Aus dem Department für Augenheilkunde Tübingen
Forschungsinstitut für Augenheilkunde

Optimising Gene Therapy for X-linked Retinitis Pigmentosa

Inaugural-Dissertation
zur Erlangung des Doktorgrades
der Medizin

der Medizinischen Fakultät
der Eberhard Karls Universität
zu Tübingen

vorgelegt von
Bellingrath, Julia-Sophia Elisabeth

2019

Dekan: Professor Dr. I. B. Autenrieth

1. Berichterstatter: Professor Dr. Dr. M. D. Fischer
2. Berichterstatter: Professor Dr. P. Martus
3. Berichterstatter: Professor Dr. A. Stahl

Tag der Disputation: 16. 07. 2019

Table of contents

LIST OF ABBREVIATIONS

AAV: adeno-associated virus

ACAID: anterior chamber-associated immune deviation

AdV: adeno virus

AF: autofluorescence

ANOVA: analysis of variance

AMD: age related macula degeneration

ARVO: The Association for Research in Vision and Ophthalmology

AU: arbitrary units

bGH: bovine growth hormone

BSA: bovine serum albumin

BSS: balanced salt solution

CAG: cytomegalovirus early enhancer and chicken beta-actin hybrid promoter

CAI: codon adaptation index

Cap: capsid proteins VP1-3 (virus protein 1-3)

CC: connecting cilium

cds: coding sequence

CEP290: centrosomal protein, 290 kilodalton

CG: cytosine-guanine dinucleotide

CpG: cytosine nucleotide occurs next to a guanine nucleotide in the linear sequence of bases co: codon optimised

chi: crossover hotspot instigator

Cre: Cre (causes recombination) protein, a recombinase

dGTP: Deoxyguanosine triphosphate

DNA: deoxyribonucleic acid

DMEM: Dulbecco's modified Eagle's medium

EBSS: Earle's Balanced Salt Solution

ECACC: European Collection of Authenticated Cell Cultures

EDTA: ethylene-diamine-tetra-acetic acid

EGFP: enhanced green fluorescent protein

ELISA: enzyme linked immunosorbent assay

EMEM: Eagle's minimal essential medium

ERG: electroretinography

EYFP: Enhanced yellow fluorescent protein

FACS: Fluorescence activated cell sorting

FBS: fetal bovine serum

FDA: Food and drug administration

FOP: frequency of optimal codons

f1ORI: origin of replication from a f1 phage

GCP: Good clinical practice

GEF: guanine nucleotide exchange factor

GFP: green fluorescent protein

GTPase: guanosine triphosphate hydrolase

HEK293T: human embryonic kidney 293 cell line with T-antigen expression

HPV: human papillomavirus

HRD: hereditary retinal degenerations

HRP: horseradish peroxidase

HSV: herpes simplex virus

ICC: immunocytochemistry

IFT: intraflagellar transport

IGF: insulin-like growth factor

IHC: immunohistochemistry

IPL: inner plexiform layer

IRES: internal ribosome entry site

ITR: inverted terminal repeat

INL: inner nuclear layer

IOP: intraocular pressure

IPL: inner plexiform layer

IRBP: interphotoreceptor retinoid binding protein

kD: kilodalton

LCA: Leber’s congenital amaurosis

LGN: lateral geniculate nucleus

MCS: multiple cloning site

MOI: multiplicity of infection

MRC: Medical Research Council (UK)

NA: not applicable

nc: negative control

NCBI: national center for biotechnology information

NGRL: National Genetics Reference Laboratory in Manchester

OCT: optical coherence tomography

OD: *oculus dexter* (right eye)

OMIM: Online Mendelian Inheritance in Man

ONL: outer nuclear layer

OPL: outer plexiform layer

ORF: open reading frame

OS: *oculus sinister* (left eye)

ORI: origin of replication

pA: polyadenylation signal

PAR: pseudoautosomal regions

PBS: phosphate buffered saline

PBS-T: phosphate buffered saline with Triton-X

pc: positive control

PCR: polymerase chain reaction

PDEδ: delta subunit of rod photoreceptor phosphodiesterase (PDE) holoenzyme

PEI: polyethylenimine

PFA: paraformaldehyde

PMMA: Polymethyl methacrylate

PVDF: polyvinylidene difluoride

qPCR: quantitative polymerase chain reaction

rAAV: recombinant adeno-associated virus

R: ratio

RA: retinoic acid

RAN: rat sarcoma (Ras)-related nuclear protein

Ras: rat sarcoma

RCC1: rat sarcoma (Ras)-related nuclear protein guanine exchange factor (RanGEF) regulator of chromosome condensation 1

Rep: replication proteins required for the AAV life cycle

RLD: rat sarcoma (Ras)-related nuclear protein guanine exchange factor (RanGEF) regulator of chromosome condensation 1 (RCC1)-like domain

RGC: retinal ganglion cell

RIPA: radio-immunoprecipitation assay

RK: rhodopsin kinase

RP: retinitis pigmentosa

RPE: retinal pigment epithelium

RPGR: retinitis pigmentosa GTPase regulator [Rpgr is the murine homologue]

RPGRIP: retinitis pigmentosa GTPase regulator interacting protein [Rpgrip is the murine homologue]

RPGRIP1: retinitis pigmentosa GTPase regulator interacting protein 1

Rpgr$^{-/y}$: transgenic mouse line with disruptive insert in murine homologue of RPGR

RT: room temperature

rTPA: recombinant tissue plasminogen activator

σ: common standard deviation

SDS-PAGE: sodium dodecyl sulfate polyacrylamide gel electrophoresis

SNR: signal-to-noise ratio

SPLICE: swift polymerase chain reaction for ligating *in vitro* constructed exons overlap extension polymerase chain reaction

SPSS: statistical package for the social sciences

SV40: Simian (vacuolating) virus 40

T: nucleotide length (in kilobases) of the transgene plasmid

TAE: tris-acetate-ethylene-diamine-tetra-acetic acid

Tm: melting temperature

TPA: tetradecanoylphorbol-13-acetate

Vb: vector backbone

vg: vector genomes

VP1-3: virus protein 1-3

WB: Western blot

WHRN: Whirlin

WPRE: woodchuck hepatitis virus post-transcriptional regulatory element wt: wild type

XCI: X-chromosome inactivation

XLPRA1: X-linked progressive retinal atrophy 1

XLPRA2: X-linked progressive retinal atrophy 2

XLRP: X-chromosome linked retinitis pigmentosa

LIST OF FIGURES

.

LIST OF TABLES

CHAPTER 1
GENERAL INTRODUCTION

1.1 The retina

1.1.1 Embryogenesis

The retina holds a unique and extraordinary position within neural tissue because it is the only part of the brain that can be visualized directly and non-invasively. These highly specialized neural cells are formed from an outpouching of the diencephalon, a secondary brain vesicle that emerges when the most cranial primary brain vesicle, the prosencephalon (forebrain) splits into tel- and diencephalon. The first morphological evidence of the retina can be seen with the emergence of optic sulci on the twenty-second day of embryonal development during the transformation of the neural plate into the neural tube, the rudiment of the central nervous system (CNS). With the completion of the neurulation process, the optic sulci become optic vesicles that are attached to the diencephalon by an optic stalk, which is later filled by the optic nerve fibres. Anteriorly, the neuroectoderm-lined optic vesicles are in contact with the surface ectoderm, which later forms the lens as well as the epithelium of the cornea. The optic vesicle invaginates and gives rise to the optic cup, which consists of a bipotential neuroretina [1, 2]. It forms two layers, which are initially separated by an intraretinal space (later termed subretinal space): the outer layer, which develops into the melanin containing retinal pigment epithelium (RPE), and the inner retinal layer [3]. While the anterior part of the inner retinal layer, the pars cecae retinae, forms the ciliary body and the unpigmented epithelium of the iris, the posterior part of the retina, the pars opticae retinae, forms what is most commonly thought of when describing the retina: the neural, light-sensing tissue of the eye (Fig. 1.1) [3].

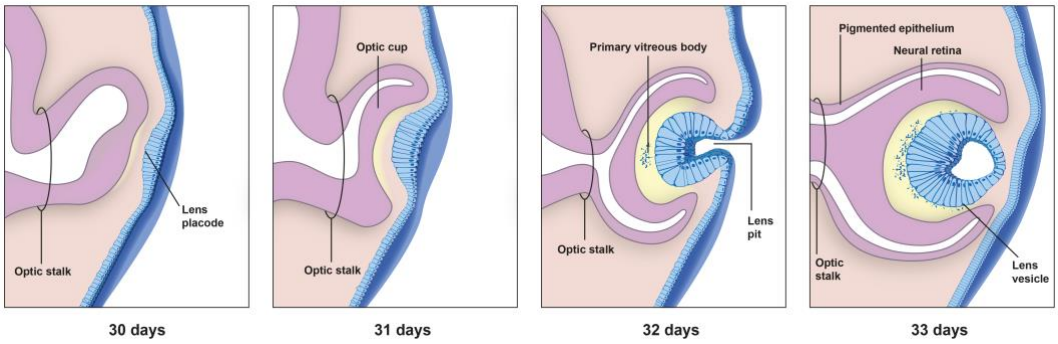

Fig. 1.1: **Embryogenesis of the human eye**. The optic vesicle arises from the diencephalon and invaginates to become the optic cup. The bipotent neuroretinal epithelium differentiates into the RPE and the neural retina, which is colonized by waves of differentiating RPC to form the ten layers of the retina. The lens develops from the lens placode, which is formed by an invagination of the surface ectoderm. The optic stalk is later filled by the optic nerve and the hyaloid retinal artery.
RPC: retinal progenitor cells, RPE: retinal pigment epithelium

Initially, the inner neural retina layer is made up of the pseudostratified epithelial lining of the neural tube but is subsequently colonized by waves of multipotent retinal progenitor cells (RPCs) moving from the intraretinal space toward the vitreous body. This wave-like migration results in the formation of the retinal layers: the cells with the ability to convert photons into an electric signals, cone and rod photoreceptors, are formed in the first and second wave of cell migration, respectively. Further cell groups to differentiate from RPCs in the first wave are ganglion cells, which are the first neurons to differentiate in all vertebrate species [4], as well as the horizontal cells, a laterally connecting retinal interneuron. The second wave of cellular migration is completed with the formation of amacrine cells, which function as inhibitory interneurons. Lastly, migration and maturation of the bipolar cells, which connect photoreceptors and ganglion cells, and Mueller retinal glial cells complete the retinal layers [4, 5]. Ganglion cell axons form the innermost retinal layer and are gathered in the optic disc to form the optic nerve, which fills out the optic stalk and connect the outwardly accessible retina to the intracerebral CNS. Retinal development begins centrally and spreads toward the periphery. By the seventh month of fetal life, a primitive fovea, which will later become the point of highest visual acuity, forms, but does not mature until several months post-partum. The intraretinal space disappears by week seven of embryonal development, but the RPE and neural retina never fuse, creating a

potential culprit for neural retinal detachment from the RPE, but also an ideal potential space for local applications of therapeutic compounds such as gene therapy.

The optic cup is surrounded by a mesenchymal capsule, which is derived from neural crest cells (NCC) and mesoderm. This mesenchymal encasing gives rise to two layers: the fibrous, avascular outer sclera, which among other things serves as an anchor for the extraocular muscles, and the vascular choroid, which serves to nourish the RPE and photoreceptors. The choroidal vessels originate from the posterior ciliary branches of the ophthalmic artery. The remaining retinal layers are nourished by the central retinal artery, a branch of the ophthalmic artery that develops from the proximal portion of the precursor hyaloid artery when the lens ceases to require vascular supply. Similar to the spatial development of the neural retina, its vascularization progresses from the optic head into the periphery, following neural differentiation. The only avascular site of the retina is the fovea. While blood supply is responsible for delivering nutrients, it also functions as an important barrier that in part regulates the immune privilege of an organ. Similar to the blood-brain or the blood-testes barrier, the blood-retina barrier partially accounts for the immune-privileged status of the eye, with the outer blood retina barrier formed by the tight junctions of the RPE and the inner blood retina barrier formed by the non-fenestrated endothelium of the retinal capillaries [6].

1.1.2 Architecture

The retina consists of ten layers, nine of which are formed by retinal neurons, Mueller glia cells and their respective synaptic connections. The RPE forms the outermost layer, which is not part of the neural retina, but is critical for preserving photoreceptor (PR) function and maintenance. It establishes the outer blood retina barrier as well as retinal adhesion, aids in the efficient processing of light waves by absorbing scattered light via its melanosomes and also plays a vital role in many metabolic needs of the retina from restoring of photopigments, over phagocytosis of shed PR outer segments to photopigment recycling and

production. Bruch's membrane lies immediately adjacent to the RPE and is formed by the fusion of RPE's basal membrane with the choriocapillaris. The second retinal layer is comprised of the photoreceptor outer segments (OS). In between these two layers lies the potential subretinal space created by the invagination of the optic vesicle discussed above. Despite the fact that based on the ontogeny, 'intraretinal space' would be the more apt term, I will follow the convention of using 'subretinal space' in the following. Connections between the Müller glial cells and PR form the outer limiting membrane (OLM), the third retinal layer, while photoreceptor nuclei form the fourth layer, the outer nuclear layer (ONL). Two other retinal layers, the sixth and the eight layer, also prominently feature neuronal nuclei and are named accordingly: the inner nuclear layer (INL) is comprised of the interneuron nuclei of bipolar, horizontal and amacrine cells as well as Mueller glial cell nuclei; the ganglion cell nuclei are contained in the ganglion cell layer. In between these three layers of cell nuclei, two synaptic layers are created: the outer plexiform layer (OPL) is formed by the synapses of the photoreceptor cells and the bipolar cells, while the inner plexiform layer (IPL) is formed by the synapses of the bipolar cells to the third neuron in the visual field, the ganglion cells. Axons of the ganglion cells make up the retinal nerve fiber layer, which is the ninth and second to last retinal layer. These axons all converge at the optic nerve papillae, the head of the optic nerve, and bundle to form the optic nerve. Finally, as a counterpart to the distal OLM, the Müller cell's proximal terminations, also called footplates, covered with their basal lamina form the tenth and innermost retinal layer, the inner limiting membrane (ILM). This ILM lies directly adjacent to the posterior hyaloid membrane of the vitreous body, which fills out the vitreous cavity towards the anterior segment of the eye (Fig. 1.2).

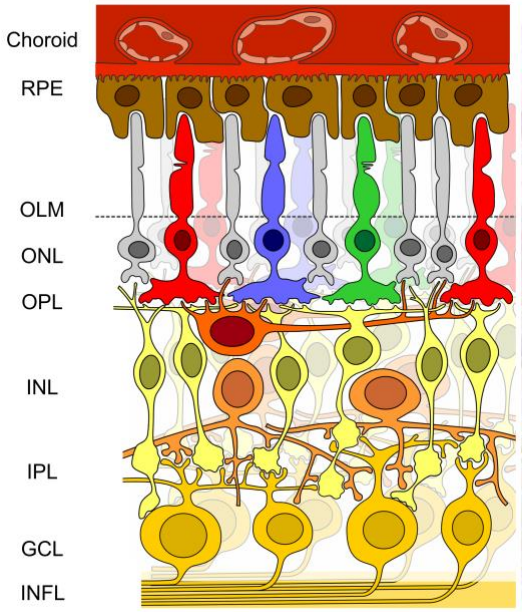

Fig. 1.2: **Layers of the retina**. Three nuclear cell layers represent the first three neurons of the visual pathway. The ONL represent PR nuclei, the INL is comprised of interneuron nuclei and the GCL is made up of ganglion cell nuclei, whose fibres form the INFL. The PR consist of rods (grey) as well as red, green and blue wave-length sensing cones (coloured accordingly). The RPE is the outermost retinal layer and vital for photoreceptor health and morphogenesis. The IPL and OPL are layers formed by synaptic connections between photoreceptors and interneurons and interneurons and GC, respectively. Only pictured on histology is the ILM, which lies adjacent to the vitreous body and is formed by the basal membrane of microglia scaffold cells. The OLM, formed by microglia cells and their connections with the PR is represented in the dotted grey line. RPE: retinal pigment epithelium; ONL: outer nuclear layer; INL: inner nuclear layer, GCL: ganglion cell layer; OPL: outer plexiform layer, IPL: inner plexiform layer, INFL: inner nerve fibre layer. Figure reprinted with alterations and permission from Dominik Fischer.

1.1.3 Visual pathway

With an area of just 1 cm^2 and a mere thickness of 150-400 microns, the transparent neural retina consists of approximately 120 million rod and 6.5 million cone photoreceptors, that synapse with one million ganglion cells via interneurons [7]. The axons of the ganglion cells form the nerve fiber layer and converge in the optic disc, the only part of the retina that cannot sense light (because it lacks the primary photoreceptors), and which corresponds to the blind spot on visual field testing. The medial optic nerve fibers are responsible for the temporal visual field and cross to the contralateral hemisphere in the optic chiasm. Together with non-crossing ipsilateral fibers responsible for the nasal components of the visual field, they form the optic tract and travel to the lateral geniculate nucleus (LGN) of the thalamus. The exception to this pathway is the

neurons involved in the pupillary light reflex, a brain stem reflex, which travel to pretectal area of the midbrain. In the LGN, the third neuron of the visual path synapses, and the light impulse reaches the primary visual cortex located around the calcarine fissure of the occipital cortex [8]. As with all neural fibers, the fibers of the visual pathway are arranged in a somatotopic fashion, with those projecting from the lower retinal reaching visual cortex via the Meyer loop while the superior retinal fibers reach the visual cortex via the dorsal optic radiation. Similar to the somatosensory homunculus, in which richly innervated parts of the body such as the hands are represented disproportionately compared with their physical side, the macula takes up the largest area of the visual cortex, even though it only takes up 20 mm^2 out of a total retina area of 1092 mm^2. This highlights the importance of the densely cone-populated macula in the subjective measure of visual acuity in humans. This pattern is shared among mammals, including the genus of *Mus muluscus* which is an important model for preclinical vision research [9].

1.1.4 Photoreceptor morphology

Photoreceptors are sensory neurons that exhibit a highly polarized structure and clearly delineated composition that is mirrored in the three of the retina's ten layers: photoreceptor outer segments form the second, photoreceptor nuclei the fourth layer and the photoreceptor synapse with interneurons make up the OPL, the fifth retinal layer. Complimentary to the outer segments (OS), photoreceptors have an inner segment (IS), two functionally and morphologically distinct compartments, which are joined by a non-motile ciliary structure, the connecting cilium (CC; Fig. 1.3 A).

The OS is a highly specialized primary (aka non-motile) cilium in which phototransduction takes place. The IS houses the PR's metabolic machinery and therefore consists of all organelles needed to provide for the high energy demand and deliver proteins for the PR's biosynthetic and metabolic functions. The OS is made up of membrane infoldings in cones and double membrane discs in rods, which are continuously shed at the tip. This loss is compensated by continuous regeneration of membrane that is synthesized at the base of the CC and

transported to the OS. The RPE phagocytoses these shed products and is thus responsible for the continued viability of the PR [10]. The layout of the 0.2 µm – wide CC shares similarities to both the composition of a motile cilium and of the microtubular transport network in the axons of neurons. Starting from the IS, it is composed of a basal body, a somewhat confusingly named connecting cilium and an axoneme (Fig. 1.3 B) [11].

It functions as a bidirectional gateway responsible for shuttling remarkable amounts of soluble and membrane-bound proteins necessary for phototransduction, including opsins, between inner and outer segments [12]. The 10 % renewal rate of the OS per day illustrates the extraordinary feat the PR undergoes to ensure its full functionality [10].

The area proximal to the basal body in the IS is termed the transition zone and functions as a gatekeeper structure that regulates the movement of proteins through the CC. The transition zone also acts as a physical redistribution barrier via transition zone fibers that allows maintenance of the vastly different protein compositions in both inner and outer segments against a concentration gradient [13]. Similar to the microtubule composition in motile cilia, the axoneme is composed of nine microtubule doublets. But, unlike the axoneme of motile cilia, it lacks the two singlets at the centre. This is referred to as a 9 + 0 configuration, in contrast to a 9 + 2 composition of a motile cilium. The motor transport proteins Dynein and Kinesin are attached to the axoneme and enable bidirectional intraflagellar transport (IFT) along the axoneme and the CC and therefore between outer and inner segments of the photoreceptor [14] Thus, the integrity of the cilium and its attached protein network is absolutely essential in maintaining the function as well as the morphology of the PR. Anything that impedes the IFT along the axoneme will lead to the severe PR malfunction and ultimately result in retinal degeneration [14].

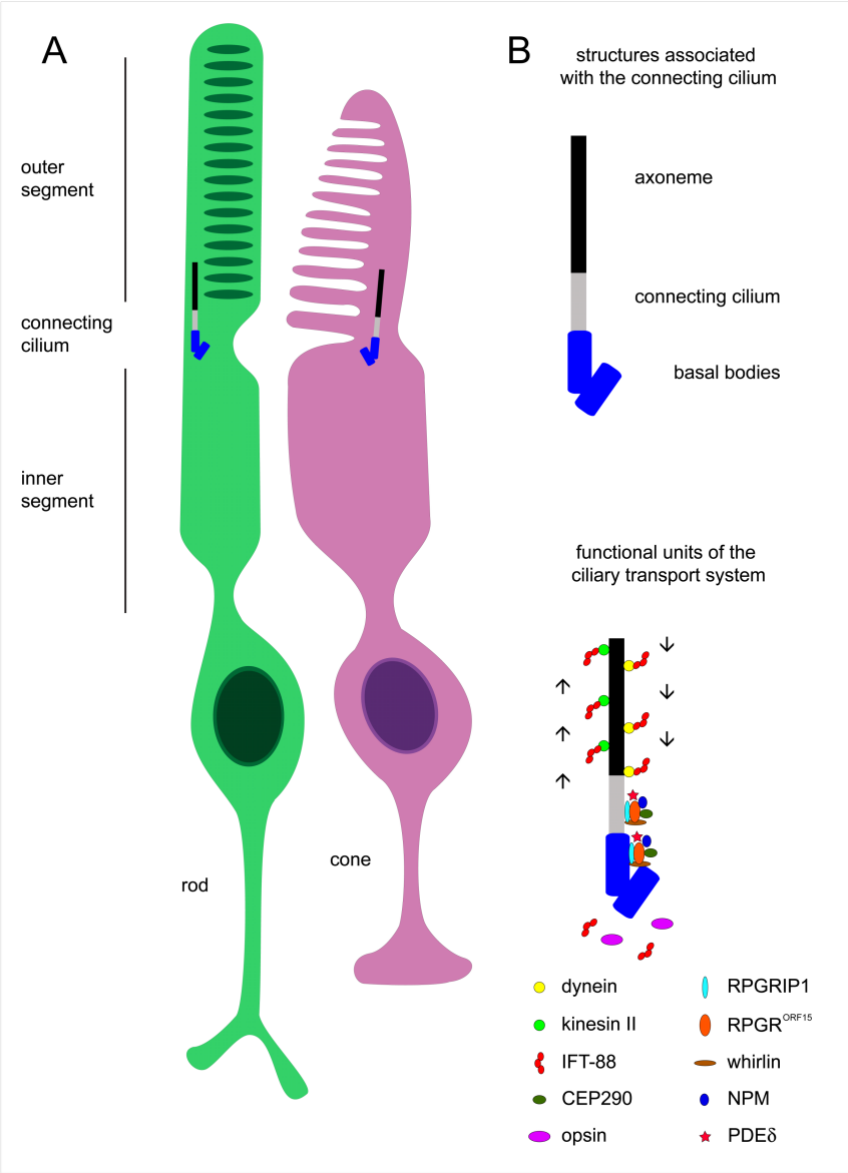

Fig. 1.3: **Photoreceptor morphology**. Photoreceptors include rods and cones, both of which have a similar basic structure: their nuclei form the retinal ONL, the IS houses the cellular machinery for the production of proteins needed to replenish the OS. The OS consists of membrane infoldings (cones) and membrane discs (rods) with light sensitive photopigments (opsins) that are continuously shed and phagocytosed by the RPE. The CC acts as a gateway to transport proteins from the IS to the OS and also a barrier that is able to uphold the steep concentration gradient between the segments (A). The non-motile CC consists of a basal body, a connecting cilium and an axoneme. Motor proteins dynein und kinesin II facilitate antero- and retrograde transport along the axoneme, while the proteins attached to the basal ganglia are part of the ciliary gateway that controls protein (e.g. opsins) movement through the CC into the OS. RPGRIP tethers $RPGR^{ORF15}$ to the connecting cilium. Other binding partners of $RPGR^{ORF15}$ are PDE6 and CEP290, as we well as NPM and whirlin, which all play a role in coordinating intraflagellar transport.
ONL: outer nuclear layer; CC: connecting cilium; RPGR: Retinitis pigmentosa GTPase Regulator; RPGRIP: RPGR interacting protein; RPE: retinal pigment epithelium; IS: inner segments; OS: outer segments
Figure reprinted with minor alterations and permission from Dominik Fischer.

1.1.5 Phototransduction and visual cycle

The first neuron in the visual pathway, made up of rod and cone photoreceptors, is perhaps the most impressive due to its ability to convert a photon first into a chemical and then into an electric signal that travels to the visual cortex. Although rods and cones operate by the same principle, they differ in their capabilities and anatomical location to complement each other's specific roles in visual perception. Rods are predominantly located in the periphery of the retina and reach their maximal density 20° from the fovea. Due to their low threshold sensitivity for light, they are responsible for achromatic sight under night-time, dark-adapted (scotopic) conditions (hence the German proverb 'In der Nacht sind alle Katzen grau'). Cones on the other hand have a relatively high threshold for light sensitivity and are responsible for high visual acuity and chromatic vision in light adapted (photopic) daytime conditions [15]. This difference in threshold and chromatic sensitivity is due to the varying amounts of opsin, the spectral sensitivities of the different opsin molecules, the molecular mechanisms of phototransduction and the intra-retinal processing of signals. Rods contain large amounts of rhodopsin and can therefore be activated by a single photon, the basic unit of light. Cones have comparatively low opsin levels and require several hundred photons for activation [16]. The number of photons correspond with the light intensity, consequently, light transmitted at night has very few photons and only has the ability to activate rods, whereas high intensity daylight would be ideal for cone activation. Cones achieve their highest density in the macular fovea, the point of highest visual acuity. The fovea is an avascular area of the retina populated exclusively by cones and thus designed to achieve high spatial, temporal and spectral resolution; it represents the point of highest visual acuity [17]. This is reflected in the 1:1:1 ratio of cone PR to bipolar to ganglion cells in the fovea, in contrast to the peripheral retina where several PR provide input into the same ganglion cell.

Photons, the basic unit of light, must pass through eight inner retinal layers to hit the outer segments of the photoreceptors. Here, they initiate a photochemical transduction cascade by activating a group of transmembrane, G-receptor coupled proteins named opsins [18]. These photopigments are coupled with 11-

cis retinal, a Vitamin A derived chromophore, which undergoes isomerization to all-*trans* retinal upon photon absorption [19]. Opsin stimulation leads to a series of chemical events which ultimately cause the levels of cGMP in the cell to fall, sodium channels to close and the photoreceptor to hyperpolarize. This results in a decrease in glutamate release from the photoreceptor synapse, which causes an excitatory or inhibitory signal to be passed along the neurons of the visual field, depending upon which interneuron the signal is transmitted to (ON or OFF bipolar cells). Thus, the electromagnetic signal is converted first to a chemical and then to an electric signal, which is passed to a sophisticated network of retinal interneurons for signal computation and then onward to the occipital cortex for visual perception.

While rods have one opsin (rhodopsin), cones have three types: short wave (S)-, medium (M)- and long wave (L)-opsins, which form the basis of colour vision [20]. These four opsins are activated by different electromagnetic wave lengths: 495 nm stimulates rhodopsin, 440-450 nm stimulate S-opsins (blue), 535-555 nm activate M-opsins and 570-590 nm activate L-opsins. Due to the wavelength by which they are stimulated, S-opsins detect blue, M-opsins detect green and L-opsins detect red colours. Cones are named after which opsin is present in them (e.g. S-cone). S-cones are predominantly located in the perifovealor region, whereas M- and L- cones are densest in the foveola, the centre of the fovea. Due to three different cone photopigments (L-, M- and S-opsin), each responsible for detecting a different wave-length, cones allow the detection of chromatic contrast, i.e. colour vision.

1.2 Retinitis pigmentosa

1.2.1 Overview

The name retinitis pigmentosa is a descriptive one, and was first used by the Dutch ophthalmologist Franciscus Donders in 1857 when writing to his colleague Hermann von Helmholtz to report the characteristic intraretinal pigment deposits seen on fundoscopy of patients with advanced RP (Fig. 1.4) [21].

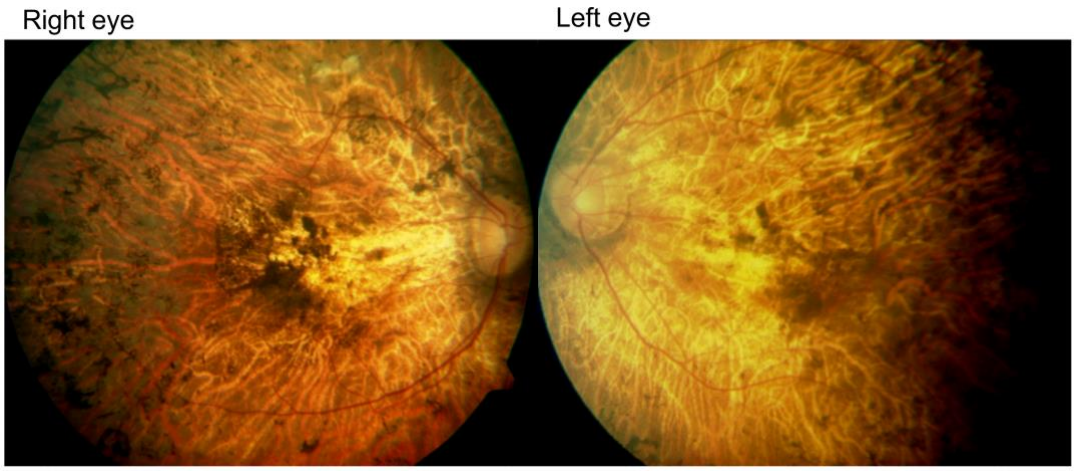

Fig. 1.4: **Fundus phenotype of a 43-year old male with *RPGR*-XLRP.** The fundus of a 43-year old male patient with *RPGR*-XLRP shows progressive disease. Typical bone spicule formation, which represents RPE migration into the neural retina secondary to photoreceptor degeneration, can be seen most prominently in the periphery and encroaching centrally.
RPGR: Retinitis pigmentosa GTPase Regulator; XLRP: X-linked Retinitis Pigmentosa

These deposits, also termed bone spicules, occur due to RPE migration into the neural retina layer secondary to photoreceptor degeneration and apoptosis [22]. The term retinitis is a misnomer owing to the fact that Donders believed the pathology to be inflammatory in origin. Only later was is discovered that rather than refer to one specific disease, the term “retinitis pigmentosa” (RP) encompasses a heterogeneous group of hereditary, monogenetic retinal diseases of which the vast majority feature a primary degeneration of rod and secondary degeneration of cone photoreceptors associated with a similar phenotypic presentation, especially toward the end of the disease course. As a whole, RP occurs with a frequency of 1:4,000 and affects more than 1 million people world-wide [23] [24] [25]. In an effort to categories this diverse group of hereditary conditions, RP can be divided by inheritance pattern. It is most commonly passed on in an autosomal-recessive manner (50-60 %), followed by an autosomal-dominant (30-40 %) and X-linked (5-15 %) pattern [26, 27]. A minority of RP are classified as sporadic (Fig. 1.5).

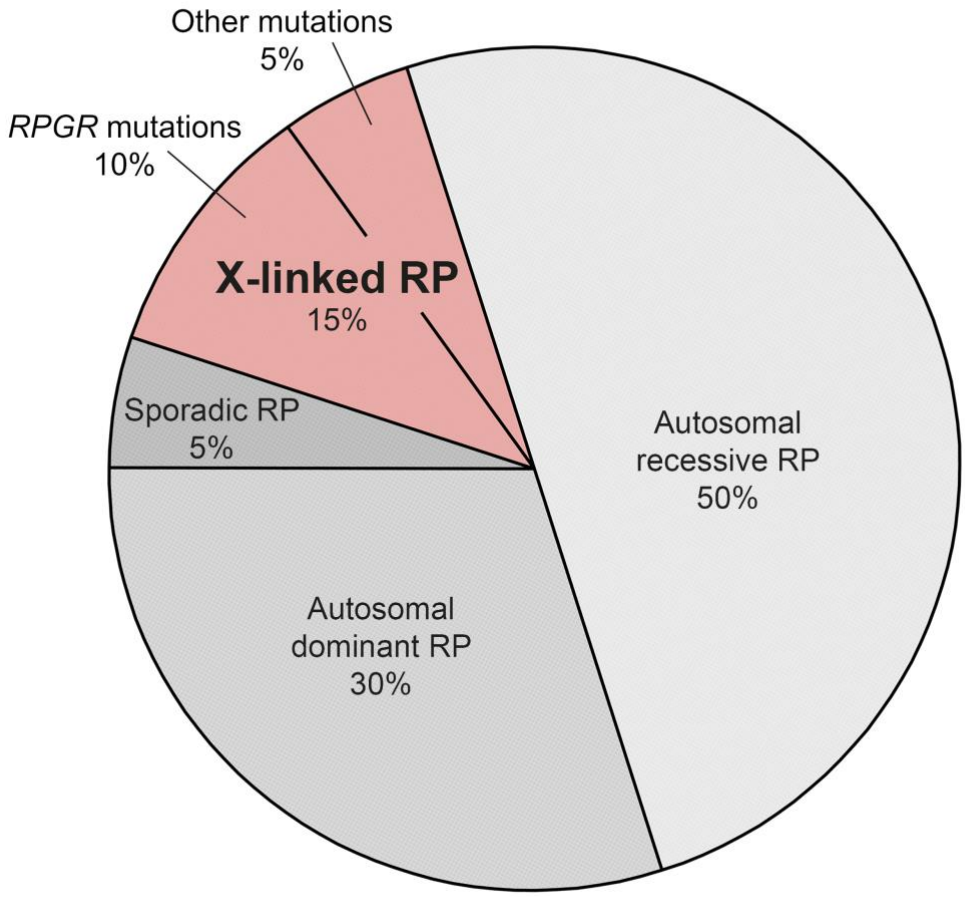

Fig. 1.5: **Distribution of Retinitis Pigmentosa by inheritance pattern.** RP is a heterogeneous group of monogenetic diseases that can further be characterized by inheritance pattern. It is most commonly passed on in an autosomal-recessive manner (50-60%), followed by an autosomal-dominant (30-40%) and X-linked (5-15%) pattern. A small minority of RP are classified as sporadic. Mutations in *RPGR*^{ORF15} cause approximately 90% of XLRP. This makes mutations in *RPGR*^{ORF15} causal for 10-20% of total RP cases.
RP: retinitis pigmentosa; XLRP: X-linked Retinitis Pigmentosa

The majority of RP is confined to the retina, but there are some notable syndromic disorders within the autosomal recessive form of RP, which together make up about 20-30 % of all RP. Usher syndrome, arguably the most well-known syndromic form of RP, manifests as hearing loss in addition to RP and accounts for 20-40 % of autosomal recessive RP. Bardet-Biedel, RP associated with kidney malformation, obesity, cognitive impairment and hypogenitalism, is also inherited in an autosomal recessive manner and makes up 5 % of all RP regardless of inheritance [28, 29]. Even though over 50 genetic loci for RP have been discovered, 40 % of genes are still unidentified [23] underscoring the

remarkable genetic heterogeneity of this disease. Of the over 50 known genes, three stand out as being responsible for a disproportionately large part of RP: *rhodopsin (RHO)* mutations cause 25 % of autosomal dominant RP, *USH2A* mutations cause 20 % of autosomal recessive RP, and, finally, mutations in *RPGR*^{ORF15} cause 70-90 % of X-linked retinitis pigmentosa. This makes mutations in *RPGR*^{ORF15} causal for 10-20 % of total RP cases [30, 31]. Since these genotypes cause a disproportionally large part of RP, they represent particularly high yield targets for developing a causative treatment.

The proteins encoded by mutated RP genes are involved in a plethora of different photoreceptor processes. Some, most notably *rhodopsin*, are involved in the phototransduction cascade, others, such as *ABCA4* and *RPE65*, encode proteins involved in Vitamin A metabolism, while others are involved in maintaining the cilium or facilitating IFT (*RPGR, USH1G, BSS1* among others), cell-to cell interaction, RNA intron splicing or pH regulation [23].

1.2.2 Clinical phenotype

In part due to the large heterogeneity of RP mutations, the rate of disease progression is highly variable between different types of RP. However, there is a general pattern of disease progression that holds true for a majority of RP patients: rod photoreceptors are the first to degenerate, causing night vision loss in adolescence coupled with progressive visual field constriction in young adulthood [23]. Due to these highly constricted visual fields, most patients become legally blind during their fifth decade of life [32, 33]. In this stereotypical disease pattern, cones are the last photoreceptors to degenerate, causing blindness during the seventh decade of life. In objective measures such as ERG, dysfunction often predates subjective perception of visual decline, with ERG studies showing dysfunction in RP patients as early as six years of age, even if these patients do not report subjective visual compromise until their teenage years [34]. Perimetry shows peripheral scotomas that enlarge over the years, but again, many patients do not realise this peripheral field loss until it is reduced to almost 50 % [35]. These findings highlight the importance and necessity of objective testing such as ERG along with psyochophysical tests such as

perimetry or visual acuity in order to accurately determine disease progression and/or response to therapy. As is to be expected, on histology, RP shows a severe disturbance of the ONL with preservation of the INL and ganglion cell layer early on in the disease. As the disease progresses, a secondary degeneration of interneurons and ganglion cells can be seen [23]. Refractive error can give an indication as to the inheritance pattern of RP. Dominant inheritance patterns tend to associate with hyperopia, whereas XLRP patients usually have a myopia of -2 diopters or more [33, 36]. This was underscored by the recent discovery of a novel *RPGR*^{ORF15} mutation responsible for both XLRP and pathologic myopia [37].

1.2.3 X-linked Retinitis Pigmentosa

The X-chromosome was first sequenced in 2005, merely a little over a decade ago. It was found to harbour 1,098 genes, of which a disproportionate number are implicated in Mendelian disease [38]. This stems from the X-chromosome inactivation (XCI) in females, a process which equalizes the dosage of X-chromosomal genes, and the hemizygosity of the X chromosome in males, which exposes recessive, monogenetic disease [38]. Also, in males, recombination between the sex chromosomes happens only in small, pseudoautosomal regions at the chromosomal tips whereas all other genes are strictly X-linked, disabling any repair mechanisms that might attenuate mutations [38].

X-chromosomal RP (XLRP) is a particularly severe and early onset form of RP that predominantly affects males, although females can be affected due to unfavourable XCI [39, 40] There is also one known, genetically verified case of a female with Turner Syndrome (X0) being affected with a full-blown picture of XLRP [41].

Twenty years before sequencing of the X-chromosome, linkage analysis was used to identify the first locus associated with XLRP. This subtype was named X-linked retinitis pigmentosa type 2 (XLRP2) and was later confirmed with help of positional cloning [42, 43]. Since then, five additional loci responsible for XLRP have been discovered: XLRP3, XLRP6, XLRP23, XLRP24 and XLRP34 (Table 1.1).

Symbol	Location on X-chromosome	*Gene*	Protein / Comment	Disease Manifestation
XLRP2	Xp11.23	*RP2*	Retinitis pigmentosa 2, similar to human cofactor C involved in beta tubulin folding	RP (10-20% of XLRP)
XLRP3	Xp11.4	*RPGR*	Retinitis Pigmentosa GTPase regulator, interacts with RPGRIP, PDE6D and IQCB 1, plays a role in ciliar transport	RP (70-90% of XLRP)
XLRP6	Xp21.3-Xp21.2	Unknown	Unknown	RP
XLRP23	Xp22.2	*OFD1*	OFD1; centrosomal protein which interacts with other ciliopathy-associated proteins including lebercilin (LCA5) and SDCCAG8.	Severe form of XLRP as well as various syndromic diseases with or without RP
XLRP24	Xq26-Xq27	Unknown	Unknown	RP
XLRP34	Xq28-qter	Unknown	Unknown	RP

Table 1.1: **Identified loci and genes responsible for XLRP.** For three of the loci, underlying genes have been identified, for the others the corresponding genes as well as putative protein functions have yet to be identified.
Table adapted from https://sph.uth.edu/retnet/home.htm.

For three of these, corresponding genes have been identified. *RP2* is responsible for XLRP2, *RPGR* for XLRP3 and *OFD1* mutations were recently identified as the causal gene in a particularly severe form of XLRP, XLRP23 (Xp22.2 locus) [44, 45].

By far the most common mutation causing XLRP are mutations in the *Retinitis pigmentosa regulator (RPGR)* gene, which is the causative mutation in 70-90 % of XLRP patients [30, 31] Although *RPGR* was identified via linkage analysis as the culprit gene causing RP3 as early as 1996 [46, 47], it could only account for less than 70 % of RP3 cases [48, 49]. This puzzle was solved with the discovery of the retina-specific isoform of $RPGR^{ORF15}$ utilizing an additional open reading frame *(ORF15)* as large terminal exon [50]. $RPGR^{ORF15}$ causes a total of 10-20 %

of all inherited retinal disease, which places it among the highest yield treatment targets for retinal dystrophies.

1.2.4 Current treatments for RP

When confronted with an RP patient, it is important to keep in mind the three extremely rare forms of RP which can indeed be treated given they are recognized early enough. All of these are syndromic RP phenotypes associated with neurologic disorders: abetalipoproteinaemia, phytanic acid oxidase deficiency (Refsum's disease), and familial isolated vitamin E deficiency (α-tocopherol transport protein deficiency). As can be inferred from the disease names, treatment consists of nutritional supplementation or food avoidance [51]. But these exceptions prove the rule that until recently, no causal treatment existed for the vast majority of RP. The only treatment approaches that had shown some promise were supportive treatments in form of high dose Vitamin A substitution, which were able to slow disease progression according to an early study, but did not succeed in arresting or reversing loss of function [34].Two therapeutic approaches have led the field in providing novel treatment options for RP and more generally for IRDs: retinal prosthesis and gene therapy. The first revolutionizing treatment for IRDs came in form of a retinal prosthesis, implanted either sub- or epiretinally [52]. This device aims to substitute the function of degenerated photoreceptors and targets patients with end stage retinal degeneration regardless of cause. Rather than modifying the disease course, as gene therapy intends to do, retinal implants aim to restore function after complete photoreceptor degeneration has occurred (and gene therapy could not function any more due to lack of target cells). Promising results have been achieved, in particular with newer generation implants [53]. Gene therapy's causative approach aims to solve degeneration by altering or preventing disease course, resulting in a highly personalized, causative approach to IRD treatment. In light of the swath of mutations responsible for IRDs and the highly selective patient selection for current clinical trials, the need for a more sweeping approach to IRD treatment is vital. Thus, the further development of the retinal implant can be seen as a complimentary field of exploration that goes hand in hand with gene therapy

IRD treatment. Gene therapy has evolved as a promising tool in the causative treatment of IRDs and will be discussed in more detail below. In addition, two promising therapies are at the horizon for IRDs. Stem cell therapy first showed promise as a treatment approach in the preclinical setting in 2006, when it was shown that rod precursor cells could successfully integrate and differentiate into into the mammalian ONL [54]. Since then, preclinical success has been translated into first-in-human phase I/II trails (NCT00874783, NCT03011541, NCT02464436) aiming to treat IRDs, including RP, with human retinal progenitor cells. First results regarding safety and tolerability of the therapy are expected as early as 2019 (NCT02464436). Genome engineering with CRISPR-Cas9 hold promise for IRDs, especially in mutations that are too large to be packaged in the conventional adeno-associated viral vectors used for gene therapy. Treatment strategies are being developed for in vivo animal models for patient cells in vitro [55].

1.3 Gene therapy

1.3.1 Concept of gene therapy

Gene therapy aims to treat diseases that result from a genetic mutation either by replacing the mutated gene, in the case of a loss of function, or by silencing the gene if it has undergone a gain of function mutation. This requires the introduction of a therapeutic gene, typically a coding sequence (cds) encoding the deficient gene, into a target cell, which then uses its own transcription- and translation machinery to continuously express the therapeutic gene. The transport of this nucleic acid can be accomplished either in form of virally vectored delivery or non-viral gene delivery. This therapeutic concept arose in the early 1970s when techniques to produce recombinant DNA were discovered that made it possible to produce cloned genes, which were shown to correct mammalian cell defects in vitro [56]. Since then, gene therapy has become a viable therapeutic strategy not only for monogenetic diseases, but also for some forms of cancer, neurologic and infectious diseases [57].

Two major concerns have plagued gene therapy from the start: firstly, an overwhelming and potentially fatal immune response to – usually systemically applied - viral vectors as well as the possibility of malignant transformation, which arises from integration of viral vectors and the activation of proto-oncogenes or inactivation of tumour suppressor genes of the genome [58, 59]. Viral vectors with a particular high risk of insertional mutagenesis are retroviral and lentiviral viruses, whose transgenes randomly integrate into the genome. The most prominent example if this occurred in a gene therapy trail for children with severe combined immunodeficiency X1 (SCID X1), where nine out of ten children contracted acute leukaemia as a result of insertional mutagenesis [58]. A milestone for gene therapy in Europe was achieved when alipogene tiparvovec (Glybera®), an AAV1-based gene therapy for patients with lipoprotein lipase deficiency (LPLD) was approved in October 2012. However, the therapy failed to meet criteria for approval by the US Federal Drug Administration (FDA) and in 2017 it as announced that uniQure, the company responsible for marketing Glybera, would not be applying for a renewal of its European licence. This makes the approval of the first ocular gene therapy, voretigene neparvovec-rzyl (AAV2-hRPE65v2; Luxturna) by the FDA in December of 2017 even more remarkable.

1.3.2. Ex- and in-vivo gene therapy

Ex-vivo gene therapy has become hugely relevant for treatment of benign and malignant hematologic conditions. The basic principle involves harvesting and selecting the appropriate cells from a patient's blood, treating them with gene therapy in vitro and re-infusing the genetically altered cells into the patient's blood stream, where they engraft and multiply. One of the most successful treatment strategies to arise from this concept is CD19 chimeric antigen receptor (CAR) T-cell therapy in the field of cancer immunotherapy [60], a therapy which has recently been approved for therapy refractive, relapsed Diffuse large B cell lymphoma (DLBCL) as well as pediatric pre B-cell acute lymphocytic leukemia (ALL) by the US Food and Drug Administration (FDA). Here, the patients T cells are extracted using apheresis and treated with a lenti- or a retrovirus and a CD19 receptor transgene which leads to CD19 receptor expression and a defined

specificity for B cells. After being expanded in vitro, these genetically engineered T-cells are then reinfused, engraft, undergo extensive proliferation and can target aberrant malignant B cells independently of HLA presentation [61]. Ex-vivo gene therapy is unique in that the vector exclusively targets the goal cells and successfully targeted cells can then be selected, while mutated or non-transduced cells can be discarded. Unfortunately, this form of gene therapy is irrelevant for gene therapy that targets tissue bound, stable, non-dividing tissue cells, which is amenable almost exclusively to in-vivo gene therapy. One exception to this rule is the targeting of corneal endothelial cells [62, 63]. When utilising in-vivo gene therapy, the transgene is administered directly to the patient in either a local or systemic manner.

1.3.3 Gene therapy and its use in ophthalmology

1.3.3.1 Benefits and drawbacks of the eye as a target for gene therapy

The success of gene therapy depends on a sufficient, long-term expression of therapeutic transgene coupled with an absence of immune-related events [64]. Due to many of its intrinsic qualities, the eye is uniquely positioned as a successful target for gene therapy. It is readily accessible, making it amenable to local injection of the viral vector. By foregoing systemic application, adverse systemic immune related events, which have plagued gene therapy in the past, are also circumvented [65]. Local immune response is also thought to be dampened due to the immune privileged status of the eye, although this hypothesis is seen in less absolute terms as human and preclinical trail data of both innate and adaptive immune response are becoming more readily available [66, 67]. The blood retina barrier is one component contributing to the immune privilege of the eye [68] and is also responsible for largely confining the viral vector to the injection space. This therefore creates a high viral vector concentration within the target tissue site. The resulting limiting of systemic spread not only increases the transduction of target cells but also lowers the systemic spread and therefore the potential targeting of germline cells, another crucial component in generating approval for a gene therapy. When thinking of the more practical side of designing a clinical trial, ocular gene therapy greatly

benefits from the eye being a paired organ. This results in an inbuilt intraindividual contralateral control which is even more valuable considering the symmetry of degeneration present in many IRDs [69]. Lastly, but perhaps most importantly, the retina harbours a particularly large amount of monogenetic degenerative diseases, making it a flag bearer for the understanding and study of monogenetically inherited conditions. As mentioned above, for most IRDs, treatment has remained elusive, which translates into an unmet need for causative therapies, which have the potential to provide a hugely benefit to individual physical and psychological health but also provide an economic benefit to society, given that IRDs are the most common cause of blindness in the working class population [70]. For all the benefits of ocular gene therapy, one drawback is the inability to directly measure transgene levels in a human clinical trial, since cells are non-dividing and their protein products locally confined. In contrast, counts of e.g. hematopoietic cells or levels of freely circulating proteins such as coagulation cascade factors can easily be determined and trended by a simple blood draw [71]. Hence functional, subjective parameters such as visual acuity, perimetry and objective measurements such as retinal thickness on OCT scan or ERG are clinically relevant surrogate markers for therapeutic transgene expression levels [72]. Hence, there is an added value of preclinical studies able to measure transgene expression with IHC or western blot.

Gene therapy in ophthalmology has been used to treat a variety of eye diseases of both the anterior and posterior segment of the eyes using Adenoviral (Ad), Lentiviral and Adeno-associated viral vectors [73]. Within the broad spectrum of efforts to treat ocular disease with gene therapy, by far the most prominent strides have been made in using it as a causal treatment option for inherited retinal disease (IRDs) using Adeno-associated viral (AAVs) vectors [73].

1.3.3.2 Modifiable factors in ocular gene therapy

Since the goal of gene therapy is to use just enough viral vector to achieve a sustained therapeutic transgene expression, it is important to think of factors that can be adjusted to achieve this. Overall, three modifiable pillars can be identified: vector delivery, the vector itself, and patient selection. Vector delivery can occur

in-vivo or ex-vivo, locally or systemically. In local administration, differing injection techniques can be harnessed. Surprisingly, ex-vivo gene therapy has indeed been used in ocular gene therapy when it was found that treating a transplanted cornea with Ad viral vectors prior to transplantation significantly prolonged transgene expression [62]. But up until now, the only viable option for IRDs is an in-vivo application of the therapeutic vector. In this setting, the vector can be delivered locally or systemically, and the eye lends itself well to gene therapy precisely because local application is possible. This decreases the likelihood of a systemic immune response and can lower the required vector dose, as well as create a tissue specificity simply by constricting the area of the vector's reach. Yet the injection technique of in-vivo viral vector delivery is a much more contested debate, which mainly focuses on whether intravitreal or subretinal delivery is more efficacious. Intravitreal injection is a significantly easier injection technique than subretinal injection, which requires a much higher level of surgical skill and experience. Therefore, it might therefore introduce less variability into a trial, especially in a multi-centre trial that involves more than one surgeon. In theory, it also allows a more even spread of the viral vector throughout the retina and thus has the potential to target the entire retina, something that is virtually impossible to achieve with subretinal injection. When thinking of RP, in which PR degeneration starts in the periphery and progresses centrally in the majority of cases, this is a relevant point, especially when considering targeting patients to prevent rather than halt (or even partially reverse) retinal degeneration. Yet a subretinal injection technique has several important advantages over an intravitreal one, the most important being its superiority in transducing the required target cells. The most common cells that require transduction by viral vectors in IRD are RPE and PR cells. The subretinal space is enclosed by exactly these cell populations, whereas intravitreal injection requires the viral vector to cross eight or nine retinal layers to arrive at these target cells. This heightens the potential for off-target effects and would most likely need a much higher vector dosing. Also, similar to the immune deviation associated with the anterior chamber of the eye (ACAID), the subretinal space has been shown to exhibit a deviant immune response [74]. This is hypothesised to play a role in the finding

that the second eye to be injected with a therapeutic vector in an LCA gene therapy approximately 2.5 years after injection of the initially treated eye did not provoke an immune response [75].

When thinking about the therapeutic viral vector itself, there are several families of viruses that have been used in gene therapy, the predominant ones being Lentiviruses, Adenoviruses (Ad) and Adeno-associated Viruses (AAV) [74]. In ocular gene therapy, AAVs have in evolved as the gold standard for gene therapy, with the number of publication and clinical trials utilizing AAV continuing to sharply increase [74]. AAVs can be modified to achieve a higher tissue specificity as well as higher transgene expression by changing the capsid or the transgene (promotor or regulatory elements). Improving capsid specificity could decrease the dose of vector and thus reduce the likelihood of an immune response as well as limit off target effects [76]. When considering transgene composition, using a cell-specific promotor increases tissue specificity, but usually represents a trade-off regarding strength of transgene expression. To combat this, regulatory elements such as woodchuck hepatitis post-transcriptional regulatory element (WPRE) are often added to the transgene cassette to make up for this [64]. The capsid can be chosen to optimally transduce target cells, but it also can be altered to decrease proteasome mediated degradation [77]. Codon optimisation can provide the great benefit of increasing transgene stability and expression levels [71, 78]. These three approaches will be discussed in the coming sections. Once a therapy is translated from bench to bedside, other points of variability present themselves. Patient selection can exert considerable influence over the success of gene therapy. This ranges from more obvious things such as the morphological and functional characteristics of the patients' disease to characteristics that are harder to determine in a scientific manner and include a stable psychological support system or realistic expectations of the therapy. Chapter 3 of this thesis will aim to procure some answers with regards to patient selection and outcome measures to determine success of clinical trials.

1.3.4 Adeno-associated virus (AAV) and its use in ocular gene therapy

Adeno-associated virus (AAV) is a single stranded DNA virus that belongs to the genus of Dependoviridae, which in turn are part of the Parvovirus family [79]. As the name Dependovirus insinuates, AAV is reliant on a helper virus to replicate and therefore is a replication-defective, non-pathogenic satellite virus for humans [80]. Wild type AAV has a genome of approximately 4.7 kB, consisting of mainly linear, single stranded DNA. Although this function is not harnessed in recombinant AAV (rAAV), it is remarkable to note that wild type AAV is the only known eukaryotic virus to integrate site-specifically on chromosome 19 in the human genome [81]. Wild type AAV (wtAAV) is packaged in an icosahedral capsid, which is made up of the three capsid proteins VP1, VP2 and VP3 [82]. In recombinant AAVs (rAAVs), the *rep* and *cap* genes that code for four replication and three capsid proteins are replaced with a transgene cassette filled with a promotor and the therapeutic transgene. Just like their wild type counterparts, they are flanked by the 145 bp-inverted terminal repeat (ITR) sequence, which aid in the formation of concatemers after the host cell DNA polymerase converts the single stranded transgene into double stranded DNA. These concatemers persist as episomal structures in non-dividing host cells [83]. Due to their greatly reduced risk of integration into the host genome, rAAVs have an extremely low risk of insertional mutagenesis [84]. Attachment to the host cell depends on interaction of capsid proteins with cellular receptors such as integrins or heparan sulfate, which is the receptor for AAV2, followed by internalization [85]. The virus is then taken up via the endosomal route and transported to the nucleus via motor proteins within seconds [85]. Twelve different serotypes of AAV have been described so far, each with a unique cell tropism [86, 87]

Besides adeno- and retroviruses, rAAVs have become some of the most important vectors in gene transfer. This is largely due to their ability to efficiently package transgenic DNA, their diverse and cell-specific tropism and their low immunogenicity as well as their ability to transduce nondividing cells. Due to their excellent safety profile in both pre-clinical animal studies and human clinical trials and adaptability to various cell lines and transgenes, rAAVs have emerged as the

gold standard for retinal gene therapy [88-90]. All major human gene therapy trials for *RPE65*-LCA, *REP1*-choroideremia and *CNGA3*-achromatopsia, have used rAAVs for viral vector delivery. A hybrid vector construct is normally used, in which the ITRs of AAV2 flank the therapeutic transgene as well as its promotor. This construct is packaged into different serotype capsids depending on the cellular tropism that is hoped to be achieved. Depending on their capsid amino acid sequence, each AAV serotype has the ability to bind to specific cell or tissue types (cellular tropism). In an effort to find AAVs that are particularly efficient at transducing a particular cell line, the capsid structures have been tested for their cellular tropism. For example, AAV2 is very efficient at transducing RPE, but not photoreceptors. Compared to AAV2, AAV8 is more successful in transducing photoreceptor cells with a dose-differential of approximately 10-fold [76, 91]. Recombinant AAV2/8 (rAAV2/8), the viral vector used in the pre-clinical mouse trail presented here, is an example of the creation of a recombinant AAV to restrict tropism to specific cell lines, in this case PRs. Creating a more specific cellular tropism possible could allow lowering of viral vector dose or achieving similar protein expression and limit off target effects that could occur with uptake in other cell lines.

Gene therapy using AAVs has been demonstrated to be safe and efficacious in several preclinical animal studies [92]. This success has been translated into human clinical trials in the proof of principle trials for patients with Leber congenital amaurosis (LCA) caused by *RPE65* mutations, which results in the lack of an essential enzyme in the Vitamin A cycle, thus causing irreversible RPE and secondary photoreceptor degeneration [76, 88, 93-96]. These studies culminated in the landmark approval of voretigene neparvovec-rzyl (AAV2-hRPE65v2; Luxturna), the first ocular gene therapy, by the US Food and Drug Administration (FDA) in December 2017. Recently, further strides were made when the first gene therapy to target photoreceptors was subretinally administered to six patients with choroideremia caused by *REP-1* mutations in a phase 1 / 2 clinical trial using AAV2 as a viral vector [72, 97].

1.3.4.1 Capsid-mutant AAV

The term capsid mutant refers to changes in the structure of capsid proteins VP1-3, most often single or multiple tyrosine (Y) to phenylalanine (F) substitutions in the amino acid sequence. Such alterations were engineered when it was observed that AAV transduction efficacy was significantly decreased by capsid tyrosine residue phosphorylation, a process mediated by epidermal growth factor receptor protein tyrosine kinase (EGFR-PTK) signalling (EGFR-PTK). Phosphorylated tyrosine residues were then tagged for proteasomal degradation by ubiquitin before they were able to reach the nucleus [98, 99]. Therefore, new AAVs with Y to F single point mutations were developed in which phenylalanine replaced each of the seven exposed tyrosine residues in VP3, making AAVs resistant to phosphorylation and subsequent ubiquitin-proteasome pathway degradation. This increased transduction efficacy up to 30-fold in vivo and 10-fold in vitro by increasing the percentage of vectors that were transported to the nucleus and therefore, therapeutic levels of transgene expression could be maintained even while using a lower vector dose [77]. Ryals *et al*. could subsequently show that the more Y to F substitutions were made, the higher the transduction efficacy became [100]. Also, where in the amino acid sequence the Y to F substitutions made influenced the efficacy of transgene expression. An AAV2 with a substitution at the 444th amino acid position showed a 10-fold higher transduction efficacy than an AAV2 with a substitution at the 730th amino acid position [101].

1.3.5 *Retinitis pigmentosa GTPase Regulator* gene

1.3.5.1 Isoforms

RPGR is located on the short arm of the X-chromosome at the Xp11.4 locus and is expressed in at least ten different isoforms, five of which are considered to be protein coding [102-105]. The constitutive variant of *RPGR* is termed *RPGR*$^{Ex1-19}$ and is expressed widely throughout the body: at the centrioles of centrosomes in dividing cells and at the transition zone of cilia [46, 47, 50, 106]. It encodes a 90 kDa protein with 19 transcribed exons, of which exons 1-10 encode a N-terminal *RCC1*-like domain (RLD), an evolutionary highly preserved domain which all

isoforms share. The dominant *RPGR* isoform of the retina is *RPGR*^{ORF15} [50, 107]. No mutation in *RPGR*$^{Ex1-19}$ has been shown to be causative for retinal disease and all mutations known to cause XLRP3 occur in the *RPGR*^{ORF15} isoform [31, 50]. In turn, this implies that substitution of RPGR^{ORF15} would be sufficient for the treatment of *RPGR*-XLRP.

1.3.5.2 Structure

RPGR^{ORF15} encodes a 1152 amino acid protein and shares exon 1-14 and part of exon 15 with the constitutive isoform *RPGR*$^{Ex1-19}$ (Fig. 1.6 B), whereas the C-terminal domain of *RPGR*^{ORF15} is unique among *RPGR* isoforms (Fig. 1.6 C).
The N-terminal domain of *RPGR*^{ORF15} consists of an amino acid structure that is very similar to the regulator of chromosome condensation (RCC1) guanine nuclear exchange factor. This N-terminal *RCC1*-like domain (RDL) is highly conserved among species and consists of six tandem repeats of 52-54 amino acids [46]. As the name implies, *RCC1* is located in the nucleus and catalyses the guanine nucleotide (GTP) exchange reaction for Ran, a small GTPase. Thus, *RCC1* plays a critical role in regulating the nucleocytoplasmic protein passage [108, 109]. The presence of a *RCC1* homology domain within *RPGR* begs the question whether the protein is a putative guanine nuclear exchange factor. This would fit with the hypothesis that it plays a role in regulating protein passageway through the connecting cilium. The unique C-terminal exon, *ORF15*, is formed by the transcription machinery skipping a splice donor site for exon 15 [50]. *ORF15* takes up a little less than half of the exonic DNA sequence and encodes for 567 amino acids. When anticipating *ORF15*'s sequence, we would expect to see a fairly even distribution of the four base pairs. Instead we see a heavy bias towards adenine and guanine nucleotides (> 98 % instead of the nominally expected level of 50 %), which make the sequence purine-rich and highly repetitive, resulting in a glycine (from GGG or GGA codons) and glutamic acid (GAG or GAA codons) rich protein sequence [50]. Due to this repetitive nature, *ORF15* is predestined for mutations during DNA replication and therefore houses a disproportionate number of mutations: it takes up less than 50 % of the cDNA sequence, but 60 % of mutations cluster on this terminal exon [50, 110].

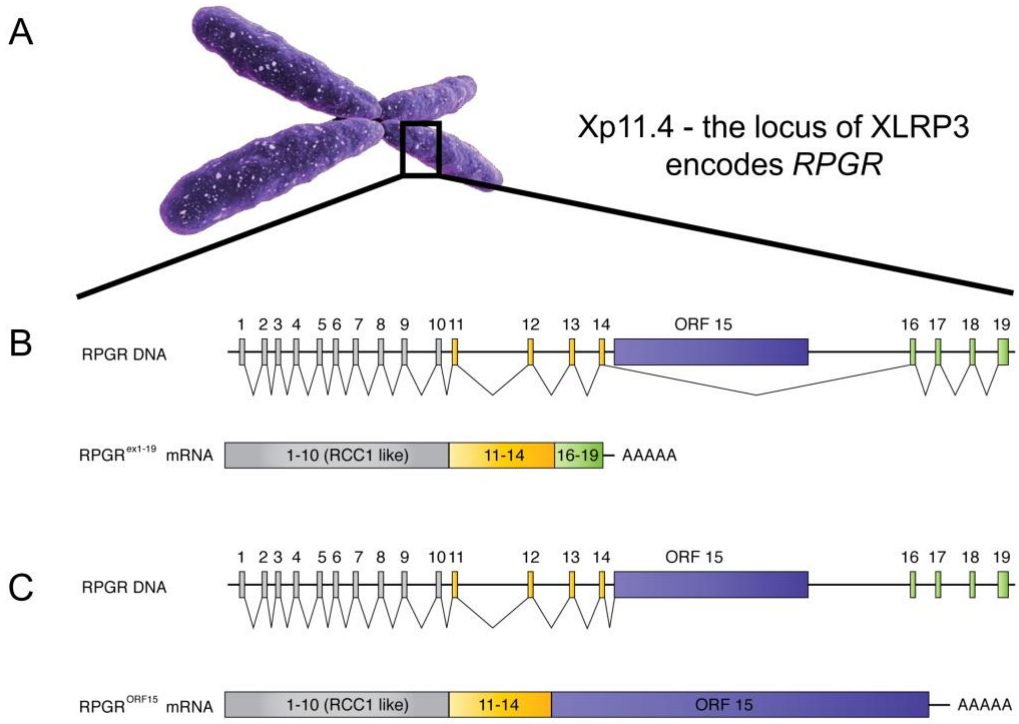

Fig. 1.6: ***RPGR* and its *RPGR*^{ORF15} isoform**. RPGR is located on the short of the X- chromosome at locus 11.4 (A). *RPGR*$^{Ex1-19}$ is the constitutive *RPGR* isoform and is ubiquitously expressed throughout the body (B). *RPGR*^{ORF15} occurs via alternative splicing and is expressed predominantly in the eye It shared the Exon 1-14, including the *RCC1* like domain with the constitutive RPGR isoform. ORF15 makes up at over half of the cDNA and mRNA (C). It is the only known form of *RPGR* that causes XLRP.
RPGR: retinitis pigmentosa GTPase regulator; *RCC1*: regulator of chromosome condensation
Figure reprinted with minor alterations and permission from Dominik Fischer.

1.3.5.3 *RPGR's* role in photoreceptor development

RPGR^{Ex1-19} und *RPGR*^{OR15} show divergent expression profiles during murine retinal development. *RPGR*$^{Ex1-19}$ is predominantly expressed during early retinal maturation and expression levels decline with further PR development [111]. In lower vertebrates, such as the zebrafish, *RPGR*$^{Ex1-19}$ is essential for retinal development, but experiments with a *RPGR*$^{-/y}$ knockout mouse model have shown it to be non-essential for PR development in higher vertebrates [112, 113]. This is supported by the fact the retina of XLPR patient shows no morphological abnormalities at the beginning of life [111]. The expression profile of *RPGR*$^{Ex1-19}$ indicates a specific but non-essential role of *RPGR*$^{Ex1-19}$ in PR development, that is not yet fully understood [114]. However, as can be impressively witnessed by

the natural disease course of *RPGR*-XLRP patients, *RPGR*^{ORF15} is essential for the maintenance of photoreceptors.

1.3.5.4 Location and function

Although the causal role of *RPGR*^{ORF15} mutations in XLRP has been well established, the function of *RPGR*^{ORF15} remains incompletely understood. Information to this end can be gained by examining the structure of *RPGR*^{ORF15}, but insight to this end can also can be gleaned from examining its binding partners in the connecting cilium (CC). The most important partner is the aptly named RPGR interacting protein (RPGRIP), a protein whose retinal isoform RPGRIP1alpha is exclusively and stably localized to the ciliary axoneme [103, 115-117]. RPGRIP's N-terminal is predicted to form a coil structure with which it binds to the ciliary axoneme [117]. Its C-terminal end binds to the *RCC1*-like, N-terminal domain of RPGR^{OR15} and therefore makes RPGRIP essential for the tethering of RPGR^{OR15} protein to the CC after its synthesis in the IS [118-120] after it is synthesized in the IS. RPGRIP is proposed to function as part of a "ciliary gate" that controls the shuttling of proteins to the OS and mutations are known to be a cause of Leber Congenital Amaurosis (LCA) type 6 [121-124]. Furthermore, another protein, SPATA7, is vital for the correct localization of RPGRIP and mutations in *SPATA7* cause LCA type 3 and juvenile RP [125]. Mutations in any of these three genes, *STATA7, RPGRIP, or RPGR*^{ORF15}, result in a similar pattern of PR degeneration, whose first sign is opsin mislocalisation to the plasma membrane, IS and ONL [113, 126]. This supports the argument that RPGR^{ORF15} might also be responsible for protein transfer from the IS to the OS. Opsin mislocalisation to the IS or CC is detectable in *RPGR*^{ORF15} mutant mammals even before PR degeneration is perceived [113, 127]. This has been observed in mammalian models such as the naturally occurring *C57BL/6J*$^{Rd9/Boc}$ mouse [127], the *Rpgr*$^{-/y}$ mouse [113] and XLRAP1 mutant dogs [128] as well as two human *RPGR*-XLRP carriers [129, 130]. Other notable binding partners that make up the *RPGR*^{ORF15} interactome are PDE6, whose binding domain overlaps with that of RPGRIP [117]. Additionally, CEP20 is an important binding partner of RPGR^{ORF15} and also forms part of the microtubule associated protein complex at the

centrosome [131]. Contrary to the C-terminal RLD, *ORF15* is not well preserved and even though it has been identified as a mutational hotspot in *RPGR*-XLRP, its function has not yet been elucidated.

1.3.5.5 Phenotype of *RPGR*-XLRP

Like all forms of XLRP and, in a broader sense, RP, *RPGR*-XLRP is known to exhibit a notoriously diverse phenotype, which results in highly variable disease progression. It usually presents as a rod-cone degeneration pattern, but a small number of patients present with a cone-rod phenotype [132]. In particular, reports show that patients with a mutation in the terminal *ORF15* exon preferentially exhibit a cone-rod degeneration pattern [25]. Although it is possible to explain this phenotypic variability with allelic heterogeneity, it is puzzling to note that this variability persists in patients with the same mutation [133] and even in dizygotic twins [134]. It has been posited that genetic modifiers may play a part in this and changes in two single nucleotide polymorphisms were shown to be associated with particularly severe disease [133].

1.3.6 Approaches and challenges in gene therapy targeting *RPGR*-XLRP

RPGR-XLRP is a model disease for gene therapy in several ways. It causes a large proportion of RP, 10 % by conservative estimate [23, 50], and no current forms of treatment exist, meaning a comprehensive patient cohort would likely profit from a causal therapeutic approach. Secondly, it is not just a prevalent, but also a severe form of RP which causes degeneration over a fairly short amount of time. This does not only make the disease more imperative to treat, but would also allow a treatment effect to be seen in a relatively short time frame [135]. Also, with the advent of genetic sequencing coupled with a clinical phenotype, it has become ever more possible to diagnose XLRP correctly, a certainty that was lacking when relying on a clinical diagnosis and history alone. However, several challenges have arisen in bringing *RPGR*-XLRP gene therapy from bench to bedside.

RPGR with its purine-rich *ORF15* region has poor sequence stability due to its highly unbalanced, repetitive nature (see 1.3.2.1), which makes it difficult to maintain sequence integrity during AAV vector production, as demonstrated by several preclinical studies that have struggled with mutated vector constructs [136-138]. Although a truncated *RPGR*^{ORF15} transgene was shown to rescue PRs in a murine preclinical study [136], this simply proves unharmful effects for one out of a myriad of possible mutations. Especially worrisome would be a mutated transgene exerting dominant negative effects that would result in an acceleration of disease progression. Indeed, Hong *et al.* showed that truncated versions of RPGR protein due to a premature stop codon lead to a degeneration that was faster in the injected eye then the natural disease progression exhibited by the control [139]. Once an unmutated therapeutic transgene has been administered, posttranscriptional processing of the therapeutic transgene presents a second challenge. The purine-rich, repetitive cDNA sequence of *ORF15* harbours potential donor splice sites which leads to a hypothesised danger of subjecting this exon-only cDNA sequence to a PR's splicing machinery used to scanning and processing intron/exon sequences. Potential splice variants arising from such an aberrant splicing could - similar to a mutated transgene - carry the potential of being ineffective or exert dominant negative effects. Even if these pitfalls have been traversed and transgene expression achieved, the expression levels must be high enough and of prolonged duration to ensure sustained restoration of function. In 2015, two important publications highlighted this problem: Jacobsen *et al.* followed three patients treated with AAV.RPE65 for up to six-years and showed that while visual sensitivity increased and peaked between one and three years after therapy, visual sensitivity progressively declined again thereafter. This rise and fall of visual sensitivity was accompanied by an invariable steady decline of photoreceptors as measured on OCT [140]. Bainbridge *et al*. independently reported similar long-term results of visual sensitivity increase in 12 patients starting at 6 months and a decrease in visual sensitivity decrease as early as one year after treatment [66]. On the flip side, administration of too high vector doses result in toxic effects [138]. These two poles highlight the importance of creating tools to optimize protein yield from

administered vectors as well as dose-escalation trials. All three of these problems are addressed by codon optimisation, a process discussed in the section below.

1.3.6.1 Preclinical studies for *RPGR*-XLRP

Developing a therapy for *RPGR*-XLRP has long been a goal due to the severity of the disease, the large proportion of RP it causes and therefore the number of people affected this disease. As in the development and approach to any disease, the creation of animal models jumpstarted a series of preclinical studies for *RPGR*-XLRP. In addition to the naturally occurring *C57BL/6J*$^{Rd9/Boc}$ mouse line, Hong *et al.* created the knockout *RPGR*$^{-/y}$ mouse model [113]. Two naturally occurring canine models, both with different microdeletions in *ORF15*, but contrasting disease courses also exist: X-linked progressive retinal atrophy 1 (XLPRA1) and 2 (XLPRA2) [128]. XLPRA1 presents with slow degeneration over years, whereas XLPRA2 presents with rapid disease progression and both are compatible with modelling human disease occurring within the first and second decades of life [90]. In addition to the preclinical study by Fischer *et al.,* three preclinical trials for *RPGR*-XLRP have been published. In 2005, Hong *et al.* were able to demonstrate evidence of long-term and substantial rescue of function, structure in their knockout *Rpgr*$^{-/y}$ mice line using a truncated murine *Rpgr*^{ORF15} transgene [136]. Subsequently, Beltran *et al.* succeeded in rescuing structure and function in two canine models of XLRP3 using human *RPGR*^{ORF15} transgene driven by two different promotors and packaged into AAV2/5 (rAAV2/5.hIRBP.hRPGRORF15 and rAAV2/5.hGRK1.hRPGRORF15) [90]. However, in 2015, the same group published results of a murine preclinical safety study, which showed *ORF15* deletions, insertions and missense mutations in the vector production process [137]. No adverse events were seen using this mutated construct, but it must be noted that due to the recorded mutations the translated protein is not wild type *RPGR*^{ORF15}. Beltran reported that the same (mutant) vector had previously been used in the dog studies (personal communication). Nevertheless, the canine studies provide therapeutic proof of principle that RPGR^{ORF15} can successfully be replaced in XLRP3 and thus provided a vital stepping stone in the quest for *RPGR*-XLRP gene therapy. The most promising

preclinical dose escalation safety study lead by Wu *et al.* was also hampered with mutations in ORF15 [138]. Four different dose categories (1×10^8, 3×10^9, 1×10^9 and 3×10^9 vg) of murine *Rpgr* and human *RPGR*^{ORF15} driven by human rhodopsin kinase (RK) promotor were tested in AAV8 and AAV9 capsids over the course of 18 months. The dose of $1x10^9$ vg in AAV8 resulted in the best outcome in the *RPGR*$^{-/y}$ mouse when using *RPGR*^{ORF15}. Interestingly enough, the ideal dose using murine *Rpgr* transgene was lower, 3×10^8 vg using both AAV8 and AAV9. Toxicity could be shown at higher doses. But during the cloning process, the purine rich, terminal *ORF15* exon once again proved amenable to mutations, with two out of five batches of vectors tainted by mutations [138].

1.4 Codon optimization

Codon optimisation attempts to address the fundamental challenges of transgene stability and protein expression levels faced in creating a gene therapy for *RPGR*-XLRP. Codon optimization is based on the principle of degeneracy, sometimes also more aptly described as redundancy, of the human genome. This simply means that for all codons, with the exception of methionine and tryptophan, a single amino acid can be encoded by anywhere from two to six differing triplet codons. This can be illustrated when looking at the ratio of possible codons to number of amino acids: there are four bases, of which three make up a base triplet, which in turn translates into an amino acid, the building block for proteins. Hence, there are 64 (4^3) possible combinations of nucleotide triplets forming a codon, which determine the amino acid. If one takes into account that three triplet sequences code of stop codons not translated into protein, there are still 61 combinations encoding for only 20 proteinogenic amino acids. In the case of glycin for example, four different triplet codons (GGG, GGA, GGC and GGU) encode this smallest amino acid, by which one can infer that several triplet codons must code for the same amino acid. These codons are then said to be redundant or synonymous. In the 1970s, it became apparent that the choice of redundant codons within genes was not arbitrary. By examining a bacteriophage that exhibited highly efficient protein expression and comparing it to another

bacteriophage that did not, Fiers *et al.* discovered that the ‘choice’ of the actual triplet out of the group of possible, synonymous combinations for any given amino acid constituted an important translational control mechanism by which cells could influence gene expression [141] as follows: The actual translation from mRNA to protein sequence in ribosomes requires tRNA molecules, which link specific codons to the corresponding amino acid. Importantly, even though synomymous codons translate for the same amino acid, each codon has a unique matching tRNA population carrying the corresponding amino acid. The amount of available such tRNA molecules differs in the cell, which in turn influences the specific efficiency of protein translation [142]. Codons with abundant levels of corresponding tRNA are dubbed “major codons”, and are preferentially used in highly expressed genes, whereas minor codons exhibit lower levels of corresponding tRNA and are used in genes with low transgene expression. This preference for certain redundant codons over others synonymous codons is termed codon bias, a widely reported phenomenon that is well preserved throughout evolution in prokaryotic and eukaryotic genomes [142-145]. In order to quantify the use of major codons and thus the strength of gene expression, Sharp *et al.* developed the codon adaptation index (CAI), a measurement of the use of major codons and thus an indication of the strength of gene expression [146]. The higher the CAI, the more major codons are used, the more rapidly this mRNA can be translated into protein and thus the more highly expressed these genes are [147]. Using a cell free model of Neurospora that allowed direct monitoring of protein translation velocity, Yu *et al*. were able to prove that the frequent use of major codons increased the speed of mRNA translation elongation [147]. But codon optimization plays a more all-encompassing role than simply increasing protein translation. For one, it can influence expression levels by modifying transcription levels through mechanism such as chromatin modification [148]. Also, by altering the speed of mRNA translation codon optimization was shown to also alter co-translational protein folding; one of the proposed mechanisms of which is affecting chaperone binding to nascent amino acid chains [147, 149]. Several analyses strengthen this finding by showing a correlation between codon usage bias and structural protein motifs, which

indicated that the mRNA sequence has a direct impact on protein folding [150, 151].

With de novo DNA synthesis becoming a broadly applicable tool, codon optimization is increasingly being used as a biotechnological tool to increase protein expression [152]. But similar to the endogenous use of codon optimization, far from simply increasing protein translation yield, goals of engineered codon optimization include elimination of GC sequences as well as avoidance of repetitive sequences and potential sites for transcription termination [153]. With codon optimization becoming more frequent, features that are taken into account when codon optimizing a gene are as follows: GC content, avoidance of repeats that might increase genetic mutations during cloning, Shine-Dalagarno-like sequences, as well as sequences that promote strong mRNA secondary structures [152]. Interestingly enough, codon optimization is more or less effective depending on which gene is targeted: it has been shown to increase protein expression by 1000-fold in some genes, while not making any difference in the protein expression in other genes [152].

1.4.1 Codon optimization and its use for *RPGR^{ORF15}*-XLRP gene therapy

Codon optimization use for translating *RPGR^{ORF15}* gene therapy into clinical trials serves a similar multifaceted goal: firstly, increased protein expression would require a lesser vector burden, which in turn would decrease the likelihood of an immune response as well as off target effects and increase the likelihood of achieving sustained therapeutic transgene expression. Since the *RPGR^{ORF15}* coding sequence takes up more than three quarters of space between the ITRs of the AAV2 transgene cassette, the prospect of not having to add additional regulatory elements such as WPRE to boost expression levels is vital. Also, and perhaps most importantly, the increased stability of the cDNA *RPGR^{ORF15}* sequence would result in a less mutation-prone transgene able to overcome a bottleneck that has hampered most *RPGR^{ORF15}* transgene sequences when developing a gene therapy *RPGR*-XLRP. Of course, potential pitfall of codon optimization could arise: unlike *wtRPGR^{ORF15}*, *RPGR^{ORF15}* is a foreign transgene

to the host, so it could be speculated that the potential for immune-mediated damage might be higher because of this. This could be exacerbated when using codon optimization on a null background, an otherwise extremely well-suited patient cohort due to the absence of dominant negative effects, since the protein is theoretically also foreign to these patients. Also, seeing the range of outcomes of codon optimization in gene translation in which gene expression is affected by codon optimization (from no change in protein translation to a 1000-fold increase), as well as considering the differing, proprietary algorithms companies provide to optimize a genetic codon sequence [152].

1.5 Aims

The aims of this thesis lie in contributing to the research that is optimising gene therapy for *RPGR*-XLRP with the goal of translating it into a clinical trial. This is achieved by looking at two very different, yet equally important angles, which are reflected in the division of the text body into the two separate chapters that follow:
The second chapter contributes to the assessment of codon-optimisation as a tool to create an $RPGR^{ORF15}$ transcript that is *i)* more stable and therefore less prone to mutations in the vector production process and *ii)* exhibits increased production efficacy as a tool as a potential way forward in treating *RPGR*-XLRP with gene therapy. This involves answering questions about translational efficacy of $coRPGR^{ORF15}$ compared to $wtRPGR^{ORF15}$ *in vitro*, as well as determining transgene expression and correct transgene localisation as an indication of $RPGR^{ORF15}$ function *in vivo*. An assessment of single-mutant (Y733F) AAV capsids as a tool to further increase therapeutic transgene expression is evaluated as well.
The third chapter contains a retrospective analysis of a two-centre, 50-patient cohort that will be on the receiving end of this *RPGR*-XLRP gene therapy. The analysis aims to elucidate functional characteristics and their development of the patient population living with *RPGR*-XLRP. Three central questions are asked when looking at the patient data: *i)* does the disease demonstrate symmetry between eyes and can the contralateral eye therefore be used as an internal

control in an interventional trial? *ii)* which subjective or objective clinical test is the most sensitive and robust outcome measure to reliably determine disease progression and in turn treatment safety and/or efficacy? *iii)* and lastly, is it possible to characterize the dynamic of disease progression to determine the optimal therapeutic window [69]? This retrospective investigation lays a foundation upon which a prospective, standardised, natural history trial can be conducted, which would allow a more in-depth and accurate assessment of these questions.

CHAPTER 2
OPTIMISING GENE THERAPY FOR X-LINKED RETINITIS PIGMENTOSA

2.1 Materials

2.1.1 Technical appliances and consumables

Product	Number	Company
Biochrom EZ Read 400 Microplate Reader	80400141	Biochrom, Cambridge, UK
Trans-Blot Turbo Transfer System	1704155	Bio-Rad, Hertfordshire, UK
PowerPac HC high-current power supply	1645052	Bio-Rad
Analogue tube rollers SRT6D	R000103298	Cole-Parmer, Staffordshire, UK
Galaxy R CO2 Incubator	CO17301001	Eppendorf, Stevenage, UK
Centrifuge	913	Hettich, Tuttlingen, Germany
Pipette Controller Pipetboy acu2	155000	Integra Biosciences, Zizers, Switzerland
Polystyrene Box	N/A	JB Packaging, Torpoint, UK
Leica CM3050 S Research Cryostat	CM3050	Leica Microsystems, Wetzlar, Germany
Leica DMIL LED Inverted Fluorescence microscope	11090137002	Leica Microsystems
R100 Rotatest Shaker	3573	Luckham, Victoria Gardens, UK
Amicon Ultra-15 Centrifugal Filter Units	UFC900308	Millipore, Feltham, UK
Snap i.d. 2.0 Protein Detection System for Western Blotting	11370220	Millipore, Billerica, USA
Retiga 2000R CCD Camera	RET2000RF M12	Qimaging, Surrey, Canada
Serological Pipette 5 ml	861253001	Sarstedt, Newton NC, USA
Serological Pipette 10 ml	861254001	Sarstedt
Serological Pipette 25 ml	861685001	Sarstedt
Tissue Culture Plate 6 Well, Standard	833920005	Sarstedt
Tissue Culture Flasks T75	833911002	Sarstedt
Tube 50 ml, 114 x 28 mm, PP	62547254	Sarstedt
Tube 15 ml, 120 x 17 mm, PP	62554502	Sarstedt
Eppendorf microtube 3810X	Z606340	Sigma-Aldrich, Dorset, UK
Polypropylene pellet pestles	Z359947	Sigma-Aldrich
Pellet pestles cordless motor	Z359971	Sigma-Aldrich

Product	Number	Company
10/20 µl XL Graduated Filter Tip 20 µl (Sterile)	S11203710	Starlab, Milton Keynes, UK
20 µl UltraPoint Graduated Filter Tip (Sterile)	S11201810	Starlab
200 µl Graduated Filter Tip (Sterile)	S11208810	Starlab
1000 µl XL Graduated Filter Tip (Sterile)	S11221830	Starlab
Disposable Scalpels No 21, sterile	507	Swann-Morton, Sheffield, UK
Pierce 96-Well Polystyrene Plates, Corner Notch	15041	ThermoFisher Scientific, Northumberland, UK
NanoDrop 1000 Spectrophotometer	N/A	ThermoFisher Scientific
Azpac Sarogold PRO Cling Wrap Film	12368039	ThermoFisher Scientific
Neubauer Counting Chamber	6310696	VWR Chemicals Prolab, Leicestershire, UK
ImmEdge Hydrophobic Barrier PAP Pen	H4000	Vector Laboratories, Burlingame, California, USA
Confocal scanning microscope	LSM710	Zeiss, Aalen, Germany

N/A: not applicable

2.1.2 Chemicals and reagents

Product	Number	Company
Tris buffered saline (10 x)	1706435	Bio Rad, Hertfordshire, UK
Trans-Blot Turbo RTA Transfer Kit, LF PVDF	1704275	Bio Rad
Trans-Blot TurboTM 5 x Transfer Buffer	10026938	Bio Rad
Trans-Blot Turbo TM Midi-size Transfer Stacks	10026915	Bio Rad
Midi-size 0.45 µm low fluorescence (LF) PVDF membrane Trans-Blot® TurboTM (BioRad)	1704275	Bio Rad
Clarity Western ECL Substrate, 200 ml	1705060	Bio Rad
Clarity Western ECL Substrate Luminol/enhancer solution	10026380	Bio Rad

Product	Number	Company
Clarity Western ECL Substrate Peroxide solution	10026381	Bio Rad
10 % Criterion TGX Precast Midi Protein Gel, 18 well, 30 µl	5671034	BioRad
7.5 % Criterion TGX Precast Midi Protein Gel, 18 well, 30 µl	5671024	BioRad
7.5 % Criterion TGX Precast Midi Protein Gel, 12 + 2 well, 45 µl	5671023	BioRad
Trans-Blot Turbo TM Midi PVDF Membrane	1704157	BioRad
BLUeye Prestained Protein Ladder	PM0070500	GeneDireX, USA
Laemmli buffer 5 x	BU117	Jena Bioscience, Jena, Germany
TransIT-LT1 Transfection Reagent	MIR2304	Mirus Bio, Wyomming, USA
Tween 20	P1379	Sigma-Aldrich, Dorset, UK
Water	W4502	Sigma-Aldrich
Phosphate buffered saline (PBS; 10 x)	P5493	Sigma-Aldrich
cOmplete, Mini, EDTA-free Protease Inhibitor Cocktail	11836170001	Sigma-Aldrich
Laemmli buffer 2 x	S3401	Sigma-Aldrich
EZBlue Gel Staining Reagent	G1041	Sigma-Aldrich
Pierce bicinchoninic acid (BCA) protein assay kit	23225	ThermoFisher Scientific, Northumberland, UK
Pierce TM BCA Protein Assay Reagent A, 1 x 500 ml	23228	ThermoFisher Scientific
Pierce BCA Protein Assay Reagent B, 1 x 25 ml	1859078	ThermoFisher Scientific
Albumin Standard 10 x 1 ml ampules	23209	ThermoFisher Scientific
Neurobasal A	10888022	ThermoFisher Scientific
Gibco B-27 Supplement	17504044	ThermoFisher Scientific
N-2 supplement	17502048	ThermoFisher Scientific
Opti-MEM Reduced Serum Medium	31985062	ThermoFisher Scientific
Radio-Immunoprecipitation Assay (RIPA) Lysis and Extraction Buffer	89900	ThermoFisher Scientific
Ethanol absolute ≥99.8 % AnalaR NORMAPUR®	20821321	VWR Chemicals Prolab, Leicestershire, UK

Product	Number	Company
Methanol absolute ≥99.8 % AnalaR NORMAPUR®	20847307	VWR Chemicals Prolab
Tissue-Tek O.C.T. compound, Sakura Finetek	25608930	VWR Chemicals Prolab

2.1.3 Media

Product	Number	Company
Dulbecco's Modified Eagle's Medium (DMEM) - high glucose	D6546	Sigma-Aldrich, Dorset, UK
L-Glutamin solution, 200 mM	G7513	Sigma-Aldrich
Fetal Bovine Serum (FBS)	F7524	Sigma-Aldrich
Hydrocortisone 21-hemisuccinate sodium salt	H2270	Sigma-Aldrich
Progesterone	P8783	Sigma-Aldrich
Putrescine dihydrochloride	P7505	Sigma-Aldrich
2-mercaptoethanol	516732	Sigma-Aldrich
Dimethyl Sulfoxide (DMSO)	D2650	Sigma-Aldrich
Penicillin/Streptomycin 10,000 U/mL	15140122	ThermoFisher Scientific, Northumberland, UK

2.1.4 Cell lines

Cell line	Description	Company
HEK293T	Human embryonic kidney cells expressing simian virus 40 (SV40) large T-antigen	European Collection of Cell Cultures (ECACC), UK
661W	Transgenic mouse retinal tumor cell line expressing simian virus 40 (SV40) T antigen	Dr. Muayyad R. Al-Ubaidi (University of Oklahoma, USA)

2.1.5 Plasmids

Plasmids	Number	Short form	Company
ITR.CAG.Kozak.coRPGRORF15.bGHpA.ITR		CAG.coRPGR	GenScript
ITR.CAG.Kozak.wtRPGRORF15.bGHpA.ITR		CAG.wtRPGR	OriGene
FIN-RK-GFP-WPRE	44358	RK.GFP	Addgene, gift from Dr Susan Semple-Rowland
AAV-EF1a-doublefloxed-chR2EYFP-WPRE-HGHpA	20298	EF1a.EYFP^doublefloxed	Addgene, gift from Dr Karl Deisseroth

2.1.6 Viruses

Virus	Short form	Origin
rAAV2/8.RK.coRPGR	rAAV2/8.coRPGR	Gift from Dr Dominik Fischer, Nuffield Department of Clinical Neuroscience, University of Oxford, UK
rAAV2/8.RK.wtRPGR	rAAV2/8.wtRPGR	Gift from Dr Dominik Fischer, Nuffield Department of Clinical Neuroscience, University of Oxford, UK
rAAV2/8.Y733F.RK.coRPGR	rAAV2/8.Y733F.coRPGR	Gift from Dr Dominik Fischer, Nuffield Department of Clinical Neuroscience, University of Oxford, UK
rAAV2/8.Y733F.RK.wtRPGR	rAAV2/8.Y733F.wtRPGR	Gift from Dr Dominik Fischer, Nuffield Department of Clinical Neuroscience, University of Oxford, UK

Virus	Short form	Origin
rAAV2/8.EF1a-doublefloxed-chR2EYFP-WPRE-HGHpA	rAAV2/8.control	Gift from Dr Dominik Fischer, Nuffield Department of Clinical Neuroscience, University of Oxford, UK
rAAV2/8.RK.GFP	rAAV2/8.GFP	Gift from Dr Dominik Fischer, Nuffield Department of Clinical Neuroscience, University of Oxford, UK

2.1.7 Primary antibodies

Anti-body	Num-ber	Company	Source / target / clonality	Anti-body iso-type	Epitope	Stock concen-tration (mg/ml)	Dilut-ion	Tech-nique
C-RPGR ^512-531	N/A	Aldevron, Freiburg, Germany	rabbit / human / polyclonal	IgG	EKSLKLSPVQKQKKQQTIGE	1,28	1:500	WB, ICC, IHC
N-RPGR ^19-35/113-129	N/A	Aldevron	rabbit / human / polyclonal	IgG	KSKFAENNPGKFWFKND, GNNEGQLGGDTEERNT	1,9	1:500	WB, ICC

Anti-body	Num-ber	Company	Source / target / clonality	Anti-body iso-type	Epitope	Stock concen-tration (mg/ml)	Dilu-tion	Tech-nique
Anti-RPGR (N-terminal) antibody produced in rabbit	HPA001593	Sigma-Aldrich Prestige Antbodies, Darmstadt, Germany	rabbit / human / polyclonal	IgG	EINDTCLSVATFLPYSSLTSGNVLQRTLSARMRRRERERSPDSFSMRRTLPPIEGTLGLSACFLPNSVFPRCSERNLQESVLSEQDLMQPEEPDYLLDEMTKEAEIDNSSTVESLGETTDILNMTHIMSLN	0,2	1:500 (WB), 1:200 (IHC)	WB, ICC, IHC
Anti-RPGR (C-terminal) antibody produced in rabbit	SAB1303617	Sigma-Aldrich	rabbit / human / polyclonal	IgG	C-terminus	0,25	1:500	WB
Rpgr Antibody (M-20)	sc-14676	Santa Cruz, Santa Cruz, Heidelberg, Germany	goat / mouse / polyclonal	IgG	near C-terminus of mouse RPGR	0,2	1:200	IHC
RPGRIP1 Antibody (E14)	sc-160753	Santa Cruz	goat / mouse and rat / polyclonal	IgG	near N-terminus of mouse RPGRIP	0,2	1:200	IHC

Anti-body	Num-ber	Company	Source / target / clonality	Anti-body iso-type	Epitope	Stock concen-tration (mg/ml)	Dilut-ion	Tech-nique
Anti-GAPDH Antibody (Clone Name: OTI2D9)	TA802519	OriGene, Cambridge, UK	mouse / human, mouse, rat, dog and monkey / monoclonal	IgG	full length human recombinant protein of human GAPDH (NP_002037)	1	1:2000	WB
Anti-beta actin	MA5-15739	ThermoFisher Scientific, Northumberland, UK	mouse / human, mouse / monoclonal	IgG	A slightly modified synthetic beta-cytoplasmic actin N-terminal peptide conjugated to KLH			

N/A: not applicable

2.1.8 Secondary antibodies

Anti-body	Num-ber	Company	Source / target / clonality	Anti-body iso-type	Epit-ope	Stock conce-ntration (mg/ml)	Dilut-on	Tech-nique
IRDye 680RD	926-68072	Li-Cor, Biotechnologies, Cambridge, UK	donkey / mouse / polyclonal	IgG	mouse IgG (H&L)	1	1:10000	WB (fluorescent)
IRDye 800CW	926-32212	Li-Cor	donkey / mouse / polyclonal	IgG	mouse IgG (H&L)	1	1:10000	WB (fluorescent)
IRDye 800CW	926-32213	Li-Cor	donkey / rabbit / polyclonal	IgG	rabbit IgG (H&L)	1	1:10000	WB (fluorescent)

Anti-body	Num-ber	Company	Source / target / clonality	Anti-body iso-type	Epit-ope	Stock conce-ntration (mg/ml)	Diluti-on	Tech-nique
IRDye 680RD	926-68074	Li-Cor	donkey / goat / polyclonal	IgG	goat IgG (H&L)	1	1:10 000	WB (fluore scent)
Donkey Anti-Rabbit IgG H&L (HRP) preabso rbed	ab985 03	Abcam, Cambridg e, UK	donkey / rabbit / polyclonal	IgG	rabbit IgG (H&L)	0,5	1:10 000	WB
Donkey Anti-Mouse IgG H&L (HRP) preabso rbed	ab987 99	Abcam	donkey / mouse / polyclonal	IgG	mouse IgG (H&L)	0,5	1:10 000	WB

2.1.9 Animals

Animal	Origin
C57BL/6J mice	The Jackson Laboratory, Bar Harbor, USA
C57BL/6J $^{Rd9/Boc}$ mice	The Jackson Laboratory, Bar Harbor, USA
Rpgr$^{-/y}$ mice	Tiansen Li, Neurobiology, Neurodegeneration & Repair Laboratory, National Eye Institute, Bethesda, USA
Rhesus macaques (*Macaca mullata*)	Medical Research Council Centre for Macaques, Porton Down, UK

2.1.10 Software

Software	Version	Company
ImageStudioLite	4.0.21	LiCor Biosciences, Nebraska, USA
Odysee Fc Imaging System	Model No 2800 S/N OFC-0377	LiCor Biosciences
Excel for Macintosh OSX	36539	Microsoft, Redmond, USA

Software	Version	Company
Statistical Package for Social Sciences version 21 by IBM (SPSS21)	21	SPSS Inc., Chicago, USA
ImageJ/FIJI	2.0.0.-rc-43/1.51s	ImageJ/FIJI

2.2. Methods

2.2.1 Cell Culture

Utilizing western blots, cell lysate of HEK293T transfected with plasmids containing codon optimized (co) *RPGR*^{ORF15} and wild type (wt) *RPGR*^{ORF15} were used to compare and quantify *RPGR*^{ORF15} transgene expression. 661W cells were employed to assess transducibility of wild type rAAV2/8 and single mutant rAAV2/8^{Y733F} vector capsids. All cell culture work was performed under a class II cell culture hood (ThermoFisher Scientific, Northumberland, UK). Cell culture flasks were stored in a Galaxy R incubator (Eppendorf AG, Hamburg, Germany). Cell culture media stored was at 4 °C and pre-warmed in a 37°-degree water bath (ThermoFisher Scientific) prior to use.

Western Blot was used to quantify transgene expression in HEK293T cells transfected with co or wt *RPGR*^{ORF15} as well as to detect transgene expression in mice unilaterally injected with AAV8.coRPGR. Immuno-labeling was used to show correct localisation of codon optimised transgene to the photoreceptor cilium and to compare transduction efficiency between wild type and single mutant (Y733F) AAV8 capsids.

2.2.1.1 Human embryonic kidney cells

HEK293T cells are derived from human embryonic kidney cells of a healthy, aborted embryo, and were immortalized by Frank Graham in Alexander van der Eb's laboratory in 1973 in Leiden, Netherlands. Transformation was achieved in Dr. Grahams 293rd experiment by culturing HEK cells with sheared adenovirus 5 (AAV5) DNA, which resulted in a 4.5 kbp insertion of the AAV5 genome into chromosome 19 of the HEK cell line. This genome fragment encodes for

E1A/E1B proteins which interfere with cell cycle control pathways and inhibit apoptosis [154, 155]. Additionally, HEK293T cells express a temperature-sensitive allele of the Simian Virus 40 (SV40) large T-Cell antigen. This considerably increases expression levels obtained with transient transfection by plasmid vectors that contain the SV40 origin of replication [156]. Additionally, SV40 T inhibits p53, which might increase proliferative drive [157].

Resuscitation

HEK293T cells were obtained from the European Collection of Cell Cultures (ECACC; UK) and aliquots of 2×10^6 cells were stored in 1.5 ml 90 % Fetal Bovine Serum (FBS; Sigma-Aldrich Company Ltd., Dorset, UK), 10 % Dimethyl sulfoxide (DMSO; Sigma-Aldrich) in liquid nitrogen at -196 °C. For resuscitation, cell vial aliquots were removed from the liquid nitrogen freezer, transported to the cell culture lab on dry ice and defrosted in a preheated water bath at 37 °C. The thawed cell suspension was pipetted into 10 ml of pre-warmed, 36 °C complete cell culture media: high glucose Dulbecco's Modified Eagle's Medium (DMEM) with 10 % FBS, 1 % 200 mM L-glutamin solution (all Sigma-Aldrich) and 1 % Penicillin/Streptomycin (ThermoFisher Scientific, Northumberland, UK) and spun down at 1200 rpm for 5 minutes at 4 °C. The supernatant was aspirated, and cells were carefully re-suspended in 1 ml DMEM and plated in a T75 flask (Sarstedt Inc., Newton NC, USA) with an additional 13 ml of DMEM. The flask was stored in a Galaxy R incubator (Eppendorf AG, Hamburg, Germany) at 37 °C with 5 % CO_2. Before fresh media was added 24 h later, cells were washed in 2 ml Phosphate Buffered Saline (PBS; Sigma-Aldrich) to remove any damaged cells. Cell proliferation rates and the resulting confluency was determined daily under direct vision with light microscopy (Leica DMIL LED Inverted Fluorescence microscope, Leica Microsystems CMS GmbH, Wetzlar, Germany) at four- and ten-times magnification and documented with Retiga 2000R CCD Camera and QCapture Pro software (both Qimaging, Surrey, Canada).

Splitting

When a cell confluency of approximately 70 % was reached, cell culture media was carefully removed from the T75 flask with a 25 ml serological pipette (Sarstedt). Preparation for splitting was undertaken with help of a gentle wash with 2 ml PBS to remove accumulated debris. Detachment of HEK293T cells from the flask bottom was induced by the addition of 1 ml PBS and a two-minute placement in an incubator. Sufficiency of cell detachment from the flask bottom was checked under direct vision with light microscopy. If the degree of detachment was deemed insufficient, mechanical force generated by tapping the flask was employed to further detach cells. Then, 9 ml of cell culture media was added, and a single cell suspension was attained by vigorously pipetting up and down. In order to achieve a 1:20 dilution, 3 ml of the generated cell suspension was added to a new, appropriately labeled T75 flask along with 3 ml of fresh cell culture media.

2.2.1.2 Mouse cone photoreceptor-like cells (661W cell line)

661W cells were cloned in the lab of Dr. Muayyad R. Al-Ubaidi from retinal tumors of a transgenic mouse line expressing the simian virus (SV) 40 T-antigen under control of the human interphotoreceptor retinol-binding protein (IRBP) promoter. In addition to SV40, immunoblot analysis of these cells in monolayer showed expression of cone - but not rod - photoreceptor proteins: blue and green cone pigments, transducin, and cone arrestin [158]. Biochemical properties also exclusively demonstrated cone characteristics. Hence, 661W cells are described as a “cone-like” photoreceptor cell line. 661W cells were obtained under material transfer agreement as a kind gift fom Dr. Muayyad R. Al-Ubaidi (University of Oklahoma, USA) and cultured according to his specifications.

Cell resuscitation and splitting

Cell storage, resuscitation and splitting were performed as described above for the HEK293T cell line, the exception being the cell media composition: 500 ml high-glucose DMEM with 40 µg/l hydrocortisone, 40 µg/l progesterone, 0.032 g/l

putrescine 40 µl/l, 2-mercaptoethanol (all Sigma-Aldrich), 100 mg/l penicillin, 100 mg/l streptomycin (ThermoFisher) and 10 % FBS (Sigma-Aldrich).

2.2.2 Animals

Retinas of three mouse lines were obtained from a pre-clinical mouse trail conducted by Fischer *et al.* [78]. Two of the mouse lines, *C57BL/6J* $^{Rd9/Boc}$ and the transgenic *Rpgr*$^{-/y}$ line, showed a well-characterised XLRP phenotype [113, 127], while the third, *C57BL/6J*, was used as a wild type control. With the goal of investigating safety and efficacy of gene therapy using an AAV2/8.RK.coRPGR vector, *C57BL/6J* and *Rpgr*$^{-/y}$ mice were injected with a AAV2/8.RK.coRPGR vector unilaterally in an unmasked randomised fashion, while the *C57BL/6J* $^{Rd9/Boc}$ mouse strain received the AAV2/8.RK.coRPGR vector in one eye and was sham-injected with AAV2/8.control in the contralateral eye in a masked and randomised manner. Both the AAV2/8.RK.coRPGR and the AAV2/8.control were diluted in BSS with 0.001 % PF-68 and injected at a dose of 1.5 x 109 vg. Retinas of all three mouse lines were used to assess for transgene expression with enhanced chemiluminescent (ECL) and Immunofluorescent Western Blot analysis as well as for assessment of correct localisation of coRPGR protein in photoreceptor ciliary body.

Throughout all stages of experimental work, mice were kept under conditions as specified by the ARVO Statement for the Use of Animals in Ophthalmic and Vision Research and UK Home Office guidelines (https://www.opt.uh.edu/onlinecoursematerials/PHOP6275/2015_Materials/PHOP6275_Class3_3_Animals_in_Research_ARVO_Statement.pdf). An ample supply of food and water was provided, animals were kept in individually ventilated cages and subjected to 12 h on/ 12 h off cyclic lighting.

2.2.2.1 *C57BL/6J* mice

The C57BL/6J mouse line is derived from the C57BL/6 mouse strain, a well-known mouse strain that has been extensively characterised both phenotypically

and genetically and is often used as a genetic background for congenic and mutant mice [159]. This inbred substrain of C57BL/6 mice was purchased from the Jackson Laboratory (Bar Harbor, USA), home of the original C57BL/6 mouse colony, and imported into the UK through Charles River Laboratories (Margate Kent, UK). It was used as wild-type control.

2.2.2.2 *Rpgr*$^{-/y}$ mice

A knockout vector was generated to create targeted disruption of exon 4-6 in the *Rpgr* gene, the murine homologue of human *RPGR*, resulting in a deletion of exon 4-6 and therefore a truncated *Rpgr* coding sequence. The vector was injected into J1ES cells and successfully targeted clones were injected into blastocytes of C57BL/6 mice to generate chimeras. Male chimeras were crossed with C57BL/6 females and nullizygous offspring were obtained by intercrossing over several generations [113]. The resulting phenotype included mislocalisation of cone opsins as well as rhodopsin depletion, which led to a slowly progressing degeneration of both rod and cone photoreceptors. Frozen embryos of the *Rpgr*$^{-/y}$ mice line were a generous gift of Tiansen Li (Neurobiology, Neurodegeneration & Repair Laboratory, NEI, Bethesda, USA) and were obtained under material transfer agreement.

2.2.2.3 C57BL/6J $^{Rd9/Boc}$ mice

The retinal degeneration 9 (Rd9) mouse is a naturally occurring mouse model of XLRP that was generated in the The Jackson Laboratory on a *C57BL/6J* background. Responsible for this phenotype is a 32-base pair (bp) duplication within the terminal exon *ORF15*, resulting in a frame-shift in the repetitive region of *ORF15* and thus a prematurely occurring stop codon. This mutation lead to substantially reduced or absent levels of *Rpgr-ORF15* on RT-PCR and non-detectable protein levels of *Rpgr-ORF15* in Western Blot. Retinal phenotype pathology included RPE pigment loss and slowly progressive decrease in outer nuclear layer (ONL) thickness [127]. Like the *C57BL/6J* mice, *C57BL/6J*$^{Rd9/Boc}$ mice were purchased from the The Jackson Laboratory and brought into the UK

through the Charles River Laboratories, where they were quarantined before transport to the Biomedical Service Center at the John Radcliffe Hospital.

Harvesting of mice eyes

After primary electrophysiological endpoints of the pre-clinical trial were established, mice were sacrificed. Eyes were quickly enucleated and appropriately processed for immunohistochemistry without fixation as detailed above and Western Blots to detect localisation of RPGR to the as well as transgene expression.

2.2.2.4 Rhesus macaque (*Macaca mullata*)

Due to their close genetic and physiological resemblance to humans as well as their natural abundance, Rhesus monkeys are the most frequently used non-human primates in biomedical and genetic research. Retinal tissue was collected from Rhesus macaque (*M. mullata*) aged 5-19 years at the Medical Research Council (MRC) Centre for Macaques (Porton Down, Salisbury, UK) that had undergone scheduled killing for separate purposes. Eyes were enucleated promptly after sedation with 10 mg kg^{-1} intramuscular ketamine and a lethal overdose of 200–300 mg kg^{-1} intravenous pentobarbitone. The tissue was placed in Neurobasal A (ThermoFisher Scientific) with 100 units/ml penicillin, 800 µl L-glutamine (both Sigma-Aldrich), 2 % B-27 supplement and 1 % N-2 supplement (both ThermoFisher Scientific). Peripheral samples of the retina were attained after appropriate dissection and transported to the laboratory in a cooled polystyrene box (JB Packaging, Torpoint UK). Lysis of peripheral retinal samples were prepared for immunofluorescent western blotting in the same manner as the mouse retinal lysates.

2.2.3 Molecular Biology

2.2.3.1 Transfection

Transfections were carried out with the goal of comparing transgene expression between wild type (wt) and codon optimized (co) *RPGR*^{ORF15}. All transfections were performed on HEK293T cells seeded in 6-well tissue culture plates (Sarstedt Inc., Newton NC, USA) at a density of 2-6 x10^5 cells per well (Graham FL 1977, Characteristics of a human cell line transformed by, Journal of general virology).

Plating of cells

When cells in a T75 flask reached 70 % confluency and were ready for passaging, cells were detached from the flask bottom and a single-cell suspension created as described above. Before splitting, 1 ml of the cell suspension was extracted and 4 ml of DMEM cell media (Sigma-Aldrich) added. This mixture was spun down at 1000 rpm for 5 min at 20 °C, the supernatant aspirated and cells re-suspended in 5 ml of DMEM cell media. A Neubauer counting chamber (VWR, Leicestershire, UK) was used to determine the number of cells/ml of suspension: twenty µl of cell suspension was pipetted onto the counting chamber surface and covered with a microslip. Cells were counted in all four squares of the counting chamber at 10 x magnification and averaged to ascertain the number of cells per ml of cell suspension and as well as the total number of cells in suspension. Based on this calculation, an appropriate amount of DMEM cell media was added to ensure the goal average of 2-6 x10^5 cells in each well. Each well was filled with 2 ml of cell suspension. Cells were incubated for 24 – 48 h until the cell confluency in each well reached 50-70 %.

Plasmids

Both plasmid constructs were flanked by AAV2 inverted terminal repeat (ITR) sequences. The initial ITR was followed by a CAG promotor, a hybrid between the early cytomegalovirus enhancer and the chicken beta-actin promotor. The CAG promotor is commonly used to promote high levels of recombinant protein

expression in mammalian cell lines [160]. This abundant expression levels also hold true for several retinal cell lines, including photoreceptors [161]. The Kozak consensus sequence 5'-(GCC)GCCRCCATGG- 3', with R being a purine, adenine or guanine, plays an important role in the initiation of translation in eukaryotes by improving the efficiency of ribosomal binding [162] and was therefore added to the immediately upstream of the plasmid start codon: 5'-GCCACC-3'. After the *RPGR*^{ORF15} transgene (either wild type or codon optimized), the Polyadenylation signal pA from the bovine growth hormone was followed by the second AAV2 ITR. For abbreviation purposes, the two plasmids will be referred to as p.CAG.wtRPGR and p.CAG.coRPGR.

The plasmids containing co and wtRPGRORF15 were designed and kindly provided by Dr Dominik Fischer. The codon optimisation process was undertaken with help of the OptimumGeneTM algorithm (GenScript, Piscataway, USA), which looked at several parameters to increase the likelihood of a stable replication and efficient protein translation: the use of major codons was increased resulting in an increase in the CAI of over 10 % (from 0.73 to 0.87). Cryptic splicing sites, premature poly-A sites, chi sites and RNA instability motifs were all sought to be minimized. GC content, CpG islands and repeat sequences and restriction sight that could potentially interfere with cloning were minimized as well.

Codon optimisation: The complete cds was subjected to the OptimumGeneTM algorithm (GenScript, Piscataway, USA) to optimize a variety of parameters that are critical to the efficiency of gene expression, including codon usage bias, GC content, CpG dinucleotides content, mRNA secondary structure, cryptic splicing sites, premature poly-A sites, internal chi sites and ribosomal binding sites, negative CpG islands, RNA instability motif (ARE), repeat sequences (direct repeat, reverse repeat, and Dyad repeat) and restriction sites that may interfere with cloning [135].

Positive control

The positive transfection control was given by a FIN-RK-GFP-WPRE plasmid (Addgene plasmid # 44358, gift from Susan Semple-Rowland) [163]. Human Rhodopsin Kinase (RK) Promotor is a photoreceptor specific promotor and HEK293T cell expression of green fluorescent protein marker was used to asses for success of transfection.

Negative control

As a negative control, AAV-EF1a-doublefloxed-chR2EYFP-WPRE-HGHpA plasmid DNA (Addgene plasmid #20298, gift from the Karl Deisseroth) was used. Double-floxing improves upon the traditional two-part scheme for spatio-temporal control of transgene expression, in which a cre-recombinase with a cell-specific promotor cuts at two loxP sites, which flank a stop codon. Ideally, excision of the stop codon and induction of transgene expression will therefore be restricted to specific tissues, However, the stop codon may insufficiently hinder the repression of transgene expression. To tackle this problem of transcriptional leakage, Sohal *et al.* modified the procedure so that the transgene, in this case the fusion gene eYFP-ChR2, is initially truly inactivated by inversion [164]. EYFP-ChR2 is therefore flanked by not one but two incompatible loxP sites (hence double-floxed) and transgene expression is subsequently achieved through serial recombination. First, the transgene is reoriented and then one of each two lox sites is excised by Cre recombinase, leaving a pair of incompatible loxP sites that are unresponsive to Cre recombinase. Since the plasmid would not come in contact with Cre recombinase this double-lox system ensures transgene expression will not occur and could therefore serve as a negative control. In addition to the EF1-alpha promotor, the woodchuck hepatitis virus post-transcriptional regulatory element (WPRE) was also contained in the plasmid, as well a human growth hormone polyadenylation signal (hGH polyA). The eYFP-ChR2 gene starts in an inverted, inactive orientation [165].

Transfection

Genomic DNA extraction with the NanoDrop 1000 Spectrophotometer (ThermoFisher Scientific), was used to determine the concentration of plasmid DNA per µl of solution. In preparation for transfection, 3.0 µl *Trans*IT®-LT1 Transfection Reagent (Mirus Bio, Wyomming, USA) was added to 250 µl of reduced serum Opti-MEM (ThermoFisher Scientific) substituted with 2 mM L-glutamine (Sigma-Aldrich Company Ltd., Dorset, UK) and placed in six sterile 1.5 ml Eppendorf microtubes 3810X (Sigma-Aldrich). The mixture was vortexed and left to incubate at room-temperature for 5 minutes. After the appropriate amount of plasmid DNA had been added to achieve a concentration of 1.0 µg of plasmid DNA per well, the mixture was incubated at room temperature for 30 minutes, and subsequently pipetted onto the wells dropwise. To ensure optimal, even distribution of the *Trans*IT®-LT1:DNA complexes, the six well plate was gently rocked back and forth.

Harvesting of transfected HEK293T cells

After 24 - 48 hours, when a strong GFP expression in the positive control indicated successful transfection, media was removed, and wells were gently washed with 1 ml PBS to remove any accumulated debris. Cells were then detached from the well surface by adding 1 ml PBS and pipetting up and down vigorously. The cell suspension was placed in 1.5 ml Eppendorf microtubes 3810X (Sigma-Aldrich) and spun down at 4 °C for 10 minutes at 1000 rpm. The supernatant was then discarded, and the cells re-suspended in 500 µl of PBS. This step was repeated, and the media completely removed. The cell pellet was stored at -80 °C or lysed directly.

Lysis of HEK293T cells

One cOmplete mini EDTA-free protease inhibitor cocktail tablet (ThermoFisher Scientific) was dissolved in 10 ml Radio-Immunoprecipitation Assay (RIPA; ThermoFisher Scientific) and incubated on ice for 30 min before use. Then, 150 µl of RIPA with dissolved protease inhibitor was pipetted onto the harvested cell pellet. The cell pellet was re-suspended and mechanically disrupted with

polypropylene pellet pestels a motor-driven grinder (both Sigma-Aldrich). After cell fragments were spun down at 14,000 rpm and 4 °C for 30 min, the protein-rich supernatant was harvested, aliquoted into 50 µl portions and stored at -20 °C.

Lysis of mouse and macaque retina

The dissected, whole retina was added to 100 µl RIPA with protease inhibitor pellet. After the retina was mechanically homogenized, the mixture was spun slowly at 4 °C for 20 min in a cold room. Then it was spun down in a centrifuge (Hettich Zentrifugen, Tuttlingen, Germany) at 14 000 rpm at 4 °C for 20 minutes. The protein-rich supernatant was collected, aliquoted in 20 µl portions and stored at -20 °C.

2.2.3.2 Transduction

Transduction agents

All viruses used for transduction were kindly provided by Dr. Dominik Fischer. The plasmids used in transfection as described above were modified for virus production in an effort to limit the expression of RPGR exclusively to photoreceptors. The cytomegalovirus early enhancer and chicken beta-actin, rabbit beta-globin hybrid (CAG) promoter, which favours ubiquitous tissue expression, was replaced a photoreceptor-specific rhodopsin kinase (RK) promotor: rAAV2/8.RK.coRPGR and rAAV2/8.RK.wtRPGR. In an effort to compare transduction efficiency of an altered capsid rAAV2/8.Y733F.RK.coRPGR and rAAV2/8.Y733F.RK.wtRPGR were also created. Similar to transfection AAV2/8. EF1a-doublefloxed-chR2EYFP-WPRE-HGHpA served as a negative control. A positive control was provided by rAAV2/8.RK.eGFP. Virus purification was performed by iodixanol gradient ultracentrifugation [166]. To remove any residual iodixinol, isolated rAAV virus was further purified and and concentrated by buffer exchange (Amicon Ultra-15; Millipore) [167]. Viral genome particle concentration as well as capsid

concentration was determined by qPCR and ELISA, respectively, and a ratio of empty to full capsids established [78].

Transduction

Despite being cells of murine origin, 661W cells were chosen for transduction due to their cone-like properties. To determine transduction efficacy of coRPGR compared with wtRPGR viral vectors as well as transduction efficacy between different viral capsids, six-well plates were seeded with 4 x 10^5 cells 661W cells per well. When cells reached a confluency of approximately 70 %, virus was diluted 1:10 and the appropriate amount added to 2 ml DMEM cell culture media to achieve a multiplicity of infection (MOI) of 10,000 vg per cell. When the positive control showed GFP expression as determined under a light microscope at 4- and 10-times magnification, the immunocytochemistry (ICC) of cells in a monolayer was performed.

2.2.3.3 Transgene detection

2.2.3.3.1 BCA Assay

The protein concentration of each aliquot was quantified using the Pierce™ bicinchoninic acid (BCA) Protein Assay Kit (ThermoFisher Scientific). The microplate procedure was used to calorimetrically quantify the amount of total protein: Reagents A and B (both Sigma-Aldrich) were mixed in a ratio of 50:1 to create a working reagent. This reagent and Albumin Standard (BSA; 2 mg/ml) were combined to create a series of nine diluted albumin standards with concentrations ranging from 25 – 2000 µg/ml, as well as a negative control void of BSA. Samples of the unknown protein aliquots were mixed with RIPA buffer to obtain a 1:10 dilution. Twenty µl of the diluted unknown protein samples was pipetted into a white 96-well microplate (ThermoFischer Scientific), and 160 µl of working reagent was added to create a 1:8 dilution. The dilution series for the known protein was added to the microplate in the same fashion. The same was done with the dilution series of known protein. A technical replicate was added for each protein well. After being placed on a shaker for 30 s, the microplate was

incubated at 37 °C for 30 minutes. Afterward, the absorbance at 562 nm was measured on a Biochrom EZ Read 400 Microplate reader with the Galapagos software (Biochrom, Cambridge, UK) and exported to an excel file. The average of the absorbance values between the technical replicate and the primary wells were taken for both known and unknown protein. The absorbance values of the dilution series coupled with the known protein concentrations provided a linear regression formula by which the protein concentration of the unknown protein was calculated. Care was taken to adjust the calculated value to the 1:10 dilution made previously.

2.2.3.3.2 SDS-PAGE

SDS-PAGE with HEK293T cells

An equal amount of protein was denatured with 2 x Laemmli buffer (Sigma-Aldrich) for 30 minutes at room temperature. Running buffer for SDS-PAGE was prepared from reverse osmosis H20 and Tris/Glycin/SDS in 10:1 parts. Ten µg total protein was loaded in each well of a Criterion™ TGX™ sodium dodecyl sulfate polyacrylamide Precast Midi Protein Gel (BioRad, Hertforshire, UK) for electrophoresis at 100 V for 1.5 h (SDS-PAGE). BLUeye prestained protein ladder (GeneDireX, UK) was added on either side of the gel to ensure a reference for protein size in kDa.

SDS Page with mouse retinal lysate

When using proteins derived from mouse retina, Laemmli buffer in 5 x concentrate (Jena-Biosciences, Jena, Germany) was used in order to allow for a higher protein concentration to be loaded into the wells. Up to 100 µg of protein was loaded in wells of 7.5 % Criterion^{TM} TGX^{TM} Precast sodium dodecyl sulfate polyacrylamide gel (Bio-Rad), 12 + 2 wells, 45 µl and ran at 100 V for 1.5 h as described above.

2.2.3.3.3. Western Blot

Western Blot with TurboBlot™

Gels containers were cracked open and gels carefully placed onto polyvinylidene difluoride (PVDF) membranes with 0.2 µm pore size (Trans-Blot® Turbo™ Midi PVDF, Bio-Rad). Proteins were blotted using the Trans-Blot® Turbo™ Transfer Starter System (Bio-Rad) according to the manufacturer's instructions. The midi setting, corresponding to the eponymous Midi PVDF Membrane, was used to blot the proteins with the 7-minute protocol, used for mixed molecular weight proteins, at 25 V. With guidance of the protein ladder, PVDF membranes were horizontally cut with disposable scalpels (Swann-Morton, Sheffield, UK) at the appropriate kD mark depending on size of the target protein and loading control. These sections were then stained independently with corresponding primary and/or secondary antibodies. For a complete list of antibodies used, see section 2.1.7 in Materials.

Enhanced Chemiluminescent (ECL) Western Blot

Snap i.d.™ protein detection system

The PVDF membranes were positioned in the wells of the SNAP i.d.™ protein detection system (Millipore Ltd., Feltham, UK). To prevent unspecific protein binding, a blocking solution consisting of 0.01M PBS with 0.1 % Triton-X (PBS-T) combined with 3 % bovine serum albumin (BSA) was mixed and added to the membranes. A vacuum was applied to draw the PBS-T through the PVDF membrane, after which 3 ml of primary antibody solution was administered and incubated at room temperature for 10 minutes followed by vacuum application. The membranes were subsequently washed three times with PBS-T, followed by the incubation with horseradish peroxidase (HRP)-linked secondary antibody for 10 minutes at room temperature. As previously described for the primary antibody, PVDF membranes were washed three times before being removed from the wells and incubated with Clarity™ Western ECL Substrate (Luminol Enhancer and Peroxide Solution, Biorad) for 3 minutes to activate chemiluminescence before imaging. Membrane sections were carefully re-assembled in between Azpack™ Sarogold™ PRO Cling Wrap Film (ThermoFisher Scientific) to prevent the membrane from drying out during the

imaging process. Images were taken with Odyssey® FC imaging system (LiCor Biosciences) on the chemiluminescent channel and exported in an uncompressed tagged image file format (.TIFF) with 1200 dpi resolution.

Optimization of ECL Western Blot

For optimization of the western blotting, a more time-intensive blocking and antibody staining procedure was used. SDS-page and blotting were undertaken as described above. The PVDF membrane was blocked with 3 % BSA in PBS-T (0.1 %) for 45 minutes on an R100 Rotatest shaker (Luckham, Appliance number 3573). The membranes were then placed in a tube with the side containing protein facing inward. Primary antibody was applied, tubes placed on an analogue roller mixer SRT6 (Cole-Parmer, Staffordshire, UK) and incubated for 1.5 hours. Afterwards, the membranes were washed with TBS 1 x and 0.1 % Tween three times for 7 minutes each and then incubated with the secondary antibody for 30 minutes, followed by an additional wash. The activation of chemical luminescence was achieved as described above.

Immunofluorescent Western Blot

In preparation for the blotting procedure, Trans-Blot® Turbo™ Transfer buffer 5 x (BioRad) was mixed with reverse osmosis water (H_2O) and ethanol absolute (AnalaR Normapur, VWR Chemicals) to create a 1 x concentration. The Midi-size 0.45 µm low fluorescence (LF) PVDF membrane Trans-Blot® Turbo™ (BioRad) was immersed in 100 % Methanol (VWR Chemicals Prolab, Leicestershire, UK) for approximately 1 minute until translucent, then transferred to a tray containing 30 ml of 1 x transfer buffer for 3 minutes. Two Trans-Blot® Turbo™ Midi-size transfer stacks (BioRad) were then submerged on a gel tray containing 50 ml of transfer buffer for 2-3 minutes. The blotting procedure was followed as described above. Depending on which antibody was used, quantitative western blot imaging was performed at 700- and 800-wave length channels for 2 minutes each.

2.2.3.3.4 EZ Blue™ Staining

To compare banding pattern between cells transfected with coRPGR and wtRPGR, an SDS-Page was performed and stained with EZBlue™ Gel Staining Reagent (Sigma-Aldrich). Ten µg of protein was added to each well of a 7.5 % Criterion™ TGX™ Precast sodium dodecyl sulfate polyacrylamide gel (Bio-Rad) and electrophoresed at 100 V for 1.5 h (SDS-PAGE). The gel was submerged in double distilled water and washed on a R100 Rotatest shaker (Luckham) for 5 minutes. This process was repeated twice before the SDS gel was submerged in EZBlue™ Gel staining reagent and incubated on the R100 Rotatest shaker for 1 hour. Afterwards, the gel was washed for 1 hour while changing water periodically. The gel was imaged with Odyssey® FC imaging system (LiCor, Nebraska, USA) at the 700-wave length channel and the file saved at 300 dpi in an uncompressed (.TIFF) file format.

2.2.3.3.5 Immunocytochemistry

The cell culture media was pipetted off each well and carefully washed with 1 ml PBS. After cells were fixed with 250 µl at 4 % for 10 minutes at room temperature they were blocked with 10 % Donkey serum in 0.2 % Triton X for 30 minutes. A wash with 1 ml PBS followed. The primary antibody solution was applied and incubated at room temperature for one hour on a R100 rotatest shaker. After the wash step was repeated twice, the Hoechst 33342 dye and secondary antibody were applied and incubated for one hour. Care was taken to protect the samples from light exposure using aluminum foil. After an additional wash step, the cells were mounted in ProLong® Gold (Life Technologies) for fluorescence microscopy.

2.2.3.3.6 Immunohistochemistry

Eyes were embedded in Tissue-Tek® O.C.T. compound (VWR Chemicals Prolab) without fixation or dehydration and stored at -80 °C for future use. The Leica CM3050 S Research Cryostat (Leica Microsystems CMS, Wetzlar, Germany) was cooled to -18 °C and the embedded tissue was cryostated into 12 µm sections and placed on a poly-L-lysine coated glass slide (Gerhard Menzel

GmbH, Thermo Fisher Scientific). The sections were dried for 5 minutes at room temperature to ensure melting of the OCT compound and to therefore prevent tissue mobilization during handling. While drying, an edge was drawn around each section with an ImmEdge^{TM} Hydrophobic Barrier PAP Pen (Vector Laboratories, Burlingame, USA) to ensure fluid containment within its margins. After sections were washed with 0.01 PBS for 1 minute, they were blocked with 10 % donkey serum in PBS containing 2 % bovine serum albumin for 10 minutes. Incubation with the primary antibody diluted in 2 % bovine serum albumin for 45 minutes followed. Sections underwent a second wash in PBS for 1 minute before they were once again incubated with fluorochrome- conjugated secondary antibodies and Hoechst 33342 dye at 1:5000 for 30 minutes. After sections were subjected to / underwent a final wash, they were mounted in ProLong Gold (Life Technologies) for fluorescence microscopy, which was performed in quick succession to the antibody staining.

A confocal scanning microscope LSM 710 (Zeiss, Aalen, Germany) was used to visualize retinal tissue sections. By harnessing the fluorescence of Hoechst 33342 dye, GFP/Alexa-488, Alexa-555, Alexa-568, and Alexa-635 with a 350-nm UV, 488-nm argon, and the 543-nm HeNe laser, XY sections through the retinal tissue were achieved and these images were processed using ImageJ software. Recreation of the XY images were achieved by merging stacks in ImageJ.

2.2.4 Statistical Analysis

2.2.4.1 ImageStudioLite

ImageStudioLite (LiCor, Nebraska, USA) was used to quantitatively analyse Western Blots. Rectangles were drawn around each band to measure the signal intensity in arbitrary units [AU]. The background was determined using samples of all sides of the rectangle and was then automatically subtracted from the signal intensity of each band. In order to account for potential differences in total protein load between wells, absolute values of the target protein were normalized by dividing them through the signal intensity of their respective loading control. Signal intensities were exported into an excel spreadsheet and SPSS for further analysis and graph creation. The signal intensity was presented in a boxplot with

a 95 % confidence interval (CI). Using the wtRPGR^{ORF15} expression as a reference point, fold increase of coRPGR^{ORF15} was depicted using bar graphs with standard deviation (SD). Kolmogorov-Smirnoff test was performed to test for normal distribution within sample groups. For normally distributed data sets, Student's t-test was applied, for non-normally distributed data sets the non-parametric Mann-Whitney test was used. Statistical significance was defined as $\alpha = 0.05$ for all tests.

2.2.4.2 ImageJ

Recreation of the XY confocal images was achieved with ImageJ [168] and FIJI [169]. Appropriate channels were selected and merged using the stack merging function. Brightness and contrast levels subsequently adjusted for optimal exposure.

Transduction efficacy was quantified by converting the colour picture to an RGB stack and measuring the grey area of the green autofluorescence channel. As described above, normalcy was tested using Kolmogorov-Smirnoff test and Student's test was used as a parametric test.

2.3 Results

2.3.1 Western Blots

2.3.1.1. HEK293T cell lysate

2.3.1.1.1 Optimisation of Western Blot protocol

Codon optimisation of RPGR leads to stable and increased gene expression in HEK293T cells

Several variables were adjusted to optimise the western blot protocol used to detect RPGR^{ORF15} protein: the amount of transfected HEK293T cell lysate loaded into a well, the antibody used to detect RPGR^{ORF15}, duration of primary and secondary antibody incubation, and the loading control used. In Fig. 1, HEK293T cell lysate previously transfected with *coRPGR^{ORF15}* and *wtRPGR^{ORF15}* plasmids was loaded into wells in three different concentrations (20 µg, 10 µg and 5 µg)

and stained with antibodies designed to target different epitopes of the human RPGR^{ORF15}. Two antibodies were specific for RPGR^{ORF15}'s N-terminal, while two other antibodies bound to epitopes in RPGR^{ORF15}'s C-terminal sequence (for more detailed information on epitope binding refer to Table 2.1.7 and 2.1.8 in the methods section). In the initial western blot series (Fig. 2.1 A) which compared three of the four antibodies, only anti-C-RPGR$^{512-531}$ was able to elicit a strong signal for all RPGR^{ORF15} protein concentrations as well as for both *coRPGR^{ORF15}* and *wtRPGR^{ORF15}* transcripts (Fig. 2.1 A).

In a head-to-head comparison of the remaining anti-N-RPGR antibody with the anti-C-RPGR$^{512-531}$ antibody, anti-C-RPGR$^{512-531}$ showed by far the strongest, clearest and most reliable protein binding signal throughout all concentrations of RPGR protein. While the anti-N-RPGR antibody bound fairly well to RPGR from the *coRPGR^{ORF15}* plasmid, the RPGR from *wtRPGR^{ORF15}* plasmid was barely able to elicit a signal.

This can be explained by future results that show *coRPGR^{ORF15}* transfected HEK293T cells elicit an average of two-fold higher RPGR expression than their HEK293T cell counterparts transfected with *wtRPGR^{ORF15}*. In an effort to determine the ideal protein loading dose for a western blot lane, 20 µg, 10 µg and 5 µg of HEK293T cell lysate transfected with both *coRPGR^{ORF15}* and *wtRPGR^{ORF15}* plasmids was loaded into three wells throughout both experiments. When looking at the RPGR staining with anti-C-RPGR$^{512-531}$ in Fig. 2.1 A, one can see that 5 µg of protein was difficult to detected, whereas 20 µg elicited a signal that produced unspecific binding. Ten µg of protein was able to show a strong antibody response within the dynamic range of signal detection and was therefore determined to be the optimal protein loading concentration. Since the loading control in form of actin consistently showed unspecific protein binding (Fig. 2.1 A and 2.1 B), the loading control was switched to the equally ubiquitously expressed anti-GAPDH (Fig. 2.2 B), which displayed more specific antibody binding.

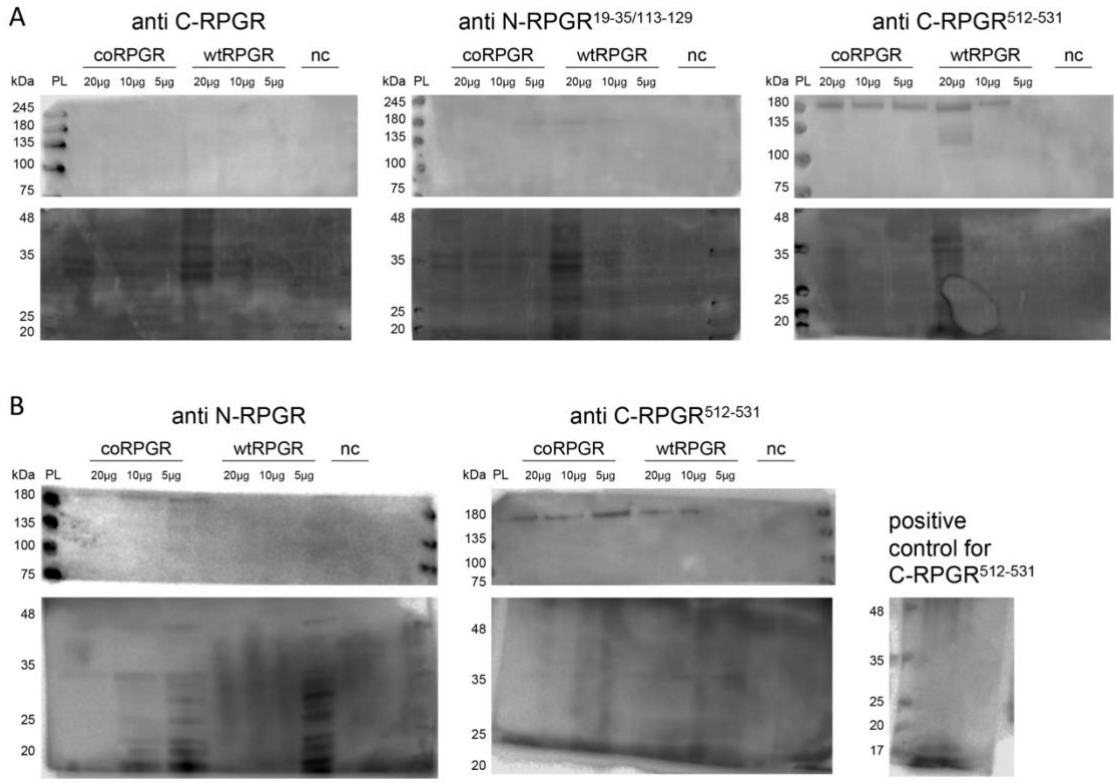

Fig. 2.1: **Optimization of western blot protocol for RPGR protein detection**. In an effort to optimize RPGR protein detection, four different antibodies designed to bind at opposite terminals and four different amino acid sequences were compared in two different experiments (A, B). Throughout both experiments, three different protein concentrations (20µg, 10µg, 5µg) were loaded into wells. The C-RPGR$^{512-531}$ antibody proved superior for protein detection, whereas a loading dose of 10µg proved ideal for a strong signal that was neither oversaturated nor too faint. A positive control was used to confirm the correct detection of C-RPGR$^{512-531}$ (B). In Figure 2C, the improvements of using a longer antibody incubation time as well as a GAPDH instead of actin loading control can be seen.
CoRPGR = codon optimised Retinitis Pigmentosa GTPase regulating gene; wtRPGR = wild type Retinitis Pigmentosa GTPase Regulator, nc = negative control, PL = protein ladder, kDa = kilo Dalton

To further optimise antibody binding, a different protocol, which required significantly longer incubation times for both primary and secondary antibody, was used (Fig. 2.2 B). This method displayed far superior results and was therefore used in all future western blot experiments.

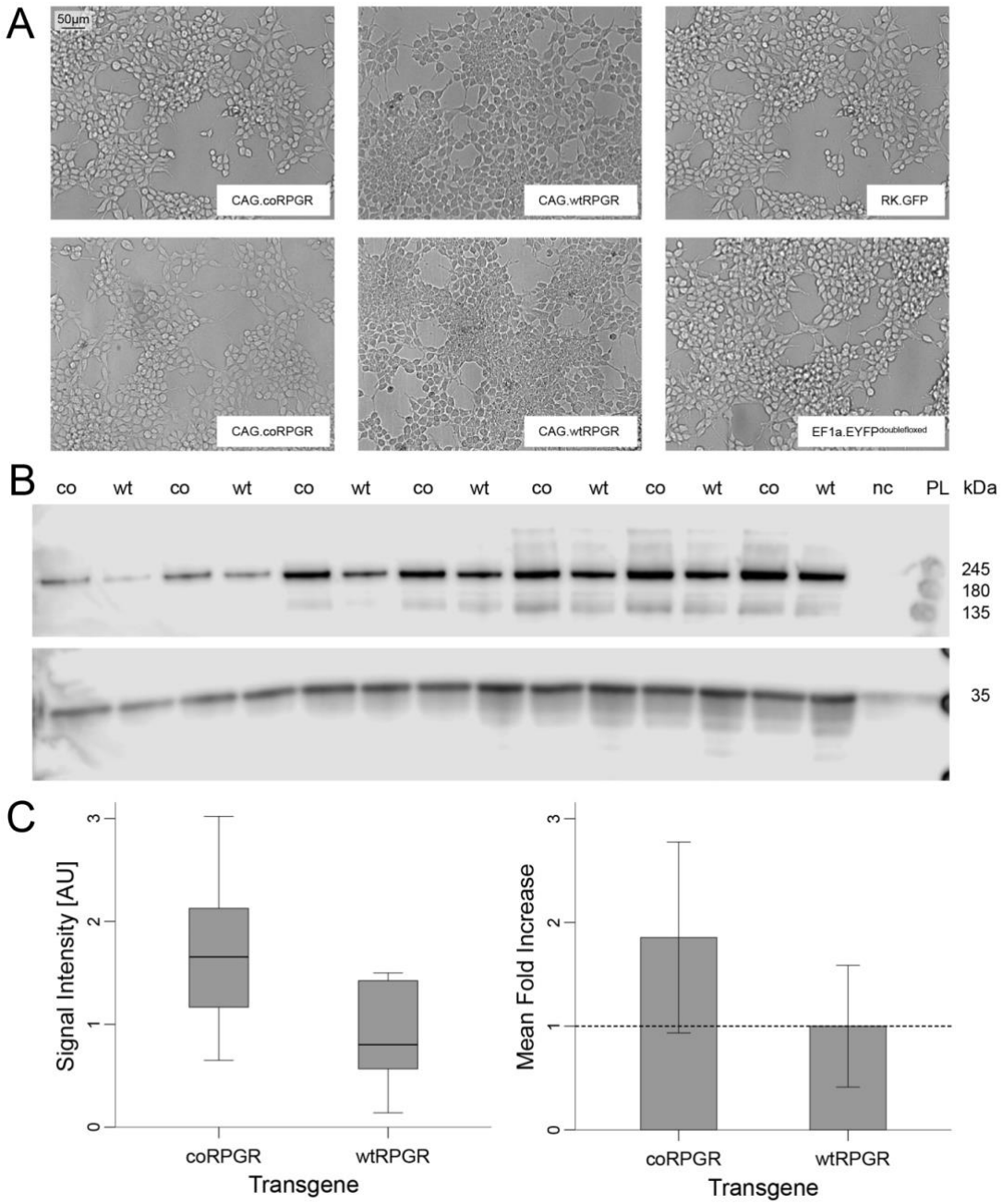

Fig. 2.2: **Depiction of sequential workflow for quantifying and comparing *coRPGR* with *wtRPGR* transgene expression**. Two wells of HEK293T cells, each paired with a technical replicate well, were transfected with *coRPGR* and *wtRPGR*-containing plasmids. The positive control was provided by a GFP plasmid, while a doublefloxed *EYFP* plasmid provided a negative control (A). Next, HEK293T cell lysate expressing *coRPGR* and *wtRPGR* transgene was loaded into wells and run on an SDS-page gel. Six technical replicates measured reproducibility of the results (B). Both the absolute signal intensity of coRPGR and wtRPGR protein bands, as well as the relative fold increase of coRPGR protein compared to wtRPGR protein were quantified (C). HEK203T cell lysate transfected with coRPGR showed a significantly stronger signal intensity ($p = 0.03$) as well as a significant mean fold increase over wtRPGR ($p = 0.03$).
CoRPGR = codon optimised Retinitis Pigmentosa GTPase regulating gene; wtRPGR = wild type Retinitis Pigmentosa GTPase Regulator; co = codon optimised, wt = wild type, nc = negative control, PL = protein ladder, kDa = kilo Dalton

2.3.1.1.2 Western Blots with HEK293T cells utilizing technical and biological replicates

Using this optimised method for western blotting, a significant difference in RPGR protein production between the HEK293T cells transfected with a plasmid-containing *coRPGR*^{ORF15} transgene and the cells transfected with a plasmid-containing *wtRPGR*^{ORF15} could be shown in two consecutive experiments.

In preparation for each experiment, wells seeded with HEK293T cells were transfected with plasmids containing *coRPGR*^{ORF15} transgene as well as *wtRPGR*^{ORF15} transgene. As a positive control to signal successful transfection, a *GFP*-containing plasmid was used. An EYFP doublefloxed plasmid was used as a negative transfection control. In the first western blot, which made use of HEK293T cell lysate from a single transfection, *co* and *wtRPGR*^{ORF15}-transfected cell lysate was loaded and run on an SDS-page gel and the bands of interest, as well as a ubiquitously expressed loading control in the form of GAPDH, were made visible via western blot. Six additional technical control bands were run alongside each original coRPGR^{ORF15} and wtRPGR^{ORF15} lane to investigate whether results were truly reproducible. Lysate of *coRPGR*^{ORF15}-transfected cells showed a clear difference in both band signal intensity and fold increase compared with *wtRPGR*^{ORF15}-transfected cell lysate. In signal intensity, coRPGR^{ORF15} lane showed a mean of 1.70 arbitrary units (AU; 95 % CI: 0.92 – 2.48), whereas wtRPGR^{ORF15} showed a mean of 0.92 AU (95 % CI = 0.42 – 1.42). Since the band intensity showed a normal distribution in all western blots utilising HEK293T cell lysate, parametric tests were used to determine significance. Using Student's *t*-test (unpaired, one-tailed) for normally distributed values, the difference between the two means was shown to be significant ($p = 0.03$). To present this band signal increase in a more meaningful manner, the fold increase achieved by transfecting cells with *coRPGR*^{ORF15}-containing plasmid was calculated using the *wtRPGR*^{ORF15}-transfected cell signal as a baseline reference. Cells transfected with *coRPGR*^{ORF15} showed a 1.86-fold increase (±SD 0.92) over *wtRPGR*^{ORF15} baseline mean of 1.00 (±SD 0.59; $p = 0.03$). While a *GFP*-containing plasmid was used as a positive control in transfection of HEK293T cells (Fig. 2.2 A) the corresponding lysate provided a negative control

throughout the blotting process. A positive control for RPGR^{ORF15} protein detection in western blots was not available.

To see whether the higher transgene expression levels results held true for biological as well as technical replicates, transfections done at three different time points (February 2015, January 2015 and June 2014) and spanning a total of nine months, were used to compare *RPGR^{ORF15}* transgene expression between HEK293T cells transfected with *coRPGR^{ORF15}* vs *wtRPGR^{ORF15}*-containing plasmid. Each biological replicate was coupled with a technical replicate (Fig. 2.3 A). Results from the previous experiment not simply replicated but amplified in this setting: mean signal intensity for coRPGR was 2.04 AU (95 % CI: 1.15 – 2.92, n = 6), compared with for 0.92 AU wtRPGR^{ORF15} (95 % CI: 0.62 – 1.28; n = 6, $p < 0.007$). The fold increase of *coRPGR^{ORF15}* transgene expression was 2.15 (±SD 0.89) compared to the baseline of 1 provided by the *wtRPGR^{ORF15}* transgene expression (±SD 0.31; $p < 0.007$; Fig. 2.3 B).

When pooling the data of the previous western blot experiments (n = 13 for both wt and coRPGR bands), coRPGR^{ORF15} bands showed a mean signal intensity of 1.86 AU (95 % CI 1.36 – 2.36) and wtRPGR^{ORF15} a mean signal intensity of 0.93 AU (95 % CI: 0.67 – 1.19), with coRPGR^{ORF15} providing a significantly higher signal intensity ($p = 0.00074$; Fig. 2.4 A). This pattern was augmented when looking at fold increase, where coRPGR^{ORF15} provided a fold increase of 2.0 (±SD 0.88) in comparison to wtRPGR (±SD 0.59). This fold increase proved highly significant ($p = 0.00071$; Fig. 2.4 B).

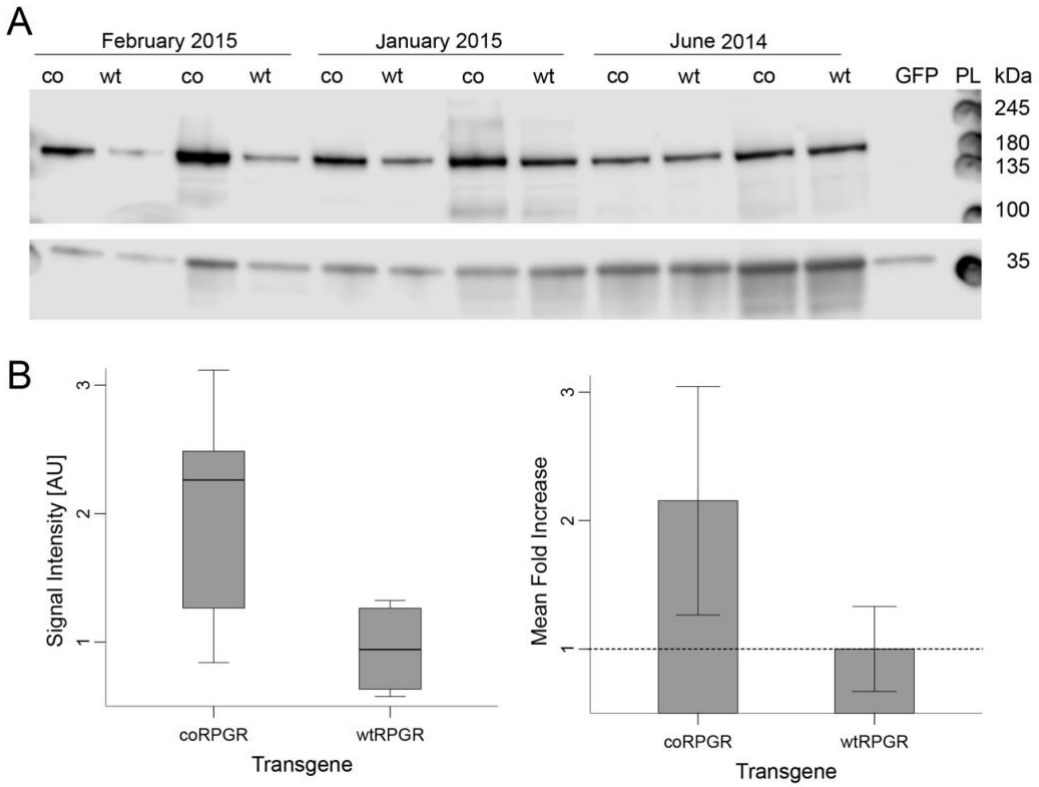

Fig. 2.3: **Western Blot utilizing technical and biologic replicates confirms superiority of *coRPGR*-containing plasmid in generating transgene expression.** Two biologic replicates in form of transfections done at different time points were added to the western blot in addition to technical replicates (A). Band signal quantification not only confirmed the superiority of *coRPGR*-containing plasmid in its ability to produce a higher transgene expression but produced amplified results (B). Signal intensity was significantly higher than that of HEK293T cells transduced with *wtRPGR* plasmid ($p < 0.007$). Compared to *wtRPGR* plasmid, *coRPGR* plasmid elicited a 2.15 increase in transgene expression compared ($p < 0.007$).
CoRPGR = codon optimised Retinitis Pigmentosa GTPase regulating gene; wtRPGR = wild type Retinitis Pigmentosa GTPase Regulator; co = codon optimised, wt = wild type, nc = negative control, PL = protein ladder, kDa = kilo Dalton

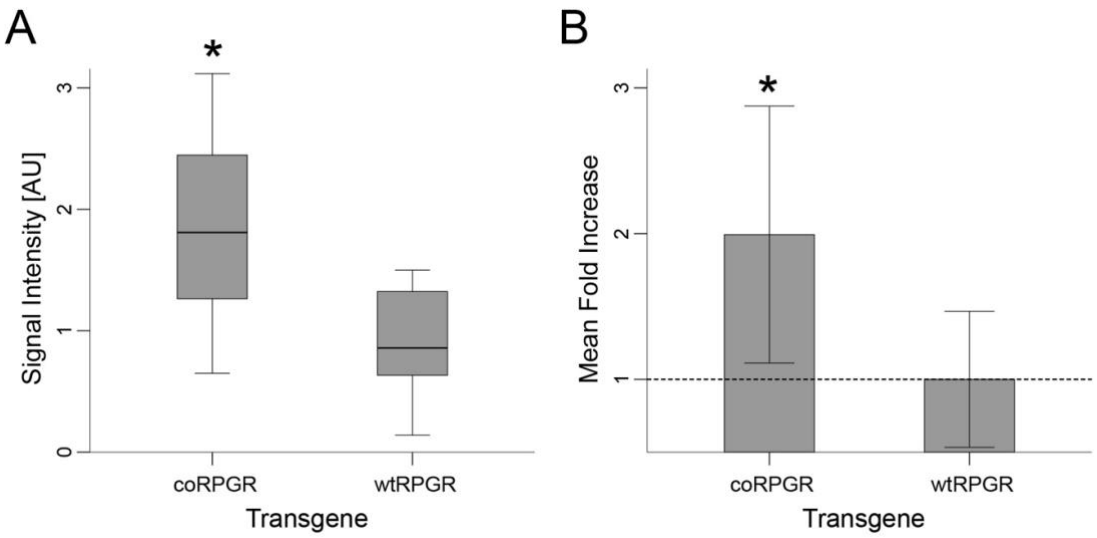

Fig. 2.4: **Combined analysis of western blot data amplifies superiority of *coRPGR*-containing plasmid to induce *RPGR* transgene expression**. Data of the previous two western blots was combined to conclusively show a significantly higher protein expression in HEK293T cells transfected with HEK293T cells. In a head to head comparison, mean signal intensity of coRPGR protein bands (n = 13) was 1.86 AU (95% CI 1.36 – 2.36) which proved significantly higher than the signal intensity of wtRPGR (0.93 AU; $p < 0.001$; A). When considering the more meaningful fold increase, coRPGR-containing transgene succeeded in doubling the transgene expression compared with wtRPGR-containing plasmid ($p < 0.001$; B).
CoRPGR = codon optimised Retinitis Pigmentosa GTPase regulating gene; wtRPGR = wild type Retinitis Pigmentosa GTPase Regulator; co = codon optimised, wt = wild type, nc = negative control, PL = protein ladder, kDa = kilo Dalton, * = $p < 0.001$

When looking at the western blots of HEK293T cells, it is important to note that the coRPGR^{ORF15} bands did not display any additional bands that were not present in the wtRPGR^{ORF15} lane, indicating the absence of erroneously spliced RPGR variants.

2.3.1.2 Western Blots using mouse retinal lysates

Therapeutic, subretinal AAV2/8.coRPGR vector injection leads to consistent, albeit variable, transgene expression in three mouse lines

As part of a pre-clinical safety and efficacy trial led by Fischer *et al.,* three mouse strains were subretinally injected with a single dose of 1.5×10^9 vg of AAV2/8.coRPGR^{ORF15} diluted in BSS with 0.001 % PF-68. The *C57BL6/J* mouse strain was used as a wild type, while the naturally occurring *C57BL6/J$^{Rd9/Boc}$* mouse strain and the generated knockout *Rpgr$^{-/y}$* mouse strain were used as models to mimic *RPGR*-XLRP in humans. When injecting the *C57BL6/J* and the

Rpgr$^{-/y}$ mouse strain, the contralateral eye was left untreated and used as an internal control, whereas the contralateral eye in *C57BL6/J*$^{Rd9/Boc}$ mice was sham-injected and acted as an internal control as well. The sham injection consisted of 1.5 x 10^9 vg of a AAV2/8.control vector, as detailed in the methods section.

Since retinal cells are non-dividing and subretinal injections only target a small part of the entire retina, RPGR^{ORF15} transgene expression was not nearly as prominent in this cell population compared with the HEK293T cell lysate. Therefore, RPGR^{ORF15} signal provided more challenging to pick up on western blot. More total protein – at times up to ten times the amount of protein used for HEK293T cell lysate - had to be loaded to adequately pick up an RPGR^{ORF15} signal. This corresponded to a stronger noise signal of other protein bands. Since these extraneous bands were present in both untreated and treated eyes, as well as the positive and negative controls, whereas an RPGR^{ORF15} could only be picked up in the treated eyes, it was inferred to be true background noise, rather than abnormally spliced or truncated RPGR variants.

Unlike western blot bands utilizing HEK293T cell lysate, RPGR^{ORF15} bands derived from mouse retinal lysate were non-normally distributed so the non-parametric Mann Whitney test was used to determine significance. The non-normal distribution was determined by the Kolmogorov Smirnoff test ($p > 0.05$).

2.3.1.2.1 *C57BL6/J* mice

Western blots display consistent and clear - albeit variable - RPGR^{ORF15} bands in the retinal lysate of nine C57BL6/J wild-type mice treated with AAV2/8.coRPGR^{ORF15} vector.

A total of nine pairs of *C57BL6/J* mice eyes, of which one eye had been treated with AAV2/8.*coRPGR* and the untreated contralateral eye served as an internal control, were assessed for RPGR^{ORF15} detection via western blot. All therapeutically injected eyes showed a variable but consistent *RPGR* transgene expression (Fig. 2.5 A). The positive control in form of HEK293T cells transfected with *coRPGR^{ORF15}* confirmed the validity of RPGR signal picked up in the mouse retina. The contralateral untreated eyes of each respective treated eye showed an absence of RPGR^{ORF15} signal, which was confirmed by negative control in

form of *GFP*-transfected HEK293T cells. In an effort to further quantify the RPGR^{ORF15} band signals, the signal intensity was measured and presented graphically. Whereas the untreated mice eyes (n = 9) had a mean signal intensity of 0.0001 AU (95 % CI 0.0001 – 0.0002), the mean RPGR signal intensity of therapeutically injected mice (n = 9) was 100-fold increased (0.0114 AU; 95 % CI: 0.019 – 0.021; p < 0.0001; Fig. 2.5 B). The wide confidence interval surrounding the RPGR^{ORF15} expression signal in treated eyes is a reflection of the wide variation in signal intensity gained from the treated lysed retina.

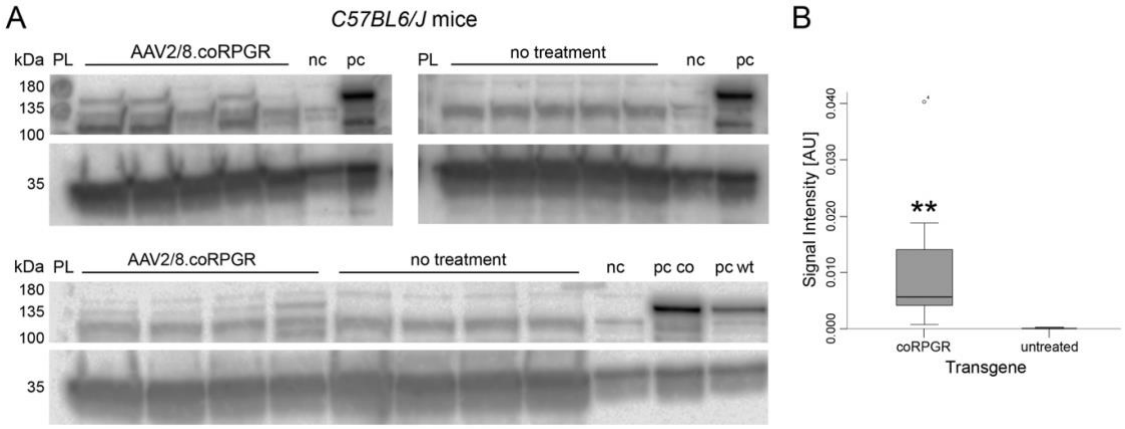

Fig. 2.5: **Consistent, albeit variable, *RPGR* transgene expression in retinal lysate of C57BL6/J mice treated with AAV2/8.*coRPGR*.** Retinal lysate of nine C57BL6/J wild-type mice treated with AAV2/8.coRPGR vector, showed consistent and clear - although variable - levels of RPGR protein on western blot. A positive control was provided by HEK293T cell lysate previously transfected with *coRPGR*-containing plasmid. The corresponding contralateral, uninjected eyes show no signs of *RPGR* transgene expression, as confirmed by the negative control, which consisted of *GFP* transfected HEK293T cells (A). These results were quantified by measuring the signal intensity of RPGR bands in arbitrary units (AU), which showed the RPGR signal being significantly more pronounced in treated mice, while the corresponding eyes showed virtually no signal (p < 0.0001; B).

It should be noted that while the *C57BL6/J* mice used as a wild type in this trial would express murine Rpgr^{ORF15}, the antibody used on Western Blotting was specific for human RPGR^{ORF15}, which meant that no protein cross contamination between endogenous and therapeutically administered protein could occur.

2.3.1.2.2 *RPGR$^{-/y}$* mice

Western blots display weak but consistent and clear RPGR^{ORF15} bands in the retinal lysate of four RPGR$^{-/y}$ mice treated with AAV2/8.coRPGR^{ORF15} vector.

Four eye pairs of *RPGR$^{-/y}$* mice, the murine homologue to XLRP in humans, which had received unilateral therapeutic injections, were analysed for RPGR^{ORF15} transgene protein expression on western blot (Fig. 2.6 A). Interestingly enough, while the mean signal was weaker than in the other two mouse lines (0.0045 [AU] compared with 0.0114 [AU] and 0.0457872 [AU], the level of protein expression was remarkably consistent in all four samples, a fact which is reflected in the small confidence interval surrounding the mean 0.0045 [AU] (95 % CI = 0.0018 – 0.0071; Fig. 2.6 B).

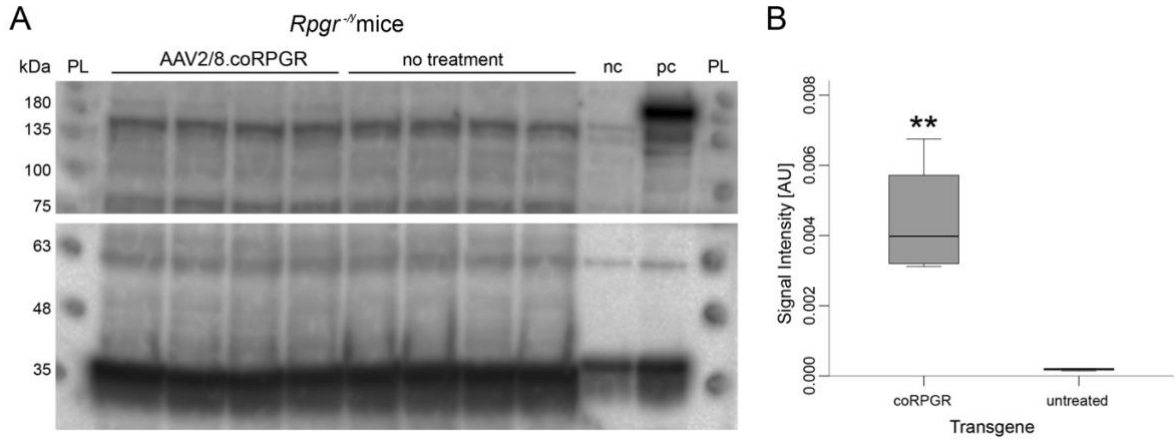

Fig. 2.6: **RPGR protein restored in RPGR$^{-/y}$ mice, the murine homologue to human *RPGR*-XLRP**. Transgene detection in RPGR$^{-/y}$ mice injected with AAV2/8.*coRPGR* showed a delicate but clear band, whereas no signal was picked up in the negative control group provided by the corresponding untreated mouse eyes (A). Compared to the untreated control eyes, therapeutically injected mouse eyes showed a significantly higher RPGR band intensity ($p < 0.0001$; B)

2.3.1.2.3 *C57BL/6J$^{Rd9/Boc}$* mice

Western blots of five mice mice treated with AAV2/8.coRPGR vector display the strongest mean signal intensity but with greatest variability.

In *C57BL/6J$^{Rd9/Boc}$* mice, the difference in signal intensities within the treated eye group (n = 5) was most apparent, a fact which is mirrored in the large confidence interval around the mean signal intensity of 0.0457872 AU (95 % CI = 0.0026 - 0.0942; Fig. 7 A and B).

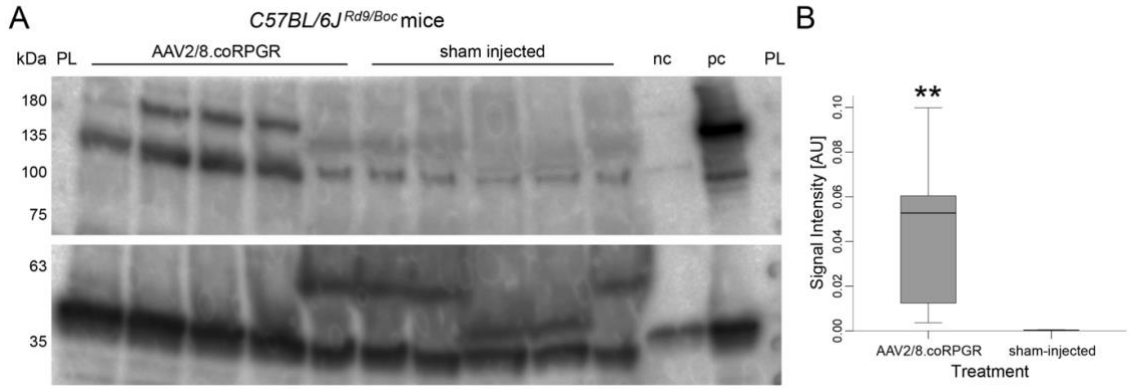

Fig. 2.7: **RPGR detection in the naturally occurring XLRP mouse model C57BL/6J$^{Rd9/Boc}$ indicates successful subretinal application of viral vector.** This western blot features the highest variability of RPGR signal. Whereas lanes two, three and four feature the strongest RPGR signal detected in any of the blots utilising mouse retinal lysate, RPGR signal in lane five is virtually undetectable (A). The mean signal intensity of treated mice eyes is remarkably strong 0.0457872 AU (95% CI = 0.0026 - 0.0942) and the highest of all mouse lines and the high variability within the treated group is reflected in the large confidence interval (95% CI = 0.0026 - 0.0942). Like the untreated control in the other mouse lines, the difference in signal intensity in therapeutically injected mice was significantly higher than in scam injected mice ($p < 0.0001$; B)

Within this group, we see by far some of the strongest RPGR^{ORF15} bands (lane two, three and four), making the mean *RPGR^{ORF15}* gene expression the highest of all mouse genotypes. Conversely, in lane five, *RPGR^{ORF15}* protein is virtually undetectable. Even though the protein load of each well is significantly less than in Fig. 6 (average of 61.2 µg of protein vs. 90 µg of protein) effects of protein overload (distortion of lanes, increased extraneous protein bands) can be seen in this gel. Just like in untreated eyes of the two other mouse lines, sham-injected eyes showed no sign of a RPGR^{ORF15} signal (0.002707 AU (95 % CI = 0.0006 – 0.0048). The difference between treated and untreated eyes was significant ($p < 0.0001$).

The immunofluorescent western blot (Fig. 2.8 A) further solidifies the trend displayed in preceding three chemiluminescent blots. In all three mouse lines, *RPGR^{ORF15}* expression is captured in the eyes of therapeutically injected mice, whereas the untreated or sham injected contralateral mouse eyes show no RPGR^{ORF15} signal, regardless of whether the eye was sham-injected or left untreated (Fig. 2.8 A). When the signal intensities of previous chemiluminescent western blots are displayed next to one other (Fig. 2.8 B), the results of the immunofluorescent western blot are mirrored in the graph. While *RPGR$^{-/y}$* has the

lowest mean signal intensity, it also has the most consistent protein expression as reflected in the smallest confidence interval, whereas *C57BL/6J*$^{Rd9/Boc}$ mice had the largest mean RPGR^{ORF15} expression, but the largest intraindividual variability within the treated eye group.

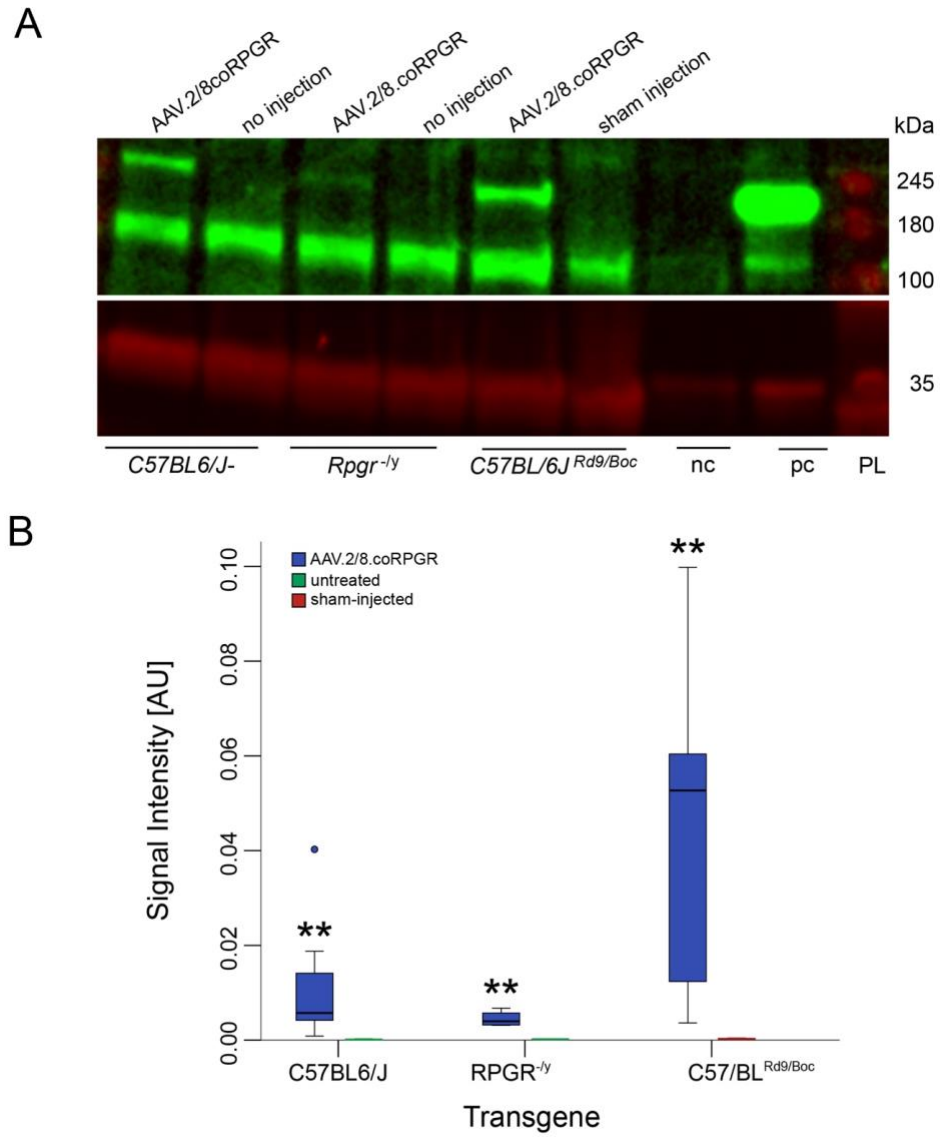

Fig. 2.8: **Immunofluorescent western blot detects RPGR protein expression in three mouse lines subretinally injected with AAV2/8.*coRPGR***. *RPGR* gene expression was found in treated eyes of all three mouse lines. RPGR signal was weakest in RPGR$^{-/y}$ mice, and strongest in C57BL/6J$^{Rd9/Boc}$ (8A). A summary of chemiluminescent western blot data mirrors the immunofluorescent blot. While RPGR$^{-/y}$ showed the least strong signal it also showed the most consistent RPGR expression (8B). An absence of RPGR signal is noted in all control eyes, regardless of whether they were treated were left untreated or sham injected with a control vector.

The immunofluorescent blot was successfully able to get rid of much of the extraneous noise present on the chemiluminescent western blots.

2.3.1.3 Rhesus macaque (*Macaca mullata*)

No endogenous levels of RPGR^{ORF15} protein could be picked up in the Rhesus macaque retina

In an effort to gage the endogenous level of RPGR^{ORF15} protein in mammals, retinas of healthy Macaques were lysed and suspected to the same western blot protocol that had been previously used. Surprisingly enough, both western blots done at separate time points failed to pick up any sign of endogenous RPGR^{ORF15} signal (Fig. 2.9 A and B).

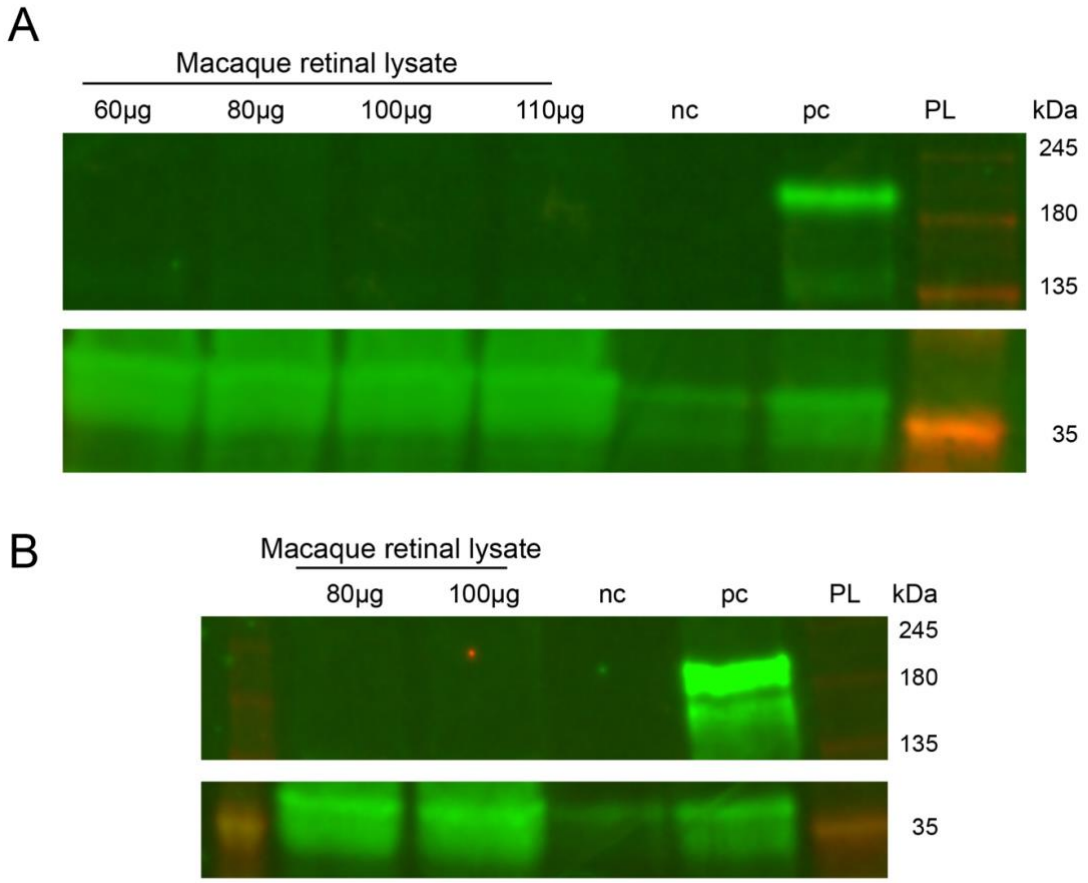

Fig. 2.9: **Two western blots of Macaque retinal lysate failed to detect endogenous RPGR^{ORF15} protein expression.** Two western blots to were unable to detect endogenous RPGR^{ORF15} protein expression in the retinal lysate of healthy Macaque retina. No RPGR^{ORF15} signal was able to be detected in either blot (A; B), whereas the positive control signale emitted a robust signal. This is most likely due to degradation of RPGR^{ORF15} by the fixation process and prolonged harvesting protocol.

2.3.1.4 EZ Blue staining of SDS-page gel

EZ Blue staining of SDS-page gel shows similar banding pattern in both coRPGR^{ORF15} and wtRPGR^{ORF15} lanes

In order to further investigate and compare the banding pattern of co and wtRPGR transfected HEK293T cells, the banding pattern was visualized by staining the SDS-page gel with EZ blue reagent (Fig. 2.10). When comparing the banding pattern of HEK293T cells transfected with *coRPGR*- and *wtRPGR*-containing plasmid, the banding pattern looked remarkably similar between the two. This further indicates the stable expression and absence of splice variants or truncated proteins in cells transfected with *coRPGR^{ORF15}*-containing plasmid.

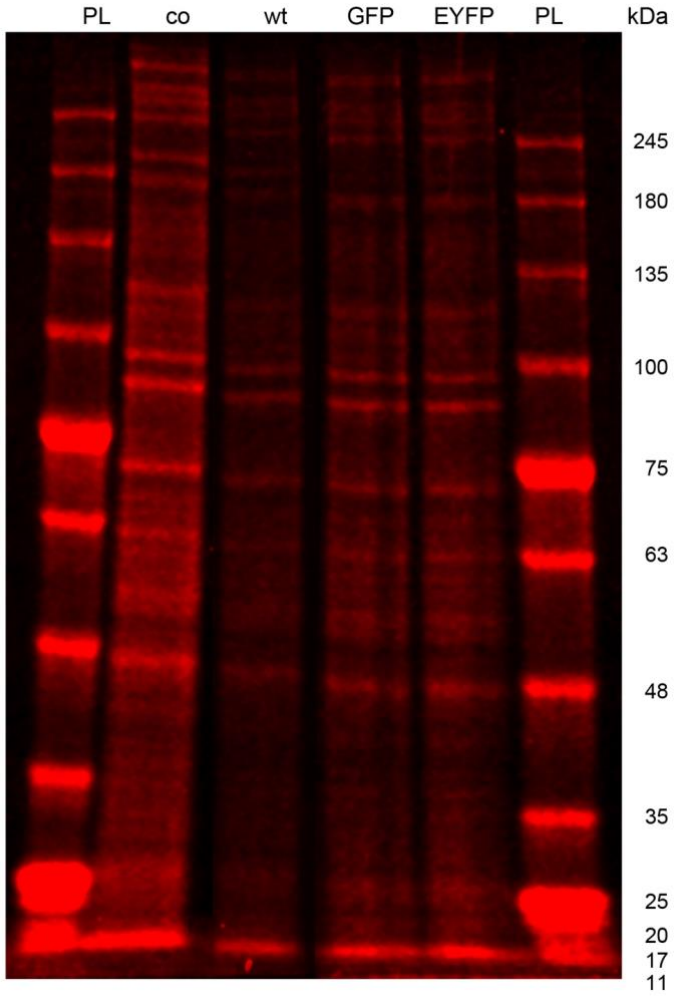

Fig. 2.10: **Similar banding pattern of HEK293T cell lysate transfected with *co* and *wtRPGR* indicates absence of splice variants or truncated of coRPGR**. EZ Blue staining of SDS page gel shows a highly similar banding pattern for both coRPGR and wtRPGR. The lack of extraneous bands in the lane with coRPGR transfected HEK293T cells indicates a lack of splice variants or truncated RPGR protein.

2.3.2 Immunocytochemistry

Single-mutant capsid results in a non-significant increase in increase in transduction efficacy of a cone-like cell line

In transducing the cone-like cell line 661W with mutant AAV2/8^{Y733F} and wild type AAV2/8 viral vectors containing *coRGPR^{ORF15}* and *wtRPGR^{ORF15}* transgene, the aim was to answer two questions:

Firstly, was the transduction using single-mutant AAV8^{Y733F} capsid more effective than transduction with wild-type AAV2/8 [100]? Secondly, was it possible to replicate the higher transgene expression of *coRPGR^{ORF15}* versus *wtRPGR^{ORF15}* that we saw in transfected HEK293T cells?

It was decided to use the cone-photoreceptor-like 661W cell line, which is derived from a murine retinal tumor, rather than HEK293T cells, a human embryonic kidney tumor cell line, in order to more closely align the cell culture experiments with the reality of therapeutic human photoreceptor transduction.

Single-mutant AAV8^{Y733F} capsid showed an increase in transduction of 661W cells when compared to the AAV2/8 wild type capsid, but this increase was non-significant ($p = 0.058$, Fig. 2.12 A). The transfection results showing increased transgene expression of coRPGR^{ORF15} in HEK203T cells could not be replicated, instead showing no significant difference in transgene expression between the two groups ($p = 0.31$, Fig. 2.12 B). The positive control was made up of 661W cells transfected with p.CAG.*coRPGR^{ORF15}* and was strongly positive, whereas the negative control, which consisted of a double-floxed EYFP plasmid, remained staunchly negative, underscoring the validity of the experiment (Fig. 2.11).

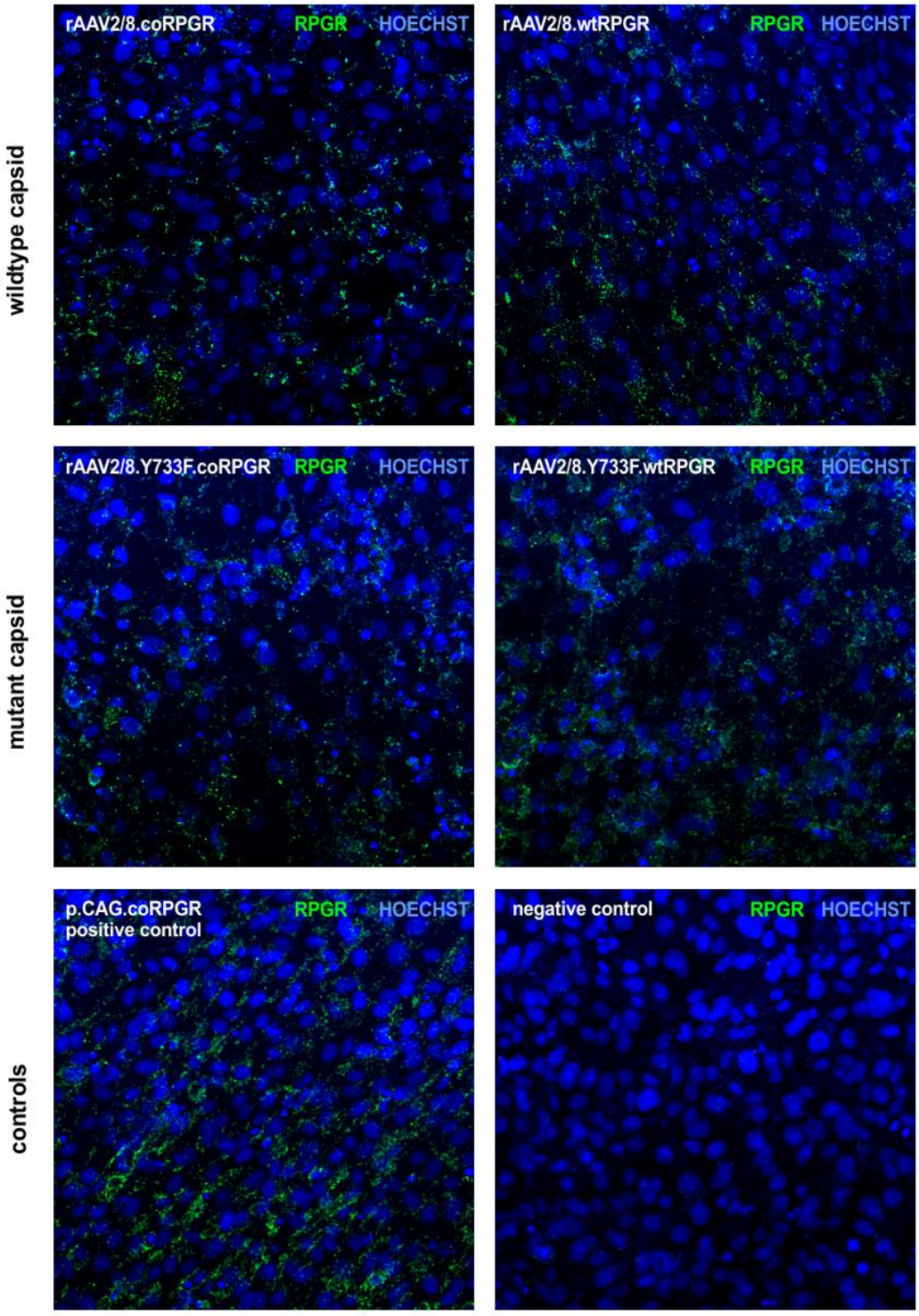

Fig. 2.11: **Comparison of transduction efficacy of two virus capsids and two transgenes in a cone-like 661W cell line.** Immunocytochemistry was used to compare transduction efficacy of single-mutant AAV8^{Y733F} capsid and wild-type AAV2/8 capsid. *CoRPGR*^{ORF15} and *wtRPGR*^{ORF15} transgenes were alternately packaged in each of the capsids with the goal of assessing transduction efficacy. The plasmid CAG.coRPGR, which had been successful in transfecting

HEK293T cells provided a positive control, while a negative control was provided by 661W cells transduced with a double-floxed EYFP plasmid.

2.3.3 Immunohistochemistry of sectioned mouse retina

Therapeutic RPGR^{ORF15} application results in gene expression and correct localisation in the connecting cilium of photoreceptors in a mouse line

Western Blot was able to show transgene expression in mouse eyes therapeutically injected with *coRPGR^{ORF15}*, but to correct photoreceptor function, the protein must not merely be expressed but also correctly localized. Immunohistochemistry (IHC) was performed on unfixed sections of mouse retina stained for the RPGR-interacting protein (RPGRIP) as well as RPGR^{ORF15}. RPGRIP is localized to the CC and it is RPGR^{ORF15}'s binding partner, making it the ideal marker to assess correct co-localisation of RPGR^{ORF15} to the connecting cilium. In all three mouse genotypes, the co-localization of RPGR^{ORF15} with RPGRIP can be visualized in the connecting cilium (Fig. 2.13). The disorganised ONL seen on the IHC slides stem from the fact that tissue remained unfixed before staining.

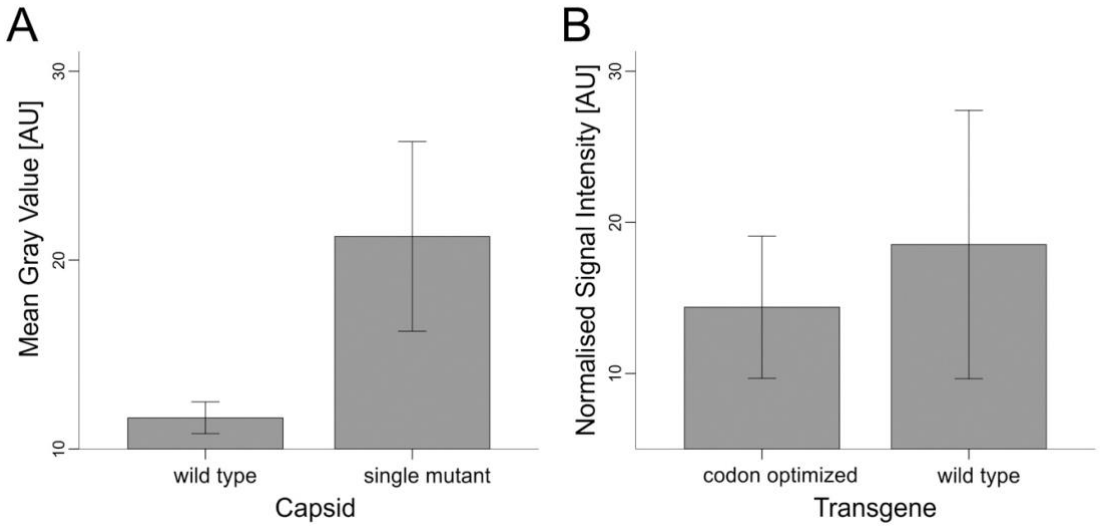

Fig. 2.12: **Statistical evaluation of transduction efficacy of two virus capsids and two transgenes in a cone-like 661W cell line.** AAV8^{Y733F} capsid showed a non-significant (p = 0.058), but increased transduction efficacy compared to wild type capsid (A). Transduction with codon-optimised RPGR did not yield a higher transduction efficacy than wild type RPGR transgene (p = 0.31; B)

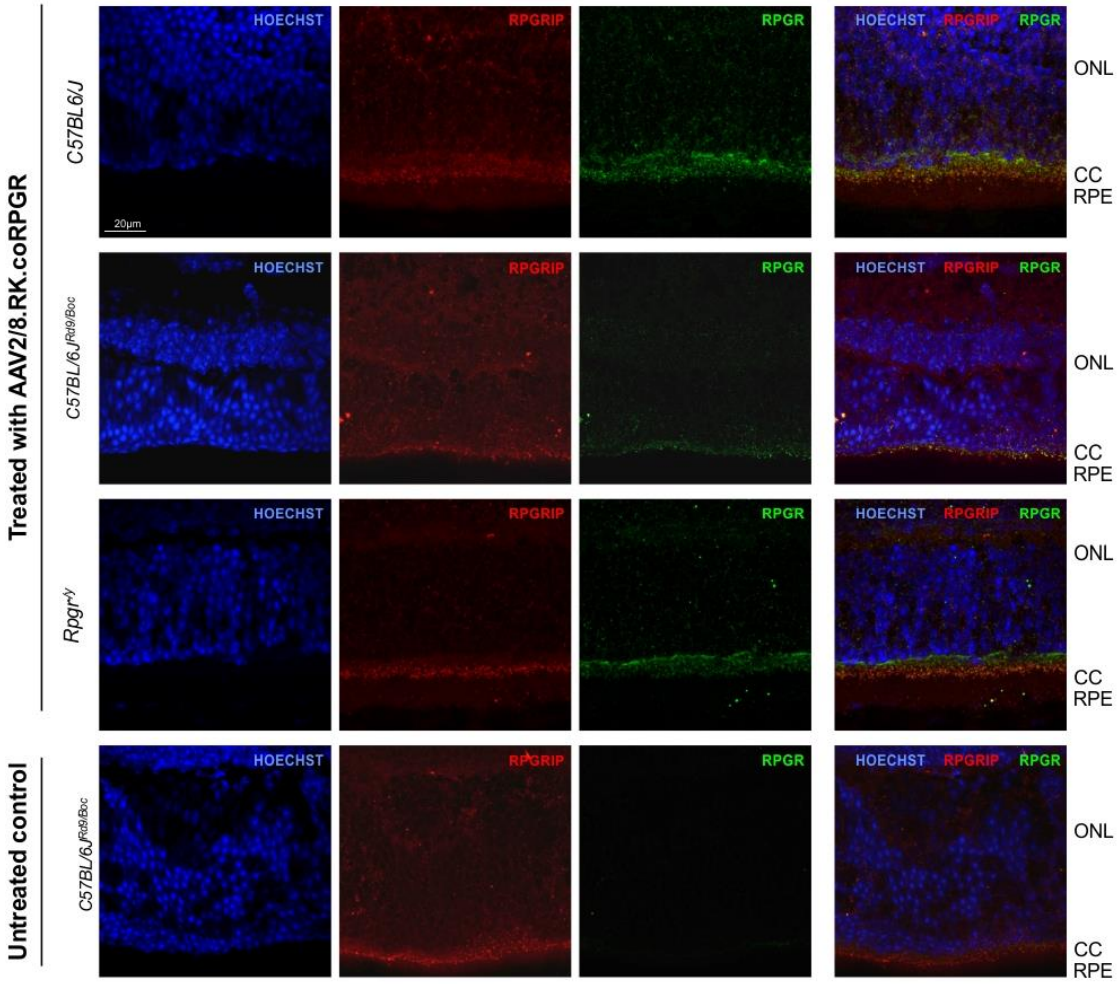

Fig. 2.13: **Retinas of therapeutically injected mouse eyes show transgene expression as well as physiological localization of RPGR to the connecting cilium.** Immunohistochemistry of mouse eyes treated with subretinal injections of AAV2/8.coRPGR showed strong transgene expression as well as correct/physiological protein localization to the connecting cilium (CC). To better distinguish between the three antibody stainings, results for each antibody staining is presented on its own before presenting the composite image. The lack of fixation, which provides crosslinks between proteins and prevents artefacts produced by the knife cutting through the tissue with shearing forces varying as a function of tissue density, results in slightly disorganised tissue architecture.

2.4 Discussion

2.4.1 *CoRPGR^{ORF15}* leads to more stable and efficient transgene expression with the potential of limiting off-target effects and immune response

CoRPGR^{ORF15} increases transcriptional efficacy

In the *codon optimized RPGR^{ORF15}* construct, the rate of low-abundance codons was reduced from 10 % to 1 % and the codon adaptation index (CAI) was therefore increased from 0.73 in the wild-type sequence to 0.87 in the codon optimized transgene sequence [78]. One of the goals of *RPGR^{ORF15}* codon optimization was to remove potential donor splice sites with the goal of reducing or even eliminating splice variants as well as to improve the stability of the *RPGR^{ORF15}* sequence during the vector production process [78]. Increasing CAI would also increase expressional efficacy based on the fact that an increased CAI means more frequent use of preferred codons with more abundant tRNA populations for efficient translational activity [148]. This phenomenon, termed codon usage bias, is surprisingly well preserved throughout evolution and exists in all pro- and eukaryotic genomes [148]. In this study, western blotting comparing RPGR^{ORF15} protein yield between *coRPGR^{ORF15}* and *wtRPGR^{ORF15}* transfected HEK293T cells was able to conclusively show a doubling of protein expression when using the codon optimized transgene sequence. Transcriptional efficacy can be seen as two sides of a coin: less transgene can achieve a higher protein yield. Less transgene burden decreases the potential for a local inflammatory response, but also for systemic spread – as well as the potential immune response that arises from it - and less risk for contiguous viral migration along the optic nerve. In a viral vector dose escalation trail, Vandenberghe *et al.* found traces of *GFP* transgene expression in the optic chiasm and lenticular nucleus at the highest dose [76]. This indicates that migration and contiguous spread of the viral vector within related tissues is dosage dependent. Thus, decreasing viral vector burden is one way to ensure transgene expression is limited to target tissues, limiting the potential for off targets effects, such as integration of the vector into the germ line or in other brain structures. Lower vector burden also

decreases the potential for an immune response, both acute and chronic, local and systemic. In the afore mentioned study, the highest dose intraocular injection lead to a formation of neutralizing antibodies targeting AAV capsids as well as the *GFP* transgene [76]. Independent studies of subretinal AAV injections in humans as well as other mammals are in line with this observation and report that high-dose AAV application undermines the idea of ocular immune privilege, causing an innate and adaptive immune response in the eye [66] [67]. If immune response is threshold dependent rather than linear to the dosage, ensuring a low viral vector load may become a vital component for gene therapy's success. Keeping an immune response at bay might also prove to be important for the long-term success of therapeutic transgene expression. In two independent, long-term gene therapy trials for *RPE65*-LCA gene therapy, a slow decline in visual function was reported after an initial boost was observed six months post subretinal injection [66, 140]. While the loss of therapeutic efficacy months after treatment could be due to a non-immune mediated mechanism, such as silencing of the episomal transgene, immune-mediated clearance must be considered as a potential cause of this long-term therapeutic decline. Translational efficacy also means a higher protein expression can be achieved from a defined amount of viral vector. This might result in a prolonged, sustained protein expression and could potentially cause a more sustained improvement of visual function. While this does not solve the problem of functional and structural photoreceptor loss over time, it does have the potential to allow for a longer time before the viral vector needs to be re-administered.

Codon optimisation has an additional benefit in that it allows an increases translational efficacy without the addition of viral, *cis*-acting regulatory elements such as WPRE that are often used to boost transcription for transgenes requiring a cell-specific promotor. This would free up space in the transgene cassette and decrease the exogenous and therefore potentially immunogenic substances being injected and - not least importantly – would make regulatory approval easier to obtain.

Indirect evidence of sequence fidelity and lack of splice variants in coRPGR^{ORF15} protein

In addition to a fold increase in transgene expression, the absence of additional bands in EZ Blue staining of SDS-page gel as well as western blot comparing wt and coRPGR^{ORF15} expression profiles, provided indirect evidence that *coRPGR^{ORF15}* transgene yielded true RPGR^{ORF15} protein without splice variants. Also, the SDS Page stained with EZ Blue showed an identical migration pattern for coRPGR^{ORF15} and wtRPGR^{ORF15}. Furthermore, the western blots of HEK293T cell lysate showed no extraneous bands in the coRPGR^{ORF15} lanes. The extraneous bands in mice retinal lysate were present in both wild type and codon optimized as well as positive and negative controls and were thus interpreted as being a result of protein overload producing unspecific antibody binding. In a liquid chromatography experiment sequencing of RPGR^{ORF15} protein Fischer *et al.* were able to sequence all but parts of the highly repetitive *ORF15* sequence and show an identical protein sequence to that transcribed from *wtRPGR^{ORF15}*. In particular, the C-terminal protein end of the protein was able to be sequenced, which ruled out premature termination of translation [78]. The increased stability and lower mutation rate of *coRPGR^{ORF15}* is vital once the necessity of a larger scale production arises in the light of clinical trials or commercialisation of *RPGR^{ORF15}* gene therapy. It could thus pass through a bottle neck that many gene therapies for *RPGR*-XLRP have struggled with in the past [138, 170]. Also, the increased translation efficacy of the *coRPGR^{ORF15}* construct would allow for a higher production yield and therefore lower production costs.

2.4.2 Detecting *coRPGR^{ORF15}* transgene expression and co-localization with RPGRIP in three different mice lines

As mentioned in the introduction, a drawback of ocular gene therapy is the inability to directly measure transgene expression. In clinical trials, downstream functional measures serve as a surrogate of successful transgene expression. Thus, the ability of a preclinical mouse trial to provide some information about the question of the scale of transgene expression is a major advantage. Transgene

expression levels were measured in two ways post-sacrifice of the animals: by western blot of retinal cell lysate and by IHC of unfixed, sectioned mouse tissue.

2.4.2.1 *CoRPGR^{ORF15}* transgene leads to consistent albeit variable expression in three different mice lines

The observation that RPGR^{ORF15} protein expression in retinal lysate of mice treated with AAV2/8.*coRPGR^{ORF15}* was not nearly as strong as the expression in transfected HEK293T cells was not surprising and can be explained in two ways: HEK293T cells divide prodigiously and can therefore selectively ramp up transgene production. In vivo retinal cells on the other hand are stable cells permanently fixed in G0 cell cycle phase and are thus incapable of dividing. To exacerbate this disadvantage, subretinal injections are only able target a very small part of the entire retina (an argument often used in favour of intravitreal injection), whereas transfection of HEK293T cells in vitro targets virtually every plated cell in a high and therefore beneficial plasmid to cell ratio. Due to these facts, RPGR^{ORF15} expression cannot be expected to be as prominent in a mouse retinal cell population compared with expression in HEK293T cell lysate. This relative weakness of the RPGR^{ORF15} signal leads to the technical challenge of RPGR^{ORF15} expression in mouse retinal cell lysate being much more difficult to detect on western blot. Consequently, more protein – at times up to ten times the amount of HEK203T cell lysate - had to be loaded to adequately detect an RPGR^{ORF15} signal. This as well as the much more diverse protein expression profile of retinal cells, corresponded to a stronger noise signal of other protein bands, even when using an RPGR^{ORF15} specific antibody. Since these extraneous bands were present in both untreated and treated eyes, as well as the positive and negative controls, whereas an RPGR could only be picked up in the treated eyes, these extraneous bands were inferred to be true background noise, rather than abnormally spliced versions of RPGR^{ORF15} protein.

Since the *invitro* transfection results convincingly showed a superiority of *coRPGR^{ORF15}* transgene compared to *wtRPGR^{ORF15}*, the preclinical mouse trail undertaken by Fischer *et al.* solely made use of an AAV2/8.*coRPGR^{ORF15}* viral vector for subretinal injection [78]. An RPGR^{ORF15} fold increase between

wtRPGR^{ORF15} and *coRPGR^{ORF15}* transgene could therefore not be assessed *in vivo*. The strength of RPGR^{ORF15} protein bands could be instead be visually assessed and compared to uninjected mouse. Protein bands were also quantified more objectively by measuring the signal strength in arbitrary units [AU]. By measuring RPGR^{ORF15}'s signal strength, several observations were made. While the *RPGR$^{-/y}$* mouse produced the least strong signal, its signal was by far the most consistent. *C57BL/6J$^{Rd9/Boc}$* mice produced the strongest signal on average but demonstrated the largest signal variability. Finally, the wild type *C57BL/6* mice fell somewhere in the middle, producing a comparably strong RPGR^{ORF15} signal on average with variable consistency. While interpreting these results, it is important to keep in mind the small cohort size (n ranges from 5 to 9 eye pairs), which are largely due to above mentioned technical challenges of producing an adequate blot, when drawing conclusions from the data presented.

Throughout all three mice lines, there was a reassuring lack of RPGR^{ORF15} signal in both untreated and sham-injected eyes. This signals two things: as mentioned above, it confirms that the RPGR^{ORF15} signal in the treatment group is a true RPGR^{ORF15} signal. Secondly, it hints at an absence of viral vector transmission into the systemic circulation, an observation that was also made in previous gene therapy trials [75]. This is extremely important when thinking about an unwanted systemic immune response or the danger that the vector might shed form the injection site and integrate into germline cells, which would be a non-compatible breach of ethics.

C57BL6/J mice

While the wide variety of signal intensity could conceivably be attributed to a number of factors (see discussion below), it could not be traced back to the quality of surgery in the pre-clinical trials. For example, the fourth lane of the bottom WB in Fig 5 A gives us one of the strongest protein expressions, the surgical notes show that the RPE was penetrated [78]. Along these same lines, surgery with a difficult AC tap and small iris prolapse produced the same results as a surgery with no complications (Fig. 5 A, lane 1 and lane 2 respectively). But it is important to point out that while minor differences in surgical quality were present, mice with

surgical quality below a defined threshold (< 7 points in a predetermined scoring system) determined by a point scoring system were eliminated from the trial as insufficient retinal transduction could not be ruled out in these animals [78]. One could argue that by doing so, surgical variability was reduced as a source of transgene expression variability.

RPGR$^{-/y}$ mice

While transgene expression was restored in all mouse lines, the *RPGR$^{-/y}$* mice provided the most consistent level of RPGR^{ORF15} expression. This could be seen as strengthening the argument that a null mutation is the best background for gene therapy due to the fact that there is no competition with endogenous RGPR^{ORF15} protein and therefore no potential of dominant negative effects of misfolded or truncated RPGR^{ORF15}. The only drawback in using null mutations would be the potential for a stronger immune response since the introduced protein would be a foreign one [76]. The codon optimised transgene is also a foreign one.

Although this would not explain the contrary strong signal intensity and wide variability in *C57BL/6J$^{Rd9/Boc}$* mice, effectively also a null mutation.

The relatively weak signal compared to the *C57BL6/J* signal might also be an indication of the challenges of rescuing a diseased retina rather than the healthy one. The retina of wild-type *C57BL6/J* mice is not hampered by degeneration, whereas the *RPGR$^{-/y}$* mice exhibit photoreceptors (PRs) marked by degeneration starting at 2.5 months of age and might not be able to uptake, transcribe and translate the vectors in as effectively and efficiently as healthy PRs would be. This hypothesis might also be used to argue for an earlier injection time point in humans, where photoreceptors exhibit the least amount of damage and thus can process the transgene most efficiently. Also, the goal of preventing rather than halting or reversing PR degeneration would be more likely to be achieved in this manner.

Considering that the two murine forms of *RPGR*-XLRP (*RPGR$^{-/y}$ and C57BL/6J$^{Rd9/Boc}$* mice) exhibits a mild phenotype compared to the human form

[113] [127] this points to the increased challenges posed by a more severely degenerated human retina when translating RPGR gene therapy into clinical *RPGR*-XLRP trials. On a more positive note, the effect on a functional level of rescuing a more severely damaged retina might be more pronounced and statistical significance of a treatment effect might be able to be shown with less patients needed in a human trial.

As with the wild-type *C57BL/6J* mice, differences in surgical quality did not influence protein expression. The eyes in 1st and 4th WB both had a small epiretinal bleed post-surgery, but there was no difference in protein expression (surgical notes of the preclinical trial notes from Fischer *et al.,* unpublished).

It could be argued that consistent RPGR^{ORF15} expression is more important than strong expression since the dose could be sequentially increased in a dose escalation trial to determine optimal dose effectiveness. This relatively weak signal in the *RPGR$^{-/y}$* mice makes the need for a *coRPGR^{ORF15}* transgene able to boost transcriptional efficacy even more apparent. And perhaps the weak expression in this knockout mouse line is an indicator that a higher dose is needed to promote sufficient RPGR^{ORF15} expression. This begs the question of what can be defined as an adequate RPGR^{ORF15} expression. The question is challenging to answer due to the lack of a mammalian positive control that could indicate normal RPGR^{ORF15} expression in humans. The lack of knowledge of which RPGR^{ORF15} dose would rescue photoreceptors as well as the recent indication from hemophilia trials that show clear relationship of dosing and treatment effect [71] are both strong reasons that a dose escalation should be part of a clinical trial.

C57BL/6J$^{Rd9/Boc}$ mice

When looking at the *C57BL/6J$^{Rd9/Boc}$* blot, the question of sources for variability in protein expression become most apparent due to a large confidence interval which can be witnessed visually (qualitatively) as well as quantitatively. If variability did not arise from surgical technique, it could have arisen from technical difficulties in lysing the mouse retina, although this also seems less than likely given that all mouse retinas were lysed using the same protocol. If the difference

in expression is indeed a true difference, the variability might be due to a heterogeneous course of disease in mice, a fact often observed in humans, even if the same mutation is present [69, 134]. Perhaps some mice exhibited faster degeneration than others, making the transgene uptake less efficient or the number of PR available for transgene uptake was decreased. Perhaps the degeneration also varied locally, and some mice were injected in an area that had been subjected to more severe degeneration than others.

When looking at the immunoblot (Fig. 8), which was done to compare all three mouse models side by side, we can see that the trend delineating itself in the individual blots holds true in the immunoblot as well. C57BL/6J$^{Rd9/Boc}$ mice have the highest and strongest RPGR^{ORF15} expression, whereas *RPGR*$^{-/y}$ mice have a weak RPGR protein band and the wild type C57BL/6J mouse falls squarely in the middle. This is an indication that the results from the western blots are not random due to technical difficulties in the experimental process but rather a true representation of transgene expression. The immunoblot also does a fair job of minimizing – though it does not eliminate – the prominent background noise present in the chemiluminescent western blots.

2.4.3 Western Blot of Macaque retinal lysate was not able to pick up endogenous RPGR expression

When looking at the strength of western blot bands in three different mouse models, it is difficult to put the RPGR^{ORF15} band strength and therefore the efficacy of RPGR expression into context, because there is no positive human or mammalian control that could serve as a benchmark for sufficient RPGR^{ORF15} expression in a healthy retina. While a strong RPGR^{ORF15} band would generally be viewed as more beneficial than a weak RPGR expression signal, perhaps high levels of RPGR^{ORF15} are actually an overexpression and would result in a toxic effect on the retina. Having a positive mammalian control would consequently also give valuable feedback if RPGR^{ORF15} was over or under dosed in the preclinical mouse trial. Hence, the western blots using lysed Macaque retina were

performed with the goal of determining a level of endogenous RPGR^{ORF15} expression.

Macaque monkeys are valuable primate models for preclinical gene therapy studies for two reasons: the axial length of their eye is similar in length to a human eye and their retina is equipped with a fovea, a structure which other mammals, such as mice or dogs, do not have. Therefore, assessment of endogenous RPGR^{ORF15} levels in the Macaque retina could provide valuable information of endogenous expression levels in their human counterpart. Unfortunately, in the two western blots of retinal lysate of healthy Macaque retinas utilizing a protein loading dose escalation, no endogenous RPGR^{ORF15} was able to be detected in either of the blots, regardless of protein amount loaded.

There are several possible hypotheses as to why endogenous Macaque RPGR^{ORF15} was not picked up in the setting of immunofluorescent western blots: perhaps endogenous expression of Macaque RPGR^{ORF15} is lower than anticipated, so that the fraction of RPGR^{ORF15} present in Macaque retinal lysate was not strong enough to produce a detectable RPGR^{ORF15} signal despite loading a large amount of protein (60 µg, 80 µg and 100 µg) in each well. If this were the case it would indicate overdosing in the treated mouse eyes and would raise questions about therapeutic protein overdosing and potential toxic effects, both direct and by triggering of the immune system. On the one hand this seems unlikely, simply due to the large amount of protein loaded. But when looking at the loading control, GAPDH, which is, contrary to RPGR^{ORF15}, a ubiquitously expressed protein, the signal is not as strong as to be expected when dealing with an ubiquitous protein. It could be therefore argued that this is an indicator that the far less highly expressed RPGR^{ORF15} is really not able to be picked up simply due to quantity.

Another explanation is that perhaps the antibody against human RPGR^{ORF15} was not able to adequately pick up Macaque RPGR^{ORF15}. The antibody used targets the less well-preserved C-terminal *ORF15* version of RPGR, which perhaps is not sequence homologous with the Macaque *RPGR^{ORF15}*.

Yet the most likely explanation is that the protocol by which the Macaque eyes were processed resulted in the RPGR^{ORF15} null signal. As mentioned in the

Methods section, all mice eyes were rapidly enucleated, placed in a lysis buffer and frozen within under 5 minutes. The tissue remained unfixed. On the other hand, the Macaque eyes were fixed and subjected to a much less rigorous harvesting timeframe than the mouse eyes. RPGR and the photoreceptor cilium are cellular organelles known to be sensitive to decay and epitope blocking due to tissue degeneration or fixation. Therefore, it is likely that RPGR^{ORF15} was degraded due to tissue fixation and a prolonged harvesting process.

2.4.3.1 Protein from coRPGR^{ORF15} transgene co-localises to RPGRIP in the connecting cilium of three mouse lines

As part of the machinery of the connecting cilium and its presumable function of shuttling protein from the inner to the outer part of the photoreceptor, RPGR^{ORF15}'s location is inextricably linked to its function. So, perhaps even more than in an enzyme disorder such as *RPE65*-LCA, it could be hypothesized that location is vital for rescuing function in *RPGR*-XLRP phenotype. All three mouse lines injected with *coRPGR^{ORF15}* show correct co-localization with RPGRIP in the CC, another essential indicator that *coRPGR^{ORF15}* transgene translates to a correct, fully-fledged and functioning RPGR^{ORF15} protein product.

Considering the functional importance successful co-localization of RPGR^{ORF15} to RPGRIP is another argument for using null mutations in RPGR gene therapy, as truncated constructs, at least those which are not subject to nonsense mediated decay, might very plausibly compete with therapeutic RPGR^{ORF15} for RPGRIP binding.

2.4.4 AAV2/8^{Y733F} fails to a induce a significant increase in transduction efficacy of 661W cells

While codon optimization creates an increased transduction efficacy by increasing protein translation, another possible way of maximizing transduction efficacy is to increase capsid affinity to target tissue by optimizing the amino acid structure of the capsid. An example of this is the use of AAV8 capsid, which targets photoreceptors with a much higher efficacy than the AAV2 capsid, which

is specific for RPE [76]. Beyond making the capsid more specific for a target cell line, the intracellular trafficking of the viral vector can be improved by modulating the capsid structure to improve the likelihood of the vector reaching the nucleus. As described previously, this has been shown to be achieved by replacing tyrosin (Y) amino acid residues with phenylalanine (F), which decreases the chance of the capsid being ubiquitinated and degraded before it can reach the nucleus [77]. In order to compare transduction efficacy of the wild type, AAV2/8 viral vector to single mutant AAV2/8^{Y733F} capsid, a murine, cone-like photoreceptor cell line was chosen to in an effort to replicate in-vivo of subretinal injection as closely as possible.

2.4.3.1 Non-significant increased transduction efficacy of single mutant Y733F capsid

On average, the single-mutant capsid does show an increased transduction efficacy, but not a significant one ($p = 0.058$). There are several points that should be considered when interpreting these results: it is described that the more capsid Y-F substitutions are made, the greater the transduction efficacity will be [100]. Ryals and Boye *et al.* show that the capsid mutants with three Y-F substitutions have a much greater transduction efficacy of 661W cells than the single capsid mutants. Therefore, it could be hypothesized that one Y-F substitution is simply not enough to generate a meaningful increase in transduction. Also, the placement of the Y-F substitution within the amino acid sequence of the capsid influences transduction efficacy as well. When looking at retinal ganglion cells, it was shown that a Y444F AAV2 single capsid mutant showed a 10-fold higher transduction efficacy than its Y730F counterpart [101]. Perhaps transduction efficacy could have been improved not only by using a vector with multiple Y to F substitutions, but also a single-mutant capsid with a substitution at a different amino acid sequence number.

In a more general argument, AAV8 is simply not the most efficient capsid for transducing 661W cells when compared to AAV1 or 2 [100] . And since 661W cells exhibit cone-like properties, but RP in the large majority of cases a rod-cone dystrophy, using cone-like cells to test transduction of a potential vector might not

be the ideal setting in which to mimic transduction for *RPGR*-XLRP treatment. Lastly, it is usually an uphill struggle to maintain a highly differentiated cellular phenotype such as that of a retinal photoreceptor in a cell culture. In fact, our 661W cells – while characterized as cone-like cells in the original publication – did not exhibit the morphology of cone photoreceptors in vitro at all. Specifically, there was no connecting cilium with a differentiated inner and outer photoreceptor segment. The lack of a connecting cilium may also indicate that the 661W cells have de-differentiated to an extent that a) RPGR expression is downregulated and no longer needed in the normal functioning of these cells and that b) opsin expression is downregulated and the RK promoter of the transgene expression cassette might not be sufficient to drive significant transgene expression in these cells.

2.4.3.2 No significance of transduction efficacy for *coRPGR^{ORF15}* over *wtRPGR^{ORF15}*

More troubling is the fact that *coRPGR* did not provide an increased transduction efficacy ($p = 0.31$), regardless of whether wild type or single-mutant Y733F capsids were used. These results stand in contrast to the HEK293T cell transfection results which showed a highly significant ($p < 0.001$) and reproducible increase in translation of coRPGR post transfection. The differences between the experiments were two-fold: the most important being that dissimilar cell lines were used (661W versus HEK293T). Secondly, the first experiment was a transfection, whereas the second was one was a transduction. Ryals *et al.* showed that compared to AAV1 and 2, AAV 8 does not lend itself well to 661W cell transduction [100]. Additionally, Vandenberghe *et al.* showed that AAV lends itself to more efficient rod rather than cone transduction [76].The HEK293T cell transfection results were reproducible with both technical and biologic replicates in different experiments at different time points. It could be argued that while whatever the cause of the non-significant difference in *co* and *wtRPGR* transgene expression in 661W cell line, the first set of experiments have shown us that the translation process is certainly more effective, so the bottleneck must not lie not in a less significant translation of protein but in the steps before the translation of

RPGR^{ORF15} protein, either in the transduction efficacy or intracellular processing. And even if transcriptional efficacy were not to be improved with codon optimization, which it was shown to do using HEK293T cells, the decreased splice variants and increased stability in the vector cloning process, make the use of codon optimization a vital component in the vector production and of success in the *RPGR* gene therapy.

2.4.3.3 Preparing for a clinical trial - which vector to use?

The end-goal of the project of optimizing gene therapy for *RPGR*-XLRP is to lay the ground work for translation of *RPGR*-XLRP gene therapy from bench to bedside. In this setting, utilizing a vector that has previously been used both in retinal and systemically administered gene therapy trials [171] [172], has thus already been approved by regulators and most importantly already been proven to be safe and effective in patients lowers the hurdles for the co*RPGR*^{ORF15}-XLRP clinical trial approval. This becomes even more relevant when the transgene being used is a novel one with a not naturally occurring cDNA sequence, as is the case in *coRPGR*^{ORF15} transgene. All these arguments were underscored by the fact that while single-mutant vector made a slightly increased vector efficacy, it was a non-significant increase. Based on this information, the decision to use the wild-type AAV2/8 viral vector in the preclinical murine trials for *RPGR*-XLRP gene therapy was made.

Based on these results, as well as further functional information of the pre-clinical mouse trail published in Fischer *et al.,* the pre-clinical approval of gene therapy utilizing *coRPGR*^{ORF15} transgene was given and a dose-escalation, Phase I/II trial (NCT03116113) is currently underway.

CHAPTER 3
RETROSPECTIVE ANALYSIS OF A 50-PATIENT *RPGR*-XLRP COHORT

3.1 Materials and Methods

The Materials and Methods utilised in the retrospective analysis of this patient cohort have previously been published by Bellingrath et al. [69].

3.1.1 Patient characteristics

A total of 50 patients, encompassing 100 eyes, were seen at two centres known for their expertise in the spectrum of IRDs: The University Eye Hospital in Tübingen, Germany, and the Oxford Eye Hospital in Oxford, United Kingdom. After an initial clinical diagnosis of RP was made and the mode of inheritance elucidated by the family history, patients were genetically sequenced to confirm *RPGR*^{ORF15} mutations as the underlying cause of RP. In cases of discordance between clinical and genetic diagnosis, the genetic diagnosis of mutation in the *RPGR*^{ORF15} gene had the final say in determining the diagnosis (e.g. in simplex cases). A total of 100 eyes were analysed in a retrospective, cross-sectional manner. The study was performed in accordance with the Declaration of Helsinki 1975 (1983 revision). After a thorough review of both electronic records at the Tübingen University Eye Hospital and paper charts at the Oxford Eye Hospital, the following data were extracted from the notes: visual acuity (VA), visual fields, electroretinography (ERG), foveal thickness as well as data from the genetic testing. Based on the pattern of PR degeneration, patients were divided into three groups: a rod-cone degeneration phenotype, the most common pattern; a cone-rod pattern of degeneration and finally, a subgroup of patients with a rod-cone phenotype featuring an affected fovea. ERG and perimetry were the tools used to divide patients into these phenotypic groups.
For all genetic testing, institutional review board approval was secured.

3.1.2 Molecular assessment

In addition to being approved by the local research as well as the respective ethical review boards, all patients were required to give written consent to genetic testing. Standard protocols were used to extract genomic DNA from peripheral

blood samples. Testing was performed at the following five institutions: Centre for Genetics and Transcriptomics (CeGaT GmbH) and the molecular genetics institutions of the Universities of Tübingen, Regensburg, München and Manchester. Methods to analyse patient DNA samples in the previously mentioned laboratories included single-strand conformation polymorphism analysis, high resolution melting curve analysis, Sanger sequencing and next-generation sequencing. Mutations found with these methods were confirmed using Sanger sequencing of PCR-amplified genomic DNA confirmed mutations [30, 110]. Between laboratories, extent and depth of analysis varied. It ranged from Sanger sequencing of solely the exon *ORF15* or the $RPGR^{ORF15}$ gene to sequencing of all coding exons of both $RPGR^{ORF15}$ as well as panel sequencing of retinal dystrophy genes [30, 110, 173]. Categorisation of mutations included dividing them according to the type of mutation: missense, nonsense, insertions, deletions, gross deletions, and splice defects. Mutations occurring within exons were further categorized by the location of the mutation, with mutations *ORF15* mutations being grouped as one and considered separate from mutations occurring in *exons 1-14*.

3.1.3 Clinical examinations

Visual acuity

Snellen charts were utilized to determine VA. If usage of pinhole improved VA, the pinhole-corrected VA was used in the data analysis. Where necessary for analysis, logMAR units were converted from original Snellen values using the formula: logMAR = -log (decimal acuity) [174].

Visual fields

An Octopus 900 or a Goldmann perimeter (Haag-Streit, Koeniz, Switzerland) were used to assess visual fields [175, 176]. The boundaries of the visual fields as well as the blind spot were determined using I4e and III4e targets. At the University Eye Hospital in Tübingen, the area (in degrees^2) was calculated using an in-built software measurement tool. Visual fields of the Oxford Eye Hospital patients were scanned from their paper records and Image J (version 2.0.0-rc-

30/1.49s, http://imagej.nih.gov/ij/; provided in the public domain by the National Institutes of Health, Bethesda, MD, USA) was used to scan and determine the area. To do so, the outlines of the I4e and III4e targets were traced and the encompassed area calculated in degrees^2 [24]. Even though it has already been shown that both methods result in comparable outcomes [177], compatibility of the two methods was tested by taking one patient's field and calculating the visual field area in degrees using both methods. Since there was only a 1 % difference between the two methodologies in the calculated area (degrees^2), the two methods were found to be compatible with one another in our study.

Foveal thickness

As has been described in previous studies [178], foveal thickness of patients in both locations was determined by scanning with spectral-domain optical coherence tomography (SD-OCT) using the Spectralis HRA+OCT platform (Heidelberg Engineering, Heidelberg, Germany) with its follow-up mode. The Caliper tool, which measures the thickness of the ONL combined with the inner and outer segment length (in other words, the PR layer), was used to determine retinal thickness in the central foveola. This thickness of the PR layer has been shown to be correlate with VA in patients with central serous chorioretinopathy [179]. In RP, there has also been some evidence shown for a relationship between foveal point thickness and VA [180]. In an effort to characterize central retinal architecture as well as measure the thickness of the remaining neuro-retinal tissue, several high-speed B-scans were recorded. With the goal of improving signal to noise ratio (SNR), n > 9 scans were averaged for each B-scan recording, the result of which was that SNR improved by the square root of n. Foveal thickness was measured in micrometers with the help of an in-built measurement tool provided by the Eye Explorer software (Heidelberg Engineering).

Elecroretinography

Patients ERG measurement was recorded with Espion (Diagnosys LLC, Lowell, MA, USA) in both centers. Measurements were taken in accordance to the

standards set by the International Society for Clinical Electrophysiology of Vision (ISCEV) 34. The following amplitudes were extracted from the ERG data: dark-adapted (DA) 0.01 cd*s, DA 3.0 cd*s, DA 10.0 cd*s, and light- adapted (LA) 3.0 cd*s single flash recordings and 30-Hz flicker.

3.1.4 Statistical Analysis

SPSS version 21 by IBM (SPSS, Inc., Chicago, IL, USA) was used for all statistical work. Statistical methods used were bivariate correlation, histograms, generalized linear mixed model analysis and Kaplan-Meyer survival curves.

Correlation between left and right eye

To determine whether or not data was normally distributed, a histogram was created using the first measurement data point of each patient was taken. Normal distribution lines were then superimposed upon this histogram. If the data values were non-normally distributed, Spearman's rho analysis was used to examine the correlation between right and left eye in the respective parameters. The first measurement of each patient was utilized for this analysis.

Progression rate analysis

There was a large variety in both the number of follow-up visits as well as the spacing in between these follow-up visits. In order to allow for this, generalized linear mixed model (GzLMM) analysis was used to determine the progression rate of disease in patients. Generally, analysis utilizing linear mixed models (LMM), is able to provide a roadmap for the longitudinal analysis of data with complex relationships and grouping of variables in more than one level. It also takes into account the relationships between a continuous, dependent variable and one or more predictor variables. Both repeated measurements and clustered data, all of which characterize the data in this study, as well as confounding interactions originating because the data stems from the same groups, can be investigated using LMMs. When comparing LMM to the more well-known repeated-measure analysis of variance, LMMs has the advantage of being able to be used for heterogenic data. This enables the inclusion of patients with

differing numbers of repeated measurements into the study. In addition to these advantages, the GzLMMs offer not only the ability to study nonlinear relationship functions, but also to investigate binary, ordinal and count variables. This offers a greater degree of depths and breadth of inquiry. In this analysis, the “subject” was represented by the patient number. The “repeated measures” variable was represented by the number of years from the first visit. By doing so, the model was able to account for difference in time between visits. The fixed effects encompassed both the intercept and the “patient age at visit” variable. The patient number was designated as a random effect. As a means of simplifying the model, only data from the left eye was used when symmetry was proven for a respective variable. Link functions was used as a tool to evaluate the linear model and gamma regression. The model with the best fit was selected depending on which had the lowest information criteria values (Akaike corrected and Bayesian). When both of the above-mentioned link functions gave similar or equal results, the more highly significant value (with a lower p-value) was given priority. The residual distribution was assessed for normality with the goal of making sure the model was fitting.

Vision Survival Analysis

Due to the previously mentioned highly variability in the spacing of patient visits, Kaplan-Meier survival curve analysis was done using both the full patient visits as well as just one visit per patient. This was done with the intention of hindering patients with many visits skewing the results. Both results are noted in the study. The following end points were used to estimate cumulative vision survival at varying ages: 6/6 vision, reading ability (defined as < 6/15), and legal blindness (defined as < 6/60).

3.2. Results

3.2.1 Patient Cohort Characterization

Due to the inheritance mode of XLRP, and the resulting variability of disease in females, the cohort was limited to 50 genetically confirmed males with mutations

in *RPGR*^{ORF15}. The patient cohort ranged in from 7 to 69 years of age. The range of patient visits spanned from single visits to a total of 17 visits per patient. A majority of patients, 34 in total, were examined between 2 and 17 times. The remaining 16 patients were seen only a single time. The average number of follow-up visits from the patients that were seen more than once was 2.4 per patient (median = 1 visit). The timespan between recurrent visits also exhibited great variability, encompassing a range from 2 - 72 months between visits (median = 14 months). The overwhelming majority of patients, 47, showed a rod-cone degeneration pattern and only 2 patients presented with a cone-rod degeneration pattern. The single remaining patient showed a rod-cone phenotype with an affected fovea (split fovea phenotype). The genotype underlying the three patients with cone-rod and rod-cone with split fovea phenotype were as follows: all of the three patients had ORF15 mutations. Of the two with a cone-rod degeneration had a deletion (c.2405_2406delAG; p.E802Gfs*32) and the other a nonsense mutation (c.2689G>T; p.E897*). The remaining patient with a split fovea phenotype displayed an underlying, hemizygous deletion (c.3077_3080delAAGG; p.E1026Gfs*62). Even though the number of phenotypic outliers was not large enough for an independent subgroup analysis, the three different patients were highlighted throughout the figures of the study [69].

Patient 20 years or younger presented 18 % of our cohort. Almost half of this cohort (44 %) were in their first decade of life at the age of first presentation. Mutations in *ORF15* and *exon 1-14* were roughly equally present in the nine patients presenting before their third decade in life: four patients had an *ORF15* mutation, while five had a mutation in *exon 1-14*. In youngest population of the patient cohort, those presenting in their first decade, one had an *ORF15* mutations and three a mutation in exons 1-14. Of the patients 18 % of patients presenting prior to their 20s, none were related, and all had different genotypes [69].

3.2.2 Molecular Assessment

All patients in this retrospective study had previously been sequenced and causative *RPGR*^{ORF15} mutations were uncovered (Fig 3.1 A, Table 3.1). The 50-patient cohort demonstrated 41 different mutations in the *RPGR*^{ORF15} gene, with 19 of those 41 mutations being the first reported mutations of their kind. Two mutations were reported several times: c.2405_2406delAG was represented seven times whereas the deletion c.2236_2237delGA mutation was present in four patients. When examining the sequence in which these mutations occur more closely, it is noticeable they both lie in repetitive, purine rich clustered sequences of *ORF15*. It should be noted that even though the sequences where the deletions occur are repetitive, the nucleotide sequences following the deletion are not identical to the deleted sequences, consequently the alignment between the shifted nucleotides remained suboptimal [69].

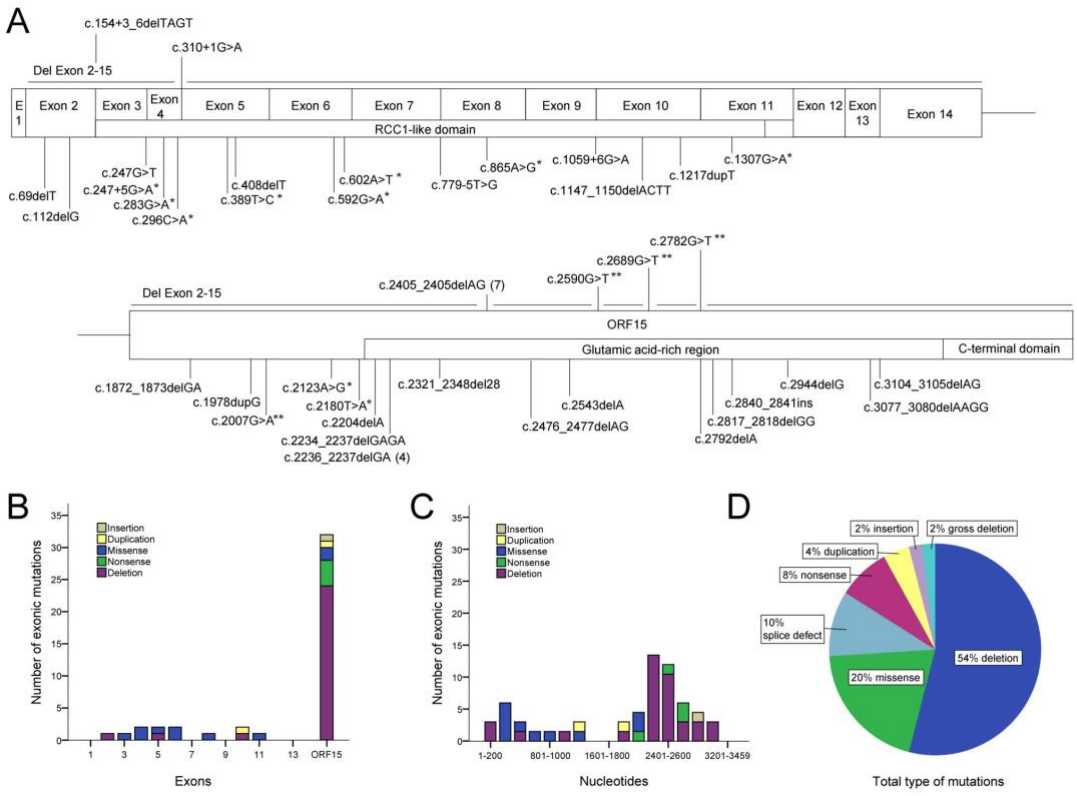

Fig. 3.1 **Overview of mutation location as well as types of mutations occurring in the 50-patient *RPGR*-XLRP cohort.** *ORF15* takes up almost half of the cDNA sequence of *RPGR*^{ORF15} (A), but houses almost three quarters of the mutations (A-C). Most mutations in the C-terminal *ORF15* were deletions, whereas missense mutations cluster in the N-terminal exons 1-14 (B and

C). Deletions make up over half of the mutations, with missense representing the second largest group at 20% (D).
Printed with permission from Julia-Sophia Bellingrath. This figure was previously published in IOVS by Bellingrath *et al.*

Pat No.	Hemizygous mutations in RPGR			Mutation type	Previously described
	Nucleotide level	Exon	Protein level		
3	gross deletion spanning exons 2-15 (length of deletion not defined)	2		gross deletion	novel
12	c.69delT	2	p.E24Kfs*44	deletion	novel
15	c.112delG	2	p.V38Yfs*30	deletion	novel
29	c.154+3_6delTAGT			splice defect	Neidhardt et al. 2008
8	c.247G>T	3	p.A83S	missense	Glöckle et al. 2014
26	c.247+5G>A			splice defect	novel
25	c.283G>A	4	p.G95R	missense	novel
17	c.296C>A	4	p.T99N	missense	Miano et al. 1999
38	c.310+1G>A			splice defect	Sharon et al. 2003
16	c.389T>C	5	p.F130S	missense	novel
42	c.408delT	5	p.F136L	deletion	Shu et al. 2007
19	c.592G>A	6	p.G198R	missense	Sharon et al. 2015
6	c.602A>T	6	p.H201L	missense	novel *
43	c.779-5T>G			splice defect	Neidhardt et al. 2008
39	c.865A>G	8	p.I289V	missense	Miano et al. 1999
37	c.1059+6G>A			splice defect	novel
41	c.1147_1150delACTT	10	p.T383Afs*13	deletion	novel
28	c.1217dupT	10	p.S407Ifs*46	duplication	novel
46	c.1307G>A	11	p.G436D	missense	Sharon et al. 2000
1	c.1872_1873delGA	15	p.E624Dfs*5	deletion	Pusch et al. 2002
22	c.1978dupG	15	p.Glu660Glyfs*4	duplication	novel
31	c.2007G>A	15	p.W669*	nonsense	Bader et al. 2003
9	c.2123A>G	15	p.E708G	missense	novel
21	c.2180T>A	15	p.M727K	missense	novel
24	c.2234_2237delGAGA	15	p.R745Kfs*69	deletion	Breuer et al. 2002
7	c.2236_2237delGA	15	p.E746Rfs*23	deletion	Vervoort et al. 2000
10	c.2236_2237delGA	15	p.E746Rfs*23	deletion	Vervoort et al. 2000
23	c.2236_2237delGA	15	p.E746Rfs*23	deletion	Vervoort et al. 2000
48	c.2236_2237delGA	15	p.E746Rfs*23	deletion	Vervoort et al. 2000

Pat No.	Hemizygous mutations in RPGR			Mutation type	Previously described
	Nucleotide level	Exon	Protein level		
30	c.2321_2348del28	15	p.E774Gfs*32	deletion	novel
14	c.2384delA	15	p.E795Gfs*20	deletion	Pusch et al. 2002
11	c.2405_2406delAG	15	p.E802Gfs*32	deletion	Vervoort et al. 2000 †
32	c.2405_2406delAG	15	p.E802Gfs*32	deletion	Vervoort et al. 2000
33	c.2405_2406delAG	15	p.E802Gfs*32	deletion	Vervoort et al. 2000
44	c.2405_2406delAG	15	p.E802Gfs*32	deletion	Vervoort et al. 2000
45	c.2405_2406delAG	15	p.E802Gfs*32	deletion	Vervoort et al. 2000
49	c.2405_2406delAG	15	p.E802Gfs*32	deletion	Vervoort et al. 2000 ‡
50	c.2405_2406delAG	15	p.E802Gfs*32	deletion	Vervoort et al. 2000 §
35	c.2476_2477delAG	15	p.R826Gfs*8	deletion	Pusch et al. 2002
27	c.2543delA	15	pE848Gfs*241	deletion	Pusch et al. 2002
40	c.2590G>T	15	p.E864*	nonsense	Pusch et al. 2002
5	c.2689G>T	15	p.E897*	nonsense	Glöckle et al. 2014 †
34	c.2782G>T	15	p.G928*	nonsense	Pusch et al. 2002
47	c.2790_2791delGG	15	p.E931Gfs*147	deletion	Shu X et al. 2007
36	c.2792delA	15	p.E931Gfs*158	deletion	Pelletier et al. 2007
13	c.2840_2841ins (length of insertion not defined)	15		insertion	novel
20	c.2944delG	15	p.E982Kfs*107	deletion	Sharon et al. 2003
2	c.2997_2998delGG	15	p.E1000Gfs*78	deletion	Pusch et al. 2002
18	c.3077_3080delAAGG	15	p.E1026Gfs*62	deletion	novel
4	c.3104_3105delAG	15	p.E1035Gfs*43	deletion	novel

Table 3.1 **Overview of Molecular Testing Results in RPGR-XLRP Patient Cohort**
Comments: RefSeq NM_001034853, NP_001030025 † Cone-rod dystrophy; * Variant of unclear pathogenicity; ‡ Uncle of patient no. 50; § Nephew of patient no. 49
Printed with permission from Julia-Sophia Bellingrath. This figure was also previously in IOVS by Bellingrath *et al.*

Location of Mutation

ORF15 has been reported to be a mutational hotspot within the *RPGR*^{ORF15} gene [50, 110], and this was particularly pronounced in the present analysis' patient cohort. Even though *ORF15* accounts for 49 % of the exonic sequence, 71 % of

mutation were found to cluster in this terminal exon (Fig.s 3.1 B, 3.1 C). A pattern concerning the type of mutation and their location regarding exon 1-14 vs. *ORF15* could also be discerned. By far the largest mutation type were deletions, 85 % of which occurred in the C-terminal *ORF15*. Only 15 % of deletions occurred in the N-terminal of $RPGR^{ORF15}$. Missense mutations, on the other hand, which made up 20 % of mutations and therefore represented the second largest group of mutations, could predominantly be found in the N-terminal exons. Eighty percent of missense mutations occurred in the first exons 1-15, and only 20 % in *ORF15*, a relationship almost inverse to the exonic location of the deletions (Fig.s 3.1 B-D). Previous studies confirm this trend [112, 181] with deletions (in/dels), and duplications clustered in the repetitive, purine (A/G)-rich *ORF15* terminal exon region, and missense mutations as well as other substitutions occurring predominantly in the first 14 exons of $RPGR^{ORF15}$ [69].

Correlation of location with severity of phenotype

Previous reports show a correlation between location of mutation and disease phenotype. To test whether such a correlation could be shown in the present cohort, VA and perimetry (III4e target intensity) of patients with mutations in *exons 1-14* were contrasted with those patients whose mutations occurred in *ORF15*. A high degree of symmetry was shown in all variables in the present patient cohort, so only data points from the right eye were considered in this analysis. Using the data set from one eye only also provided assurance that the data set would not be skewed by the use of two dependent variables. One patient visit for each patient was used as to not skew the data set by patients that had been examined a disproportionate number of times. Significant variability, but no significant difference in VA or perimetry could be shown between mutations located between in *exons 1-14* and *ORF15* (VA $p = 0.9$; perimetry $p = 0.58$; Fig.s 3.2 A and B).

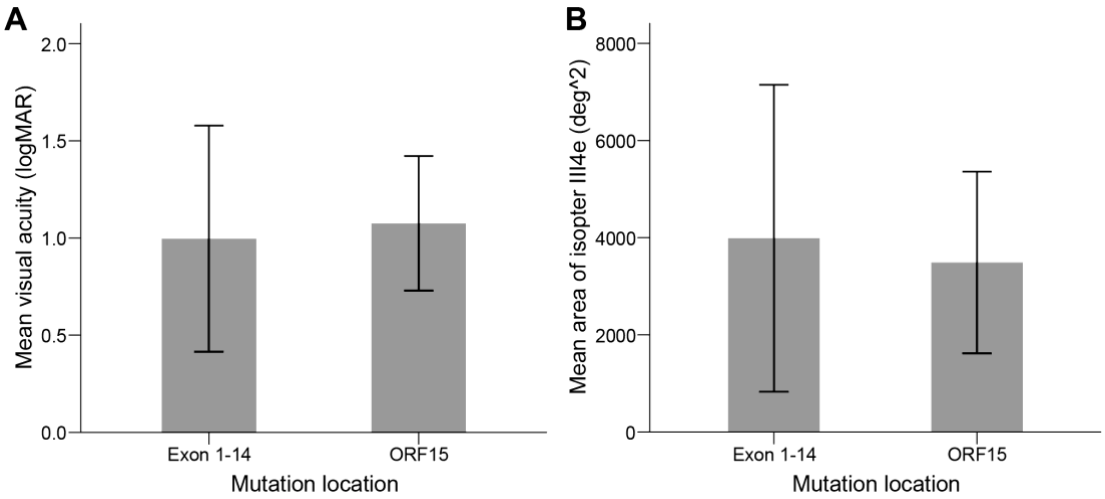

Fig. 3.2 **Correlation of genotype with phenotype between mutations located on *exon 1-14* and *ORF15***. Contrary to previous studies, no evidence of a genotype to phenotype correlation could be shown when examining VA (A) or perimetry (B) as a stand-in for phenotype.
Printed with permission from Julia-Sophia Bellingrath. This figure was also previously in IOVS by Bellingrath *et al.*

In order to eliminate differences in progression between patients as a possible confounder, these results were replicated by the analysis of patients all in their fourth decade of life, which provided a back-up to the previously mentioned results [69].

3.2.3 Analysis of disease symmetry between eyes

All four parameters (VA, ERG, foveal thickness and perimetry) were assessed for symmetry of disease. In every one of these parameters a highly significant degree of symmetry could be shown (p in all four measures < 0.001; Fig 3). Foveal thickness demonstrated the least amount of robustness with regards to symmetry between eyes ($n = 35$; $rho = 0.75$; $p < 0.001$; Fig 3 B). A much higher amount of symmetry was demonstrated by VA, a measurement of central visual function ($n = 50$; $rho = 0.85$; $p < 0.001$; Fig. 3.3 A). Perimetry using the III4e isopter showed an even higher degree of symmetry ($rho = 0.96$, $n = 38$, $p < 0.001$; Fig. 3.3 C). Even though correlation analysis of isopter I4e proved to be even more symmetrical ($rho = 0.97$, $n = 30$, $p < 0.001$), this is likely an overestimation caused by a floor effect, since 40 % of I4e measurements were nearly 0 in both eyes. Not enough data was available to analyse isopter Ve. ERG serves as perhaps the least variable and therefore most objective measure of retinal function and as

such is a particularly valuable measure. The comparison of ERG b-wave amplitude of right and left eyes showed symmetry in all measurements, although a confounding floor effect was noted in some measurements. The highest symmetry not subjected to a floor effect was seen in DA single-flash responses to a 3 cd*s stimulus (rho = 0.98, n = 32, p < 0.001; Fig. 3.3 D). Interestingly, there was no significant difference in symmetry in the three patients with cone-rod or rod-cone phenotype with split fovea compared to the majority of patients with rod-cone dystrophy [69].

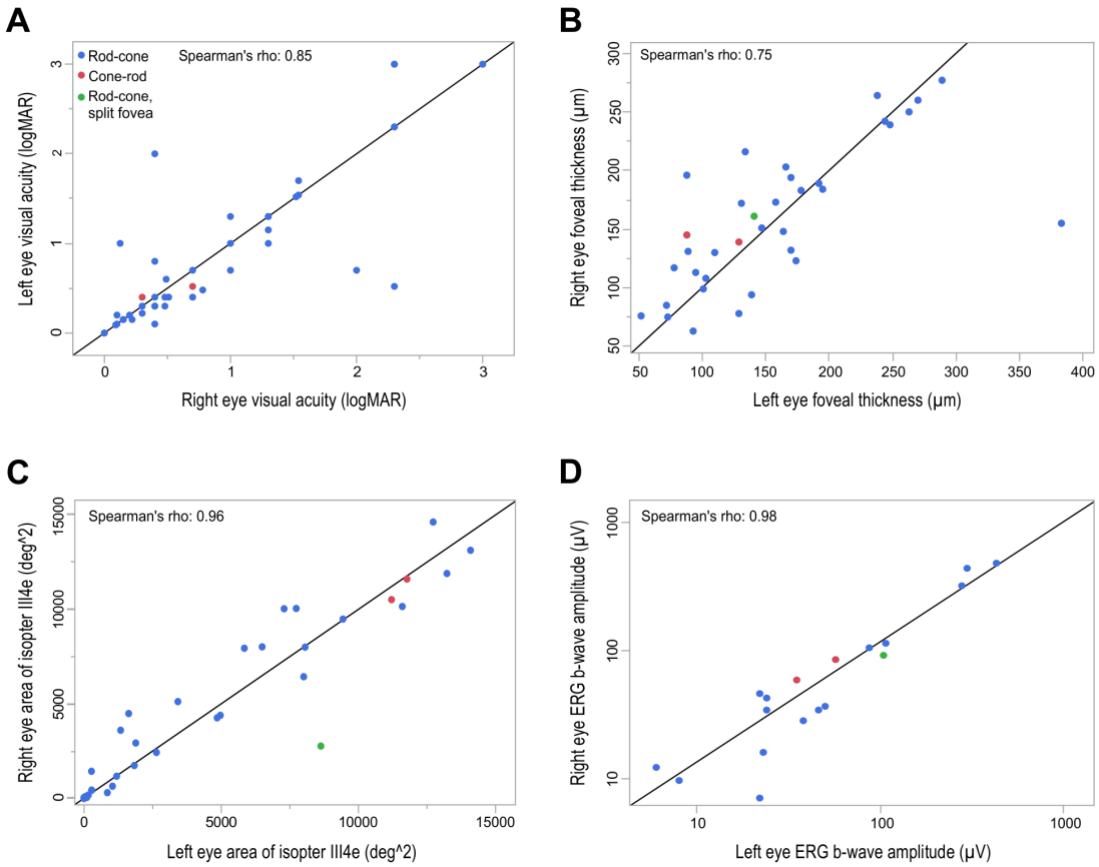

Fig. 3.3 **Symmetry analysis of a 50 patient *RPGR*-XLRP cohort.** In all measures, disease proved symmetrical between eyes. Foveal thickness exhibited the least amount of symmetry (A), whereas both kinetic perimetry using the III4e target (C) and ERG b-wave amplitude provoked by DA 3.0 cd*s flash (D) demonstrated remarkable similarity between both eyes. Degeneration and its effect on central visual function was fairly symmetrical (B).
Printed with permission from Julia-Sophia Bellingrath. This figure was previously published in IOVS by Bellingrath *et al.*

3.2.4 Analysis of disease progression

When looking at disease progression of *RPGR*-XLRP in this cohort, the same morphologic and functional parameters used to screen for symmetry were used

for evaluation of disease progression. As can be seen in Fig. 4 A and 4 B, the two parameters VA and foveal thickness were the most helpful in characterizing disease progression. The most fitting function to describe disease development over time was a logarithmic function. Logarithmic progression rates are reported in Table 3.2.

Age group (range in years)	**Estimated average yearly progression rate [CI: 95%]**			
	Visual Acuity (LogMAR / year)	**Foveal thickness** (µm / year)	**Perimetry III4e** (deg^2 / year)	**ERG b3.SF** (µV / year)
7 - 20	0.01 [0, 0.04]	-2.35 [-2.67, -0.93]	-416.44 [-88.83, -1165.17]	0 [0, 0]
21 - 40	0.03 [0.01, 0.11]	-1.91 [-1.84, -0.89]	-131.07 [-13.23, -761.75]	0 [0, 0]
41 - 60	0.07 [0.01, 0.39]	-1.51 [-1.18, -0.83]	-33.64 [-1.41, -462.03]	0 [0, 0]

Table 3.2 **Average disease progression rate per age group.**

Perimetry as measured with the III4e isopter was only able to describe disease progression in the first two decades of life, owing to the fact that by ages as early as 20-25, visual field loss can be nearly complete. This early loss of visual fields introduces a floor effect prompted by the fact that all patients present with a near complete loss of visual fields. This floor effect results in a lack of discriminatory power in efficacy analysis. In contrast to the other three parameters, disease progression as measured by ERG (Fig. 3.4 D, Table 3.3) did not show a correlation with age. As in the symmetry analysis, patients with the cone-rod or rod-cone dystrophy with split fovea did not manifest as outliers during disease progression analysis [69].

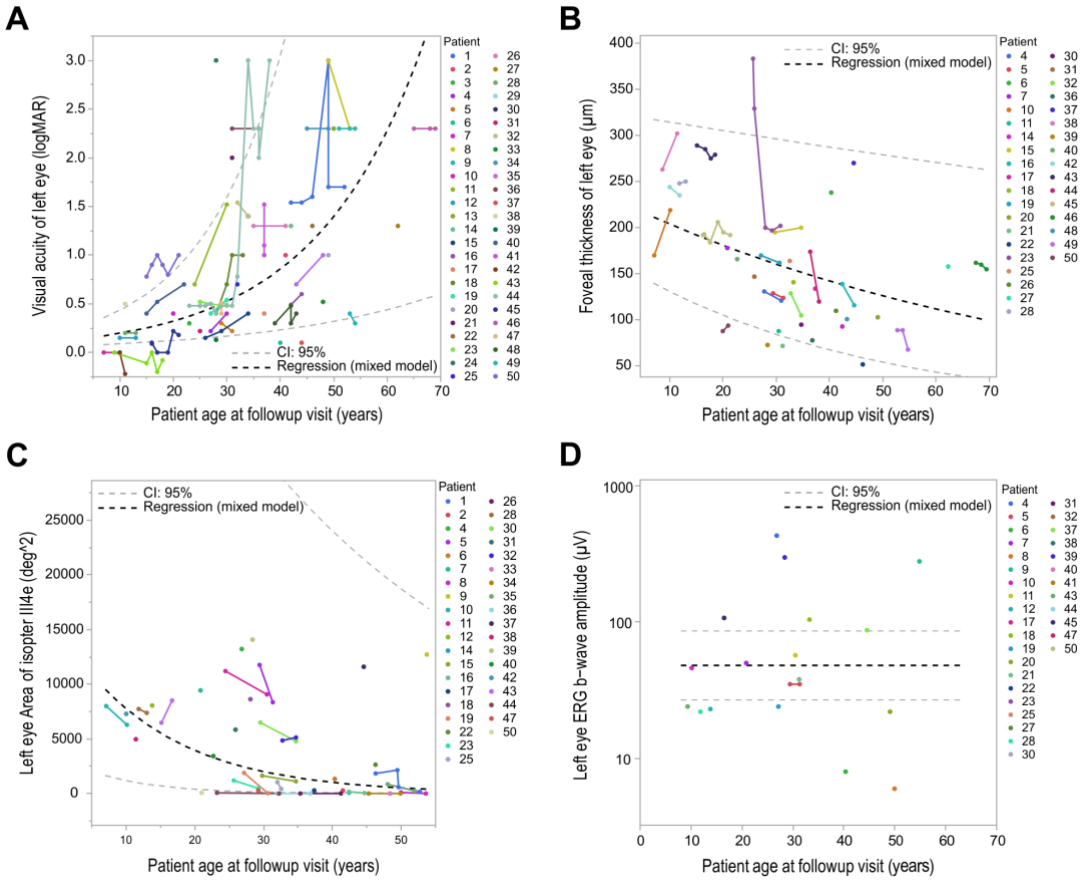

Fig. 3.4. **Analysis of progression of XLRP3 patients examining left eye VA, III4e target perimetry, foveal thickness and ERG DA 3.0 cd*s flash.** A logarithmic function best described the relationship between age and VA (A) as well as foveal thickness (B). Increased foveal thickness was the result of epiretinal membrane formation in some of the patients. Yet these were not excluded, since it would not have changed the outcome of the analysis. Once again, when examining III4e target perimetry (C) a logarithmic function best described the outcome. No correlation could be shown between age and ERG DA 3.0 cd*s flash (D).
Printed with permission from Julia-Sophia Bellingrath. This figure was also previously in IOVS by Bellingrath *et al.*

A. Visual Acuity progression			
Model Term	**Coefficient**	**CI 95%**	**P-Value**
Intercept	-2.116	[-2.747, -1.485]	< 0.001
Age at visit	0.049	[0.032, 0.065]	< 0.001
Number of levels	47		
Gamma Distribution. Log link function			
B. Foveal thickness progression			
Model Term	**Coefficient**	**CI 95%**	**P-Value**
Intercept	5.438	[5.095, 5.780]	< 0.001
age at visit	-0.012	[-0.022, -0.003]	0.012
Number of levels	36		
Gamma Distribution. Log link function			
C. Perimetry III4e progression			
Model Term	**Coefficient**	**CI 95%**	**P-Value**
Intercept	9.638	[8.188, 11.087]	< 0.001
Age at visit	-0.068	[-0.112, -0.025]	0.003
Number of levels	34		
Gamma Distribution. Log link function			
D. ERG b3.SF progression			
Model Term	**Coefficient**	**CI 95%**	**P-Value**
Intercept	3.872	[3.872, 4.453]	< 0.001
Age at visit	0	[0.000, 0.000]	1
Number of levels	18		
Gamma Distribution. Log link function			

Table 3.3 Mixed model disease progression coefficients

3.2.5 Subgroup analysis of disease progression

The phenotypic heterogeneity and the heterogeneity in disease progression has been widely described among RP patients as a whole. To see whether this phenomenon was curbed when looking at patients with mutations not just in the same gene, but also in the identical genetic sequence, two deletions that were present in subgroups of seven and four patients, respectively, were analyzed.

RPGR mutation c.2405_2406delAG

This was the largest subgroup and was comprised of seven patients with the identical c.2204_2205delAG; p.E802Gfs*32 mutation. Within this group, patient No. 49 and patient No. 50 were second degree relatives as noted in Table 1. Even in this patient group with identical mutations, no correlation could be established between disease progression and age (Fig. 3.5). Moreover, patient no. 11 exhibits a degeneration favouring cones, a cone-rod phenotype, while the other six patients manifested as the far more prevalent rod-cone phenotype [69].

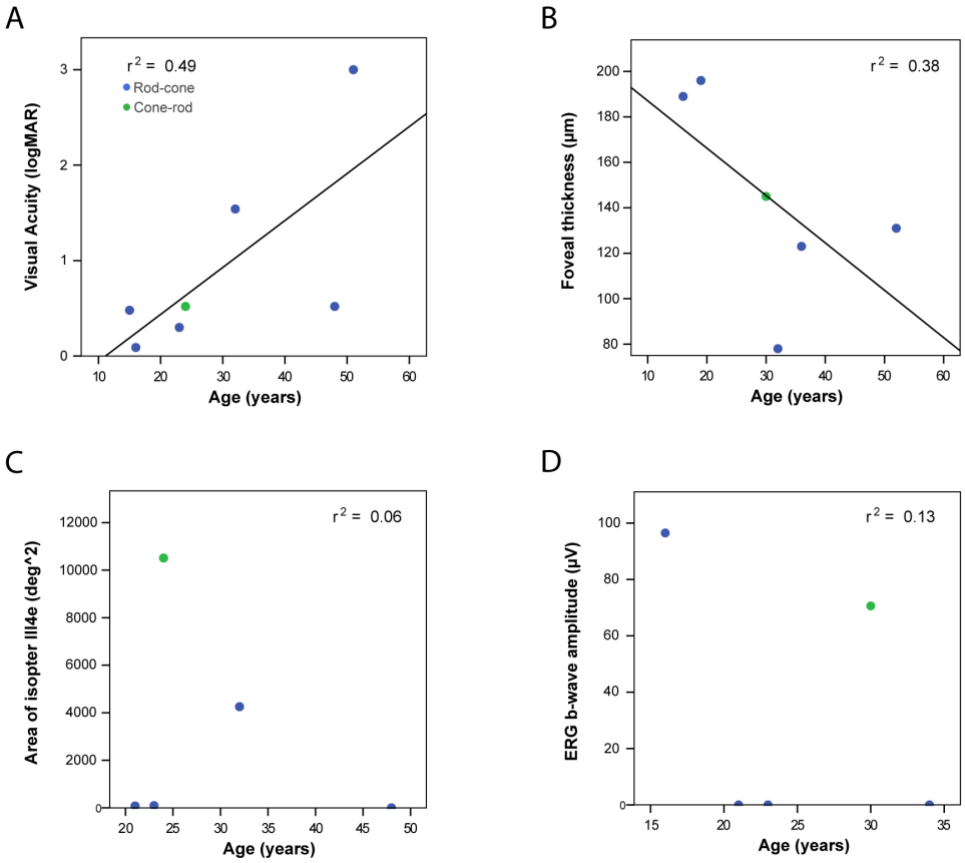

Fig. 3.5 **Disease progression analysis in seven patients with c.2405_2406delAG mutation.** Despite demonstrating an identical correlation, no uniform disease progression could be identified in any of the parameters. Even the phenotype varied, with one patient presenting with a cone-rod phenotype while the other six patients all demonstrated a rod-cone phenotype.
Printed with permission from Julia-Sophia Bellingrath. This figure was previously published in IOVS by Bellingrath *et al.*

RPGR mutation c.2236_2237delGA

Four patients of our cohort study presented with the c.2236_2237delGA, p.E746Rfs*23 genotype (Fig. 3.6). When looking exclusively at VA (R2 = 0.58, n = 4; P = 0.11; Fig 6 A) and foveal thickness (R2 = 0.96, n = 4, p = 0.05 Fig 6 B), the progression appeared to exhibit similarities. Yet ERG showed a wide degree of variation regarding symmetry and displayed a range from 0.50 (DA 3.0 cd*s) to a fairly symmetrical value of 0.81 (LA 3.0 cd*s; Fig 6 D). 30 Hz flicker had an R2 of 0.79 (n = 4, p < 0.01). When looking at perimetry, neither I4e nor III4e target showed a homogenous disease progression (Fig. 3.6 C). When looking at the patient data more closely, one can see that this is the result of patient No. 48 presenting as an outlier with particularly poor results in the I4e target perimetry, but patient No. 7 showing a relatively well preserved III4e target perimetry [69].

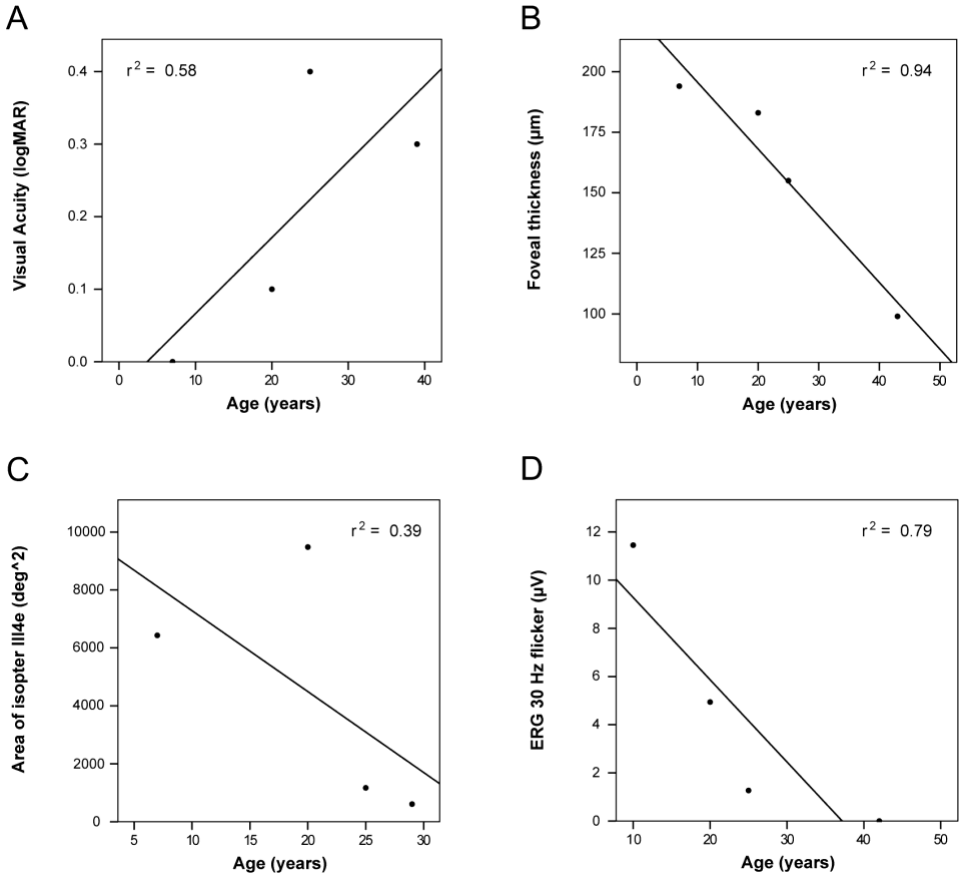

Fig. 3.6 **Disease progression analysis in seven patients with c c.2236_2237delGA mutation.** In this cohort, VA (A) and foveal thickness (B) showed a fair degree of symmetry, while perimetry (C) and ERG (D) did not. All patients presented with a rod-cone phenotype.
Printed with permission from Julia-Sophia Bellingrath. This figure was also published in IOVS by Bellingrath *et al.*

3.2.6 Kaplan Meier Survival Curves

While many measures, in particular the objective ones such as ERG and perimetry may be clinically robust, relevant and important, the most meaningful outcome measure for the patient is arguably VA. With the goal of estimating decline of VA, even in the face of a large variability between patients, Kaplan Meier survival curves were used to calculate a survival curve (Fig. 3.7). Three meaningful cutoff points for both the patient and the physician were used: loss of 6/6 vision (0.0 logMAR), loss of reading ability (0.4 logMAR), and a drop of vision under the limit for legal blindness (1.0 logMAR). Right and left eye are shown separately in this context and this once again reveals the high amount of symmetry between eyes (Fig. 3.7 A and B).

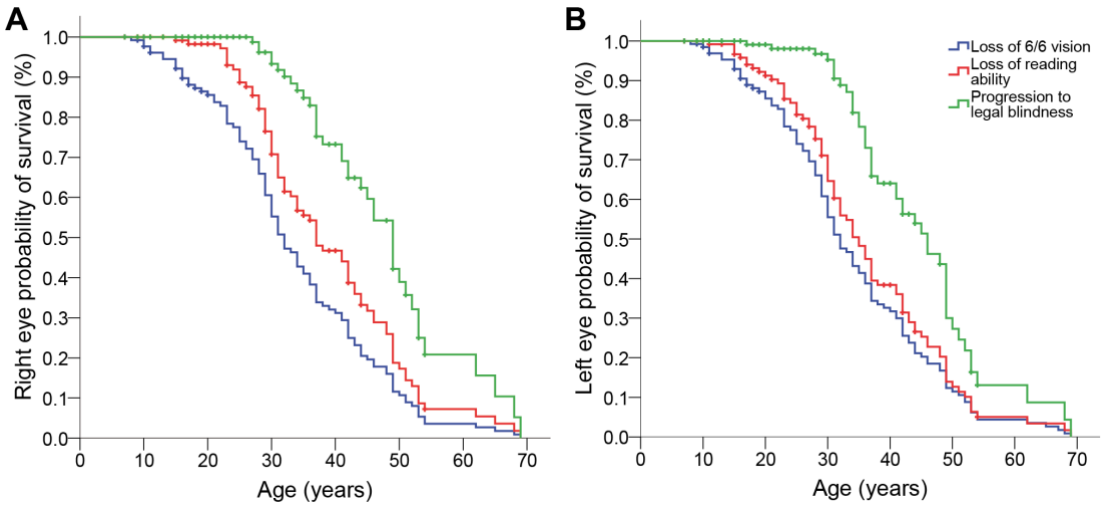

Fig. 3.7 **Kaplan-Meier survival curves for the right and left eye of *RPGR*-XLRP patients.** for right eyes (A) predicted a loss of 6/6 vision at a mean age of 34 years (+/- 2.9; 95% confidence interval), a loss of reading ability at 39 years (+/- 2.6), and progression to legal blindness at 48 years (+/- 1.6). KMCs for left eyes (B) were similar, estimating a loss of 6/6 vision at a mean of 34 years (+/- 2.4), a loss of reading ability at 37 years (+/- 2.5), and a reaching of the legal limit for legal blindness at 45 years (+/- 3.1).
Printed with permission from Julia-Sophia Bellingrath. This figure was also previously in IOVS by Bellingrath *et al*.

The most severe loss of VA was shown to happen in the third and fourth decade of life. To illustrate this more clearly, the following data can be considered: At 20 years of age, more than 80 % of patients demonstrated 6/6 vision and more than 90 % of patients were predicted to be capable of reading. In contrast to this, by age 40, over 20 % of patients are predicted to be legally blind and 50 % of patients are predicted to have lost reading ability. Merely 30 % retain 6/6 vision

in this age bracket. When looking at all age groups and all 50 patients, the mean estimated survival time for 6/6 vision was 34 years (+/-/2.9; 95 % confidence interval). A loss of reading ability occurred at 39 years (+/-2.6) and patients reached the legal limit for blindness at age 48 (+/- 1.6) [69]

3.3 Discussion

The present study confirms the severity of XLRP caused by mutations *RPGR*^{ORF15}. This can be seen in the early disease onset, which results in patients presenting as young as seven years of age. Nine patients presented before the age of 20 [69]. This is even more remarkable when one considers that, as mentioned in the introduction, a subjective loss in visual acuity or visual fields is not noted until a considerable part of the peripheral rods have already degenerated [23]. One potential confounder is the fact that some patients might already have a sibling or a relative that has known XLRP and present before subjective changes in VA or visual fields or nyctalopia occur. In the present study, none of the patients under the age of 20 had a relative being concurrently treated at the same institutions. There were four patients who presented under the age of 10, and three of them had mutations in exons 1-14 [69]. This could be interpreted as mutations at the N-terminal presenting earlier in age, but due to the extremely small sample size, the statistical power is too low to make a reliable hypothesis.

Almost three quarters of mutations occurred in the terminal *ORF15* exon, strongly confirming this C-terminal, purine rich exon as a mutational hotspot of the *RPGR*^{ORF15} gene. Contrary to previous reports however, *ORF15* mutations could not be shown to have a more or severe phenotype. Neither could they be shown to have a different phenotype regarding the phenotypic pattern of degeneration. In general, no genotype-phenotype relationship could be shown in regard to *ORF15* mutations compared to *exon 1-14* mutations [69]. These results differ from Sharon *et al.* and Fahim *et al*. who demonstrate a milder disease phenotype in patients with C-terminal *ORF15* mutations than in patients with mutations in Exon 1-14 [31, 133]. It has been postulated that such a genotype-phenotype relationship could be explained by nonsense mediated decay not applying to

mutations in the terminal *ORF15* exon and this might allow the transcribed truncated protein to retain residual function [31, 128]. However, it has also been shown by Hong *et al.* that a gain-of function mutation in *ORF15* causes more severe disease progression than a null mutation due to dominant negative effects [139]. Another argument against genotype phenotype correlation in this context is provided when looking at the naturally occurring canine models of *RPGR*-XLRP, termed X-linked progressive retinal atrophy. Both dogs with X-linked progressive retinal atrophy (XLPRA1) have mutations in *ORF15*, occurring 52 nucleotides apart from each other, but one shows a slow progression (XLPRA1), the other more severe degeneration (XLPRA2). This falls in line with the results of the present patient cohort analysis, where a clear genotype-phenotype remains elusive.

Symmetry in RP has been previously reported: as early as 1979, Massof *et al.* analyzed VA and perimetry (V4e) of a 60-patient cohort [182]. In this genetically unclassified cohort, the authors reported high symmetry between right and left eye. Subclassification of RP was determined by clinical phenotype and family history alone, and only 4 % showed an X-linked inheritance pattern [182]. Moreover, the cohort most likely showed a large genetic heterogeneity. This present study adds the vital observation that the symmetry proposed for the hugely genetically variable disease of RP holds true for XLRP patients with mutations occurring in $RPGR^{ORF15}$ [69]. With treatments becoming more targeted and personalized, information about more specific patient cohorts is a vital part of running clinical trials for new drugs or therapies. The results show that in clinical trials with *RPGR*-XLRP patients, the contralateral eye can be used as an internal control to measure treatment efficacy [69]. This practice has already been established in phase 1 and phase 2 clinical trials for Leber Congenital Amaurosis (LCA) [66, 140]. But in previous trails for RP treatment, regulatory agencies have wanted an interindividual control, despite evidence of a symmetrical RP phenotype [183]. The present study is able to show that the assumption of bilateral symmetry holds true not only for VA and perimetry, but also for foveal thickness and ERG b-wave amplitudes. ERG is a particularly interesting parameter in that it is an objective marker of photoreceptor function, unlike VA,

which can fluctuate according to the patient's general state of concentration and well-being. Also, in recent long-term results of gene therapy trails for LCA, while VA and perimetry initially improved post treatment before declining again after six months, a continuous and steady decline of photoreceptor function in ERG was noted [66, 140]. This uniqueness of ERG might make this parameter useful as a long-term indicator of photoreceptor function. The greatest symmetry in the present patient cohort could be shown for perimetry using isopter area III4e, but its utility could be limited by the early loss of visual fields in *RPGR*-XLRP patients [69]. In a clinical trial setting with adult patients, a lack of progression could be impossible to prove due to this floor effect. A further possibility would be to utilize more sensitive perimetry measure (Ve) in the hopes of warding off the floor effect [69].

When considering both the results of the symmetry and progression rate, VA could very well be the best choice to measure treatment efficacy. It is a functional outcome measure with an arguably the greatest subjective value to the patient. According to the present data, VA is less variable in younger patients [69]. Although it should be noted that test-retest variability could not be measured in this retrospective trail and would have to be assessed in the setting of a prospective trial. Both VA and perimetry are subjective measures. This psychophysical nature could be seen as problematic, especially in an unmasked trial. In an effort to limit test-retest variability, Bittner *et al.* were able to show a limitation to < 20 % in perimetry, but not further. This was achieved by using a single, experienced operator [184]. This setting might be probable to achieve in a single-center trial, but is highly unlikely to be in a multi-center trial. However, to generate adequate numbers in an *RPGR*-XLRP clinical trial, a multi-center clinical trial would most likely have to be conducted. ERG is in the unique position of offering an objective, quantitative outcome measure, that also displays high symmetry [69]. Unfortunately, with regards to disease progression, the present study was not able to show a correlation between ERG values [69]. Additionally, full-field ERG is generated as a sum potential and - contrary to perimetry -does not feature a spatial resolution, a particular drawback when using subretinal injection, where the therapy is limited to a particular spot in the retina where one

thus would expect to see a particular effect. Multifocal ERG data could provide a solution to this, but could not be analyzed in this retrospective, cross-sectional study due to lack of data. As a result of these findings, a prospective trail measuring multifocal ERG, VA, perimetry, and OCT data is needed to further compare the advantages of each outcome measure [69]. Additionally, based on several studies, the width of the photoreceptor ellipsoid zone (EZ) on OCT has the potential to become a highly relevant outcome measure for disease progression in XLRP3 [184-187]. A correlation between loss of visual field and thinning of the EZ in the transitional zone could be shown by Birch *et al.* [185]. EZ width is a potentially extremely robust marker due to its low repeat variability and its lack of susceptibility to floor effects regarding disease progression analysis. It is in the unique position of being a morphologic, and hence objective, outcome measure that correlates with the subjective perimetry measurements.

As is evident from our subgroup analysis, even if patients carry the same mutation, a uniform disease progression or phenotype cannot be predicted [69]. This finding is hugely relevant for daily clinical practice and counseling, even in fields like prenatal counseling that is becoming more and more influenced by advancements in genetics. This evidence of considerable phenotypic variability in patients with identical mutations is conflicting. This is most likely to due to both the lack of statistical power in the extremely limited patient numbers as well as the possibility of unknown genetic and epigenetic confounders that may be influencing disease progression. Fahim *et al.*, identified two SNPs associated with either a more or less severe disease progression [133]. Perhaps more research into these genetic and epigenetic modifiers might pave the way for discovering variability of genotype-phenotype relationship and eventually enable a more precise prediction of prognosis for patients and their offspring.

As determined by Kaplan-Meier curves, the most impressive decline in VA occurs between the ages of 20 and 40 years [69]. Our results determining the median age for blindness were further strengthened by those of Sandberg *et al.*, who determined the median survival age to be 45 years of age in their respective *RPGR*-XLRP cohort [188]. There are several different markers that can be used in a clinical trial to define treatment efficacy, one of them being lack of

progression. In this scenario, our analysis indicated patients should be selected before or at the beginning of this rapid rate of disease progression [69]. Another clinical endpoint may be to show VA gain, in addition to simply a lack of progression. In this case, patients perhaps should be chosen toward the end or after the period of sharp decline in VA [69]. To this end, Beltran *et al.* recently utilized a canine model to demonstrate that treatment during this intermediate disease stage is capable of significantly slowing and even arresting disease progression [189]. This finding has the potential to widen the therapeutic window of intervention in patients with *RPGR*-XLRP.

In total, our results stipulate that degeneration between right and left eye are symmetrical [69]. Therefore, it is legitimate to use the contralateral eye as an internal control in the setting of an interventional, therapeutic trial. The highest symmetry was seen in the VA and foveal thickness as outcome measures. In younger patients where disease has not yet fully advanced, perimetry with III4e target intensity could present a promising outcome measure. Standing in contrast to previous studies, we could not show a genotype phenotype relationship between mutations occurring in *ORF15* and in mutations occurring outside of it. Nor did identical mutations guarantee a similar disease progression or even a similar phenotype. Survival curve analysis as related to vision showed the steepest decline in the third and fourth decade of life, while the median age to reach legal blindness was 48 years. In the light of these results, a prospective, observational trail with genetically conformed *RPGR*-XLRP patients would be needed to further explore the endpoint utility [69].

ABSTRACT

Purpose

Mutations in *RPGR*^{ORF15} cause 70 to 90 % of the monogenetic disease X-linked retinitis pigmentosa (XLRP), making this gene a high-yield target for causal treatment with gene therapy. Due to the purine-rich, repetitive nature of the terminal *ORF15* exon, maintaining transgene sequence fidelity has proven to be a road-block in translational efforts. This thesis contributes to the optimisation of a gene therapy for *RPGR*-XLRP in two ways: firstly, it aims to investigate codon optimization and use of mutant AAV capsids as a means to overcome the inherent instability of *RPGR*^{ORF15} and increase transgene expression. Secondly, analysis of pre-treatment characteristics in a cohort of 50 *RPGR*-XLRP patients will assist both future prospective observational and interventional trials by determining symmetry of disease, rate of progression and suitability of outcome measures as endpoints for clinical trials.

Methods

In the first part of the thesis, Western Blot was used to quantify transgene expression in HEK293T cells transfected with codon optimised (co) or wild type (wt) *RPGR* plasmids as well as to detect transgene expression in mice unilaterally injected with AAV2/8.*coRPGR*. Immunolabeling was used to show correct localisation of codon optimised transgene to the photoreceptor cilium and to compare transduction efficiency between wild type and single mutant AAV8^{Y733F} capsids. In the thesis' second part, a retrospective, cross-sectional analysis of 50 patients extracted visual acuity, visual fields (I4e and III4e targets), foveal thickness and ERG data points (ISCEV standard protocol) alongside molecular genetic data. Symmetry and progression were assessed using linear regression and cross-sectional analysis, respectively. Kaplan-Meyer Curves were used to estimate cumulative 'survival' of three important levels of visual function (full vision, reading ability, threshold to legal blindness) with age.

Results

HEK293T cells transfected with p.*coRPGR* showed an increase in protein expression ($p < 0.005$) and demonstrated a superior transgene stability compared to the wild type control. Three different mouse lines, *C57BL/6J*, *C57BL/6J* $^{Rd9/Boc}$ and *Rpgr*$^{-/y}$, treated with AAV2/8.*coRPGR* showed a reliable, albeit variable transgene expression and demonstrated co-localisation with RPGR interacting protein (RPGRIP) in the connecting cilium. Mutant capsid (AAV8^{Y733F}) failed to show a significant increase in transduction of 661W cone-like photoreceptor cells ($p = 0.058$). In the retrospective analysis of clinical data from XLRP patients, 73 % of exonic mutations occurred in *ORF15*. Yet no clear genotype-phenotype relationship could be established between mutations located in these two parts of the *RPGR* gene and patients with *ORF15* mutations did not have a significantly different visual acuity ($p = 0.9$) or visual field (III4e; $p = 0.6$) than those with mutations in exons 1-14. Comparison of both eyes revealed a strong symmetry of degeneration in all outcome measures, with visual fields (I4e $\rho = 0.99$; III4e $\rho = 0.96$) and ERG (30 Hz flicker $\rho = 0.95$) exhibiting the highest symmetry. Disease progression eluded description by a simple function. Kaplan-Meier curve (KMC) analysis predicts the most severe decline in vision between the third and fourth decade of life.

Conclusions

Codon optimisation of *RPGR* significantly increased transgene levels in HEK293T cells compared to a wild type *RPGR* expression cassette. AAV2/8.coRPGR injected mouse eyes reliably expressed RPGR protein that correctly localised to the photoreceptor connecting cilium in mouse models of *RPGR*-XLRP.

High symmetry in all outcome measures confirm that the contralateral eye can be used as an internal control in an *RPGR*-XLRP gene therapy trial. The variability between patients makes an intra-individual control preferable to an inter-individual control. According to these findings, the most sensitive parameter to measure disease progression and treatment success in an interventional *RPGR*-XLRP trial seems to be kinetic visual field using the III4e target.

Overall, these two pillars of research contribute to the foundation enabling translation of *RPGR*^{ORF15} gene therapy into a clinical trial.

ZUSAMMENFASSUNG

Hintergrund

Mutationen in dem *RPGR*^{ORF15} Gen sind für 70 bis 90 % der X-chromosomal vererbten Retinitis Pigmentosa (XLRP) verantwortlich. Aufgrund dessen ist dieses Gen ein besonders vielversprechendes Target für die Entwicklung einer kausalen, gentherapeutischen Behandlungsstrategie. Allerdings stellte in bisherigen präklinischen Studien die Bewahrung der Transgen-Sequenz des Purin-reichen, repetitiven und terminalen Exons *ORF15* den limitierenden Faktor in diesen Bestrebungen dar. Diese Dissertation trägt auf zwei Weisen zu der Weiterentwicklung einer Gentherapie für *RPGR*-XLRP bei: Zum einen werden Methoden der Codon-Optimierung und die Anwendung mutierte AAV-Kapside evaluiert um die inhärente Transgen-Instabilität zu überwinden und die Protein-Expression zu steigern. Zum anderen wird durch eine retrospektive Querschnittsanalyse 50 *RPGR*-XLRP Patienten der Grundstein für prospektive Beobachtungs- und Interventionsstudien gelegt, indem die Symmetrie der Erkrankung, die Progressionsrate und der bestgeeignete Parameter für einen primären Endpunkt zukünftiger Studien untersucht wurden.

Methoden

Western Blots wurden genutzt, um die *RPGR*^{ORF15} Transgen-Expression in zwei Szenarien zu quantifizieren: zum einen in HEK293T Zellen, die mit Codon-optimierten (co) oder Wildtyp (wt) *RPGR*-Plasmiden transfiziert wurden, zum anderen in drei verschiedenen Mausstämmen, dessen Augen unilateral mit AAV.*coRPGR*^{ORF15} injiziert wurden. Die Lokalisation des *coRPGR*^{ORF15} Transgens in Photorezeptor-Zilien dieser unilateral mit AAV2/8.*coRPGR*^{ORF15} injizierten Mäuse wurde anhand von Immunfärbung demonstriert. Ebenso wurde die Immunhistochemie dazu verwendet, die Transduktions-Effizienz zwischen Wildtyp und mutierten AAV8^{Y733F}-Kapsiden in Zapfen ähnlichen 661W Zellen zu vergleichen. Im zweiten Teil der Arbeit wurden klinische Datenpunkte wie Sehschärfe, Perimetrie (I4e und III4e), foveale Dicke, ERG nach ISCEV-Standard, sowie genetische Mutationsanalysen von 50 *RPGR*-XLRP Patienten

aus zwei Behandlungszentren extrahiert. Symmetrie und Progression wurden anhand linearer Regressions- und Querschnittsanalysen untersucht. Kaplan-Meier-Kurven (KMC) wurden verwendet, um den Erhalt der Sehschärfe im Altersverlauf anhand drei wichtiger Parameter (volle Sehschärfe, Lesevermögen und die Gesetzesdefinition von Blindheit) zu analysieren.

Ergebnisse

HEK293T Zellen, die mit p.*coRPGR*^{ORF15} transfiziert wurden, zeigten eine signifikant höhere Protein-Expression ($p < 0.005$) und demonstrierten eine überlegene Transgen-Stabilität gegenüber den Wildtyp Kontrollen. Drei verschiedene, mit AAV2/8.*coRPGR*^{ORF15} behandelte Mauslinien (*C57BL/6J*, *C57BL/6*$^{Rd9/Boc}$ and *Rpgr*$^{-/y}$*),* demonstrierten eine stabile Transgen Expression und zeigten eine physiologische Co-lokalisation mit RPGR-interagierendem Protein (RPGRIP) im Zilium der Photorezeptoren. Das mutierte AAV8^{Y733F}-Kapsid zeigte keine signifikant erhöhte Transduktions-Effizienz der zapfenähnlichen 661W-Zellen ($p = 0.058$). In der retrospektiven Querschnittsanalyse von 50 *RPGR*-XLRP-Patienten zeigten sich 73 % der Mutationen in dem terminalen *ORF15* Exon. Es konnte keine Genotyp-Phenotyp-Korrelation zwischen Mutationen etabliert werden, die in *ORF15* und *Exon1-14* des *RPGR*-Gens auftraten, und somit wiesen Patienten mit *ORF15* Mutationen keine bessere Sehstärke ($p = 0.9$) oder weiteres Gesichtsfeld (III4e; $p = 0.6$) auf als Patienten mit *Exon1-14* Mutationen. Es zeigte sich eine hohe Symmetrie der Degeneration in allen klinischen Parametern, wobei die Perimetrie (I4e $\rho = 0.99$; III4e $\rho = 0.96$) und das ERG (30 Hz flicker $\rho = 0.95$) die höchste Symmetrie aufwiesen. Die Progression der Erkrankung konnte nicht mit einer einfachen Funktion beschrieben werden. Die KMC Analyse zeigte die am schnellsten progrediente und stärkste Degeneration der Sehschärfe zwischen der dritten und vierten Lebensdekade.

Zusammenfassung

Die Codon-Optimierung des *RPGR*^{ORF15} Gens erhöht signifikant die Transgene-Expression in HEK293T Zellen im Vergleich mit der Wildtyp *RPGR*^{ORF15}

Transgene-Expressions-Kassette. Augen von *RPGR*-XLRP Maus-Modellen, die mit AAV2/8.coRPGR^{ORF15} injiziert wurden, exprimieren beständig das RPGR^{ORF15} Protein, welches sich physiologisch in dem Photorezeptor-Verbindungs-Zilium lokalisierte.

Eine hohe Symmetrie aller klinisch erhobenen Parameter bestätigt, dass das kontralaterale Auge als eine intra-individuelle Kontrolle in einer *RPGR*-XLRP-gentherapeutischen Studie verwendet werden kann. Die hohe Variabilität zwischen Patienten zeigt, dass diese intra-individuelle Kontrolle einer inter-individuellen Kontrolle vorzuziehen ist. Gemäß den Ergebnissen der Studie ist die kinetische Perimetrie mit dem III4e Target der sensitivste Parameter, um das Voranschreiten der Degeneration sowie den Therapieerfolg in einer *RPGR*-XLRP Interventionsstudie zu messen.

REFERENCES

1. Araki, M. and T.S. Okada, *Differentiation of lens and pigment cells in cultures of neural retinal cells of early chick embryos.* Dev Biol, 1977. **60**(1): p. 278-86.
2. Coulombre, J.L. and A.J. Coulombre, *Regeneration of neural retina from the pigmented epithelium in the chick embryo.* Dev Biol, 1965. **12**(1): p. 79-92.
3. Fuhrmann, S., *Eye morphogenesis and patterning of the optic vesicle.* Curr Top Dev Biol, 2010. **93**: p. 61-84.
4. Young, R.W., *Cell differentiation in the retina of the mouse.* Anat Rec, 1985. **212**(2): p. 199-205.
5. Wallace, V.A., *Concise review: making a retina--from the building blocks to clinical applications.* Stem Cells, 2011. **29**(3): p. 412-7.
6. Francis-West, G.C.S.S.B.B.P.R.B.P.H., *Larsen's Human Embryology*. Fifth Edition ed.: Elsevier
7. Osterberg, G., *Topography of the layers of the human retina.* Acta Ophthalmol Suppl, 1935: p. 1–103.
8. Hubel, D.H. and T.N. Wiesel, *Brain mechanisms of vision.* Sci Am, 1979. **241**(3): p. 150-62.
9. Jeon, C.J., E. Strettoi, and R.H. Masland, *The major cell populations of the mouse retina.* J Neurosci, 1998. **18**(21): p. 8936-46.
10. Young, R.W., *The renewal of photoreceptor cell outer segments.* J Cell Biol, 1967. **33**(1): p. 61-72.
11. Wolfrum, U. and A. Schmitt, *Rhodopsin transport in the membrane of the connecting cilium of mammalian photoreceptor cells.* Cell Motil Cytoskeleton, 2000. **46**(2): p. 95-107.
12. Sung, C.H. and A.W. Tai, *Rhodopsin trafficking and its role in retinal dystrophies.* Int Rev Cytol, 2000. **195**: p. 215-67.
13. Spencer, M., P.B. Detwiler, and A.H. Bunt-Milam, *Distribution of membrane proteins in mechanically dissociated retinal rods.* Invest Ophthalmol Vis Sci, 1988. **29**(7): p. 1012-20.
14. Hosch, J., B. Lorenz, and K. Stieger, *RPGR: role in the photoreceptor cilium, human retinal disease, and gene therapy.* Ophthalmic Genet, 2011. **32**(1): p. 1-11.
15. Pacione, L.R., et al., *Progress toward understanding the genetic and biochemical mechanisms of inherited photoreceptor degenerations.* Annu Rev Neurosci, 2003. **26**: p. 657-700.
16. Hecht, S., S. Shlaer, and M.H. Pirenne, *Energy, Quanta, and Vision.* J Gen Physiol, 1942. **25**(6): p. 819-40.
17. Hendrickson, A.E. and C. Yuodelis, *The morphological development of the human fovea.* Ophthalmology, 1984. **91**(6): p. 603-12.
18. Schnapf, J.L. and D.A. Baylor, *How photoreceptor cells respond to light.* Sci Am, 1987. **256**(4): p. 40-7.
19. Yau, K.W., T.D. Lamb, and D.A. Baylor, *Light-induced fluctuations in membrane current of single toad rod outer segments.* Nature, 1977. **269**(5623): p. 78-80.

20. Nathans, J., D. Thomas, and D.S. Hogness, *Molecular genetics of human color vision: the genes encoding blue, green, and red pigments.* Science, 1986. **232**(4747): p. 193-202.
21. Hwa, S.G.J., *Rhodopsin Structure, Function, and Involvement in Retinitis Pigmentosa*. 2008: Springer Science & Business Media.
22. Li, Z.Y., D.E. Possin, and A.H. Milam, *Histopathology of bone spicule pigmentation in retinitis pigmentosa.* Ophthalmology, 1995. **102**(5): p. 805-16.
23. Hartong, D.T., E.L. Berson, and T.P. Dryja, *Retinitis pigmentosa.* Lancet, 2006. **368**(9549): p. 1795-809.
24. Wright, A.F., et al., *Photoreceptor degeneration: genetic and mechanistic dissection of a complex trait.* Nat Rev Genet, 2010. **11**(4): p. 273-84.
25. Pawlyk, B.S., et al., *Photoreceptor rescue by an abbreviated human RPGR gene in a murine model of X-linked retinitis pigmentosa.* Gene Ther, 2016. **23**(2): p. 196-204.
26. Bunker, C.H., et al., *Prevalence of retinitis pigmentosa in Maine.* Am J Ophthalmol, 1984. **97**(3): p. 357-65.
27. Grondahl, J., *Estimation of prognosis and prevalence of retinitis pigmentosa and Usher syndrome in Norway.* Clin Genet, 1987. **31**(4): p. 255-64.
28. Haim, M., *Epidemiology of retinitis pigmentosa in Denmark.* Acta Ophthalmol Scand Suppl, 2002(233): p. 1-34.
29. Macrae, W.G., *Retinitis pigmentosa in Ontario - a survey.* Birth Defects Orig Artic Ser, 1982. **18**(6): p. 175-85.
30. Bader, I., et al., *X-linked retinitis pigmentosa: RPGR mutations in most families with definite X linkage and clustering of mutations in a short sequence stretch of exon ORF15.* Invest Ophthalmol Vis Sci, 2003. **44**(4): p. 1458-63.
31. Sharon, D., et al., *RP2 and RPGR mutations and clinical correlations in patients with X-linked retinitis pigmentosa.* Am J Hum Genet, 2003. **73**(5): p. 1131-46.
32. Bird, A.C., *X-linked retinitis pigmentosa.* Br J Ophthalmol, 1975. **59**(4): p. 177-99.
33. Fishman, G.A., M.D. Farber, and D.J. Derlacki, *X-linked retinitis pigmentosa. Profile of clinical findings.* Arch Ophthalmol, 1988. **106**(3): p. 369-75.
34. Berson, E.L., *Retinitis pigmentosa. The Friedenwald Lecture.* Invest Ophthalmol Vis Sci, 1993. **34**(5): p. 1659-76.
35. Szlyk, J.P., et al., *Perceived and actual performance of daily tasks: relationship to visual function tests in individuals with retinitis pigmentosa.* Ophthalmology, 2001. **108**(1): p. 65-75.
36. Berson, E.L., B. Rosner, and E. Simonoff, *Risk factors for genetic typing and detection in retinitis pigmentosa.* Am J Ophthalmol, 1980. **89**(6): p. 763-75.
37. Parmeggiani, F., et al., *Identification of novel X-linked gain-of-function RPGR-ORF15 mutation in Italian family with retinitis pigmentosa and pathologic myopia.* Sci Rep, 2016. **6**: p. 39179.

38. Ross, M.T., et al., *The DNA sequence of the human X chromosome.* Nature, 2005. **434**(7031): p. 325-37.
39. Comander, J., et al., *Visual Function in Carriers of X-Linked Retinitis Pigmentosa.* Ophthalmology, 2015. **122**(9): p. 1899-906.
40. Souied, E., et al., *Severe manifestations in carrier females in X linked retinitis pigmentosa.* J Med Genet, 1997. **34**(10): p. 793-7.
41. Zhou, Q., et al., *A heterozygous mutation in RPGR associated with X-linked retinitis pigmentosa in a patient with Turner syndrome mosaicism (45,X/46,XX).* Am J Med Genet A, 2018. **176**(1): p. 214-218.
42. Bhattacharya, S.S., et al., *Close genetic linkage between X-linked retinitis pigmentosa and a restriction fragment length polymorphism identified by recombinant DNA probe L1.28.* Nature, 1984. **309**(5965): p. 253-5.
43. Schwahn, U., et al., *Positional cloning of the gene for X-linked retinitis pigmentosa 2.* Nat Genet, 1998. **19**(4): p. 327-32.
44. Webb, T.R., et al., *Deep intronic mutation in OFD1, identified by targeted genomic next-generation sequencing, causes a severe form of X-linked retinitis pigmentosa (RP23).* Hum Mol Genet, 2012. **21**(16): p. 3647-54.
45. Hardcastle, A.J., et al., *Evidence for a new locus for X-linked retinitis pigmentosa (RP23).* Invest Ophthalmol Vis Sci, 2000. **41**(8): p. 2080-6.
46. Meindl, A., et al., *A gene (RPGR) with homology to the RCC1 guanine nucleotide exchange factor is mutated in X-linked retinitis pigmentosa (RP3).* Nat Genet, 1996. **13**(1): p. 35-42.
47. Roepman, R., et al., *Positional cloning of the gene for X-linked retinitis pigmentosa 3: homology with the guanine-nucleotide-exchange factor RCC1.* Hum Mol Genet, 1996. **5**(7): p. 1035-41.
48. Buraczynska, M., et al., *Spectrum of mutations in the RPGR gene that are identified in 20 % of families with X-linked retinitis pigmentosa.* Am J Hum Genet, 1997. **61**(6): p. 1287-92.
49. Fujita, R., et al., *Analysis of the RPGR gene in 11 pedigrees with the retinitis pigmentosa type 3 genotype: paucity of mutations in the coding region but splice defects in two families.* Am J Hum Genet, 1997. **61**(3): p. 571-80.
50. Vervoort, R., et al., *Mutational hot spot within a new RPGR exon in X-linked retinitis pigmentosa.* Nat Genet, 2000. **25**(4): p. 462-6.
51. Grant, C.A. and E.L. Berson, *Treatable forms of retinitis pigmentosa associated with systemic neurological disorders.* Int Ophthalmol Clin, 2001. **41**(1): p. 103-10.
52. Zrenner, E., *Fighting blindness with microelectronics.* Sci Transl Med, 2013. **5**(210): p. 210ps16.
53. Edwards, T.L., et al., *Assessment of the Electronic Retinal Implant Alpha AMS in Restoring Vision to Blind Patients with End-Stage Retinitis Pigmentosa.* Ophthalmology, 2018. **125**(3): p. 432-443.
54. MacLaren, R.E., et al., *Retinal repair by transplantation of photoreceptor precursors.* Nature, 2006. **444**(7116): p. 203-7.
55. Burnight, E.R., et al., *CRISPR-Cas9 genome engineering: Treating inherited retinal degeneration.* Prog Retin Eye Res, 2018. **65**: p. 28-49.
56. Friedmann, T., *A brief history of gene therapy.* Nat Genet, 1992. **2**(2): p. 93-8.

57. Buning, H., *[Gene Therapy - What is it? "Healing" with genes].* Pharm Unserer Zeit, 2011. **40**(3): p. 194-201.
58. Hacein-Bey-Abina, S., et al., *LMO2-associated clonal T cell proliferation in two patients after gene therapy for SCID-X1.* Science, 2003. **302**(5644): p. 415-9.
59. Raper, S.E., et al., *Fatal systemic inflammatory response syndrome in a ornithine transcarbamylase deficient patient following adenoviral gene transfer.* Mol Genet Metab, 2003. **80**(1-2): p. 148-58.
60. Sadelain, M., R. Brentjens, and I. Riviere, *The promise and potential pitfalls of chimeric antigen receptors.* Curr Opin Immunol, 2009. **21**(2): p. 215-23.
61. June, C.H. and M. Sadelain, *Chimeric Antigen Receptor Therapy.* N Engl J Med, 2018. **379**(1): p. 64-73.
62. Oral, H.B., et al., *Ex vivo adenovirus-mediated gene transfer and immunomodulatory protein production in human cornea.* Gene Ther, 1997. **4**(7): p. 639-47.
63. Beutelspacher, S.C., et al., *[Comparison of several viral vectors for gene therapy of corneal endothelial cells].* Ophthalmologe, 2005. **102**(12): p. 1168-74.
64. Klein, R., et al., *WPRE-mediated enhancement of gene expression is promoter and cell line specific.* Gene, 2006. **372**: p. 153-61.
65. Wilson, J.M., *Lessons learned from the gene therapy trial for ornithine transcarbamylase deficiency.* Mol Genet Metab, 2009. **96**(4): p. 151-7.
66. Bainbridge, J.W., et al., *Long-term effect of gene therapy on Leber's congenital amaurosis.* N Engl J Med, 2015. **372**(20): p. 1887-97.
67. Reichel, F.F., et al., *AAV8 Can Induce Innate and Adaptive Immune Response in the Primate Eye.* Mol Ther, 2017. **25**(12): p. 2648-2660.
68. Weaver, K.M.M.C., *Janeway's Immunobiology*. 9th edition ed.: Garland Science.
69. Bellingrath, J.S., et al., *High Symmetry of Visual Acuity and Visual Fields in RPGR-Linked Retinitis Pigmentosa.* Invest Ophthalmol Vis Sci, 2017. **58**(11): p. 4457-4466.
70. Liew, G., M. Michaelides, and C. Bunce, *A comparison of the causes of blindness certifications in England and Wales in working age adults (16-64 years), 1999-2000 with 2009-2010.* BMJ Open, 2014. **4**(2): p. e004015.
71. Rangarajan, S., et al., *AAV5-Factor VIII Gene Transfer in Severe Hemophilia A.* N Engl J Med, 2017. **377**(26): p. 2519-2530.
72. MacLaren, R.E., et al., *Retinal gene therapy in patients with choroideremia: initial findings from a phase 1/2 clinical trial.* Lancet, 2014. **383**(9923): p. 1129-37.
73. Bennett, J. and A.M. Maguire, *Gene therapy for ocular disease.* Mol Ther, 2000. **1**(6): p. 501-5.
74. Willett, K. and J. Bennett, *Immunology of AAV-Mediated Gene Transfer in the Eye.* Front Immunol, 2013. **4**: p. 261.
75. Bennett, J., et al., *Safety and durability of effect of contralateral-eye administration of AAV2 gene therapy in patients with childhood-onset blindness caused by RPE65 mutations: a follow-on phase 1 trial.* Lancet, 2016. **388**(10045): p. 661-72.

76. Vandenberghe, L.H., et al., *Dosage thresholds for AAV2 and AAV8 photoreceptor gene therapy in monkey.* Sci Transl Med, 2011. **3**(88): p. 88ra54.
77. Zhong, L., et al., *Next generation of adeno-associated virus 2 vectors: point mutations in tyrosines lead to high-efficiency transduction at lower doses.* Proc Natl Acad Sci U S A, 2008. **105**(22): p. 7827-32.
78. Fischer, M.D., et al., *Codon-Optimized RPGR Improves Stability and Efficacy of AAV8 Gene Therapy in Two Mouse Models of X-Linked Retinitis Pigmentosa.* Mol Ther, 2017. **25**(8): p. 1854-1865.
79. Goncalves, M.A., *Adeno-associated virus: from defective virus to effective vector.* Virol J, 2005. **2**: p. 43.
80. Xiao, W., et al., *Adenovirus-facilitated nuclear translocation of adeno-associated virus type 2.* J Virol, 2002. **76**(22): p. 11505-17.
81. Kotin, R.M., et al., *Site-specific integration by adeno-associated virus.* Proc Natl Acad Sci U S A, 1990. **87**(6): p. 2211-5.
82. Xie, Q., et al., *The atomic structure of adeno-associated virus (AAV-2), a vector for human gene therapy.* Proc Natl Acad Sci U S A, 2002. **99**(16): p. 10405-10.
83. Clark, K.R. and M. Penaud-Budloo, *Evaluation of the fate of rAAV genomes following in vivo administration.* Methods Mol Biol, 2011. **807**: p. 239-58.
84. Duan, D., et al., *Circular intermediates of recombinant adeno-associated virus have defined structural characteristics responsible for long-term episomal persistence in muscle tissue.* J Virol, 1998. **72**(11): p. 8568-77.
85. Bartlett, J.S., R. Wilcher, and R.J. Samulski, *Infectious entry pathway of adeno-associated virus and adeno-associated virus vectors.* J Virol, 2000. **74**(6): p. 2777-85.
86. Gao, G., et al., *Clades of Adeno-associated viruses are widely disseminated in human tissues.* J Virol, 2004. **78**(12): p. 6381-8.
87. Schmidt, M., et al., *Adeno-associated virus type 12 (AAV12): a novel AAV serotype with sialic acid- and heparan sulfate proteoglycan-independent transduction activity.* J Virol, 2008. **82**(3): p. 1399-406.
88. Jacobson, S.G., et al., *Gene therapy for leber congenital amaurosis caused by RPE65 mutations: safety and efficacy in 15 children and adults followed up to 3 years.* Arch Ophthalmol, 2012. **130**(1): p. 9-24.
89. Pang, J.J., et al., *Long-term retinal function and structure rescue using capsid mutant AAV8 vector in the rd10 mouse, a model of recessive retinitis pigmentosa.* Mol Ther, 2011. **19**(2): p. 234-42.
90. Beltran, W.A., et al., *Gene therapy rescues photoreceptor blindness in dogs and paves the way for treating human X-linked retinitis pigmentosa.* Proc Natl Acad Sci U S A, 2012. **109**(6): p. 2132-7.
91. Allocca, M., et al., *Novel adeno-associated virus serotypes efficiently transduce murine photoreceptors.* J Virol, 2007. **81**(20): p. 11372-80.
92. Boye, S.E., et al., *A comprehensive review of retinal gene therapy.* Mol Ther, 2013. **21**(3): p. 509-19.
93. Maguire, A.M., et al., *Safety and efficacy of gene transfer for Leber's congenital amaurosis.* N Engl J Med, 2008. **358**(21): p. 2240-8.

94. Bainbridge, J.W., et al., *Effect of gene therapy on visual function in Leber's congenital amaurosis.* N Engl J Med, 2008. **358**(21): p. 2231-9.
95. Cideciyan, A.V., et al., *Human RPE65 gene therapy for Leber congenital amaurosis: persistence of early visual improvements and safety at 1 year.* Hum Gene Ther, 2009. **20**(9): p. 999-1004.
96. Bennett, J., et al., *AAV2 gene therapy readministration in three adults with congenital blindness.* Sci Transl Med, 2012. **4**(120): p. 120ra15.
97. Edwards, T.L., et al., *Visual Acuity after Retinal Gene Therapy for Choroideremia.* N Engl J Med, 2016. **374**(20): p. 1996-8.
98. Douar, A.M., et al., *Intracellular trafficking of adeno-associated virus vectors: routing to the late endosomal compartment and proteasome degradation.* J Virol, 2001. **75**(4): p. 1824-33.
99. Duan, D., et al., *Endosomal processing limits gene transfer to polarized airway epithelia by adeno-associated virus.* J Clin Invest, 2000. **105**(11): p. 1573-87.
100. Ryals, R.C., et al., *Quantifying transduction efficiencies of unmodified and tyrosine capsid mutant AAV vectors in vitro using two ocular cell lines.* Mol Vis, 2011. **17**: p. 1090-102.
101. Petrs-Silva, H., et al., *High-efficiency transduction of the mouse retina by tyrosine-mutant AAV serotype vectors.* Mol Ther, 2009. **17**(3): p. 463-71.
102. Kirschner, R., et al., *RPGR transcription studies in mouse and human tissues reveal a retina-specific isoform that is disrupted in a patient with X-linked retinitis pigmentosa.* Hum Mol Genet, 1999. **8**(8): p. 1571-8.
103. Roepman, R., et al., *The retinitis pigmentosa GTPase regulator (RPGR) interacts with novel transport-like proteins in the outer segments of rod photoreceptors.* Hum Mol Genet, 2000. **9**(14): p. 2095-105.
104. Neidhardt, J., et al., *Identification and characterization of a novel RPGR isoform in human retina.* Hum Mutat, 2007. **28**(8): p. 797-807.
105. Schmid, F., et al., *Mutation- and tissue-specific alterations of RPGR transcripts.* Invest Ophthalmol Vis Sci, 2010. **51**(3): p. 1628-35.
106. Iannaccone, A., et al., *Clinical and immunohistochemical evidence for an X linked retinitis pigmentosa syndrome with recurrent infections and hearing loss in association with an RPGR mutation.* J Med Genet, 2003. **40**(11): p. e118.
107. Hong, D.H., et al., *RPGR isoforms in photoreceptor connecting cilia and the transitional zone of motile cilia.* Invest Ophthalmol Vis Sci, 2003. **44**(6): p. 2413-21.
108. Gorlich, D. and I.W. Mattaj, *Nucleocytoplasmic transport.* Science, 1996. **271**(5255): p. 1513-8.
109. Sazer, S. and M. Dasso, *The ran decathlon: multiple roles of Ran.* J Cell Sci, 2000. **113 (Pt 7)**: p. 1111-8.
110. Pusch, C.M., et al., *Ten novel ORF15 mutations confirm mutational hot spot in the RPGR gene in European patients with X-linked retinitis pigmentosa.* Hum Mutat, 2002. **20**(5): p. 405.
111. Megaw, R.D., D.C. Soares, and A.F. Wright, *RPGR: Its role in photoreceptor physiology, human disease, and future therapies.* Exp Eye Res, 2015. **138**: p. 32-41.

112. Shu, X., et al., *RPGR mutation analysis and disease: an update.* Hum Mutat, 2007. **28**(4): p. 322-8.
113. Hong, D.H., et al., *A retinitis pigmentosa GTPase regulator (RPGR)-deficient mouse model for X-linked retinitis pigmentosa (RP3).* Proc Natl Acad Sci U S A, 2000. **97**(7): p. 3649-54.
114. Wright, R.N., D.H. Hong, and B. Perkins, *Misexpression of the constitutive Rpgr(ex1-19) variant leads to severe photoreceptor degeneration.* Invest Ophthalmol Vis Sci, 2011. **52**(8): p. 5189-201.
115. Hong, D.H., et al., *Retinitis pigmentosa GTPase regulator (RPGRr)-interacting protein is stably associated with the photoreceptor ciliary axoneme and anchors RPGR to the connecting cilium.* J Biol Chem, 2001. **276**(15): p. 12091-9.
116. Boylan, J.P. and A.F. Wright, *Identification of a novel protein interacting with RPGR.* Hum Mol Genet, 2000. **9**(14): p. 2085-93.
117. Remans, K., et al., *C2 domains as protein-protein interaction modules in the ciliary transition zone.* Cell Rep, 2014. **8**(1): p. 1-9.
118. Zhao, Y., et al., *The retinitis pigmentosa GTPase regulator (RPGR)-interacting protein: subserving RPGR function and participating in disk morphogenesis.* Proc Natl Acad Sci U S A, 2003. **100**(7): p. 3965-70.
119. Patil, H., et al., *Structural and functional plasticity of subcellular tethering, targeting and processing of RPGRIP1 by RPGR isoforms.* Biol Open, 2012. **1**(2): p. 140-60.
120. Li, T., *Leber congenital amaurosis caused by mutations in RPGRIP1.* Cold Spring Harb Perspect Med, 2014. **5**(4).
121. Reiter, J.F., O.E. Blacque, and M.R. Leroux, *The base of the cilium: roles for transition fibres and the transition zone in ciliary formation, maintenance and compartmentalization.* EMBO Rep, 2012. **13**(7): p. 608-18.
122. Sung, C.H. and M.R. Leroux, *The roles of evolutionarily conserved functional modules in cilia-related trafficking.* Nat Cell Biol, 2013. **15**(12): p. 1387-97.
123. Rachel, R.A., T. Li, and A. Swaroop, *Photoreceptor sensory cilia and ciliopathies: focus on CEP290, RPGR and their interacting proteins.* Cilia, 2012. **1**(1): p. 22.
124. Dryja, T.P., et al., *Null RPGRIP1 alleles in patients with Leber congenital amaurosis.* Am J Hum Genet, 2001. **68**(5): p. 1295-8.
125. Eblimit, A., et al., *Spata7 is a retinal ciliopathy gene critical for correct RPGRIP1 localization and protein trafficking in the retina.* Hum Mol Genet, 2015. **24**(6): p. 1584-601.
126. Won, J., et al., *RPGRIP1 is essential for normal rod photoreceptor outer segment elaboration and morphogenesis.* Hum Mol Genet, 2009. **18**(22): p. 4329-39.
127. Thompson, D.A., et al., *Rd9 is a naturally occurring mouse model of a common form of retinitis pigmentosa caused by mutations in RPGR-ORF15.* PLoS One, 2012. **7**(5): p. e35865.
128. Zhang, Q., et al., *Different RPGR exon ORF15 mutations in Canids provide insights into photoreceptor cell degeneration.* Hum Mol Genet, 2002. **11**(9): p. 993-1003.

129. Adamian, M., et al., *Rod and cone opsin mislocalization in an autopsy eye from a carrier of X-linked retinitis pigmentosa with a Gly436Asp mutation in the RPGR gene.* Am J Ophthalmol, 2006. **142**(3): p. 515-8.
130. Aguirre, G.D., et al., *Retinal histopathology of an XLRP carrier with a mutation in the RPGR exon ORF15.* Exp Eye Res, 2002. **75**(4): p. 431-43.
131. Chang, B., et al., *In-frame deletion in a novel centrosomal/ciliary protein CEP290/NPHP6 perturbs its interaction with RPGR and results in early-onset retinal degeneration in the rd16 mouse.* Hum Mol Genet, 2006. **15**(11): p. 1847-57.
132. Zahid, S., et al., *Phenotypic conservation in patients with X-linked retinitis pigmentosa caused by RPGR mutations.* JAMA Ophthalmol, 2013. **131**(8): p. 1016-25.
133. Fahim, A.T., et al., *Allelic heterogeneity and genetic modifier loci contribute to clinical variation in males with X-linked retinitis pigmentosa due to RPGR mutations.* PLoS One, 2011. **6**(8): p. e23021.
134. Walia, S., et al., *Discordant phenotypes in fraternal twins having an identical mutation in exon ORF15 of the RPGR gene.* Arch Ophthalmol, 2008. **126**(3): p. 379-84.
135. Fischer, M.D., *Retinitis Pigmentosa GTPase Regulator Gene Replacement: a potential treatment for X-linked Retintis Pigmentosa*. 2016, University of Oxford.
136. Hong, D.H., et al., *A single, abbreviated RPGR-ORF15 variant reconstitutes RPGR function in vivo.* Invest Ophthalmol Vis Sci, 2005. **46**(2): p. 435-41.
137. Deng, W.T., et al., *Stability and Safety of an AAV Vector for Treating RPGR-ORF15 X-Linked Retinitis Pigmentosa.* Hum Gene Ther, 2015. **26**(9): p. 593-602.
138. Wu, Z., et al., *A long-term efficacy study of gene replacement therapy for RPGR-associated retinal degeneration.* Hum Mol Genet, 2015.
139. Hong, D.H., et al., *Dominant, gain-of-function mutant produced by truncation of RPGR.* Invest Ophthalmol Vis Sci, 2004. **45**(1): p. 36-41.
140. Jacobson, S.G., et al., *Improvement and decline in vision with gene therapy in childhood blindness.* N Engl J Med, 2015. **372**(20): p. 1920-6.
141. Fiers, W. and H. Grosjean, *On codon usage.* Nature, 1979. **277**(5694): p. 328.
142. Ikemura, T., *Codon usage and tRNA content in unicellular and multicellular organisms.* Mol Biol Evol, 1985. **2**(1): p. 13-34.
143. Sharp, P.M. and W.H. Li, *Codon usage in regulatory genes in Escherichia coli does not reflect selection for 'rare' codons.* Nucleic Acids Res, 1986. **14**(19): p. 7737-49.
144. Comeron, J.M., *Selective and mutational patterns associated with gene expression in humans: influences on synonymous composition and intron presence.* Genetics, 2004. **167**(3): p. 1293-304.
145. Plotkin, J.B. and G. Kudla, *Synonymous but not the same: the causes and consequences of codon bias.* Nat Rev Genet, 2011. **12**(1): p. 32-42.
146. Sharp, P.M. and W.H. Li, *The codon Adaptation Index--a measure of directional synonymous codon usage bias, and its potential applications.* Nucleic Acids Res, 1987. **15**(3): p. 1281-95.

147. Yu, C.H., et al., *Codon Usage Influences the Local Rate of Translation Elongation to Regulate Co-translational Protein Folding.* Mol Cell, 2015. **59**(5): p. 744-54.
148. Zhou, Z., et al., *Codon usage is an important determinant of gene expression levels largely through its effects on transcription.* Proc Natl Acad Sci U S A, 2016. **113**(41): p. E6117-E6125.
149. Koutmou, K.S., A. Radhakrishnan, and R. Green, *Synthesis at the Speed of Codons.* Trends Biochem Sci, 2015. **40**(12): p. 717-718.
150. Pechmann, S. and J. Frydman, *Evolutionary conservation of codon optimality reveals hidden signatures of cotranslational folding.* Nat Struct Mol Biol, 2013. **20**(2): p. 237-43.
151. Pechmann, S., J.W. Chartron, and J. Frydman, *Local slowdown of translation by nonoptimal codons promotes nascent-chain recognition by SRP in vivo.* Nat Struct Mol Biol, 2014. **21**(12): p. 1100-5.
152. Gustafsson, C., et al., *Engineering genes for predictable protein expression.* Protein Expr Purif, 2012. **83**(1): p. 37-46.
153. Quax, T.E., et al., *Codon Bias as a Means to Fine-Tune Gene Expression.* Mol Cell, 2015. **59**(2): p. 149-61.
154. Berk, A.J., *Recent lessons in gene expression, cell cycle control, and cell biology from adenovirus.* Oncogene, 2005. **24**(52): p. 7673-85.
155. Sha, J., et al., *E1A interacts with two opposing transcriptional pathways to induce quiescent cells into S phase.* J Virol, 2010. **84**(8): p. 4050-9.
156. Lin, Y.C., et al., *Genome dynamics of the human embryonic kidney 293 lineage in response to cell biology manipulations.* Nat Commun, 2014. **5**: p. 4767.
157. Lilyestrom, W., et al., *Crystal structure of SV40 large T-antigen bound to p53: interplay between a viral oncoprotein and a cellular tumor suppressor.* Genes Dev, 2006. **20**(17): p. 2373-82.
158. Tan, E., et al., *Expression of cone-photoreceptor-specific antigens in a cell line derived from retinal tumors in transgenic mice.* Invest Ophthalmol Vis Sci, 2004. **45**(3): p. 764-8.
159. Mekada, K., et al., *Genetic differences among C57BL/6 substrains.* Exp Anim, 2009. **58**(2): p. 141-9.
160. Rita Costa, A., et al., *Guidelines to cell engineering for monoclonal antibody production.* Eur J Pharm Biopharm, 2010. **74**(2): p. 127-38.
161. Charbel Issa, P., et al., *Assessment of tropism and effectiveness of new primate-derived hybrid recombinant AAV serotypes in the mouse and primate retina.* PLoS One, 2013. **8**(4): p. e60361.
162. Kozak, M., *Point mutations define a sequence flanking the AUG initiator codon that modulates translation by eukaryotic ribosomes.* Cell, 1986. **44**(2): p. 283-92.
163. Semple-Rowland, S.L., et al., *Expression characteristics of dual-promoter lentiviral vectors targeting retinal photoreceptors and Muller cells.* Mol Vis, 2010. **16**: p. 916-34.
164. Sohal, V.S., et al., *Parvalbumin neurons and gamma rhythms enhance cortical circuit performance.* Nature, 2009. **459**(7247): p. 698-702.

165. Smedemark-Margulies, N. and J.G. Trapani, *Tools, methods, and applications for optophysiology in neuroscience.* Front Mol Neurosci, 2013. **6**: p. 18.
166. Hermens, W.T., et al., *Purification of recombinant adeno-associated virus by iodixanol gradient ultracentrifugation allows rapid and reproducible preparation of vector stocks for gene transfer in the nervous system.* Hum Gene Ther, 1999. **10**(11): p. 1885-91.
167. Lipinski, D.M., et al., *CNTF Gene Therapy Confers Lifelong Neuroprotection in a Mouse Model of Human Retinitis Pigmentosa.* Mol Ther, 2015. **23**(8): p. 1308-1319.
168. Schneider, C.A., W.S. Rasband, and K.W. Eliceiri, *NIH Image to ImageJ: 25 years of image analysis.* Nat Methods, 2012. **9**(7): p. 671-5.
169. Schindelin, J., et al., *Fiji: an open-source platform for biological-image analysis.* Nat Methods, 2012. **9**(7): p. 676-82.
170. Deng, W.T., et al., *Stability and Safety of an AAV Vector for Treating RPGR-ORF15 X-linked Retinitis Pigmentosa.* Hum Gene Ther, 2015.
171. Nathwani, A.C., et al., *Long-term safety and efficacy of factor IX gene therapy in hemophilia B.* N Engl J Med, 2014. **371**(21): p. 1994-2004.
172. Liu, Y., et al., *AAV8-antiVEGFfab Ocular Gene Transfer for Neovascular Age-Related Macular Degeneration.* Mol Ther, 2018. **26**(2): p. 542-549.
173. Glockle, N., et al., *Panel-based next generation sequencing as a reliable and efficient technique to detect mutations in unselected patients with retinal dystrophies.* Eur J Hum Genet, 2014. **22**(1): p. 99-104.
174. Holladay, J.T., *Proper method for calculating average visual acuity.* J Refract Surg, 1997. **13**(4): p. 388-91.
175. Wiethoff, S., et al., *Retinal nerve fibre layer loss in hereditary spastic paraplegias is restricted to complex phenotypes.* BMC Neurol, 2012. **12**: p. 143.
176. Fischer, M.D., et al., *A new method to monitor visual field defects caused by photoreceptor degeneration by quantitative optical coherence tomography.* Invest Ophthalmol Vis Sci, 2008. **49**(8): p. 3617-21.
177. Rowe, F.J. and A. Rowlands, *Comparison of diagnostic accuracy between Octopus 900 and Goldmann kinetic visual fields.* Biomed Res Int, 2014. **2014**: p. 214829.
178. Fischer, M.D., et al., *Structural and functional changes of the human macula during acute exposure to high altitude.* PLoS One, 2012. **7**(4): p. e36155.
179. Matsumoto, H., T. Sato, and S. Kishi, *Outer nuclear layer thickness at the fovea determines visual outcomes in resolved central serous chorioretinopathy.* Am J Ophthalmol, 2009. **148**(1): p. 105-10 e1.
180. Kacar, D.G.M.D.E.E.S.T.D.A.D.H., *Evaluation of demographical, clinical and imaging characteristics of 304 retinitis pigmentosa (RP) patients screened for retinal prosthesis candidacy.* IOVS Abstract Issue, 2016. **57**(12).
181. Wright, A.F. and X. Shu, *Focus on Molecules: RPGR.* Exp Eye Res, 2007. **85**(1): p. 1-2.
182. Massof, R.W., et al., *Bilateral symmetry of vision disorders in typical retinitis pigmentosa.* Br J Ophthalmol, 1979. **63**(2): p. 90-6.

183. Birch, D.G., et al., *Randomized trial of ciliary neurotrophic factor delivered by encapsulated cell intraocular implants for retinitis pigmentosa.* Am J Ophthalmol, 2013. **156**(2): p. 283-292 e1.
184. Bittner, A.K., M.H. Iftikhar, and G. Dagnelie, *Test-retest, within-visit variability of Goldmann visual fields in retinitis pigmentosa.* Invest Ophthalmol Vis Sci, 2011. **52**(11): p. 8042-6.
185. Birch, D.G., et al., *Rates of decline in regions of the visual field defined by frequency-domain optical coherence tomography in patients with RPGR-mediated X-linked retinitis pigmentosa.* Ophthalmology, 2015. **122**(4): p. 833-9.
186. Birch, D.G., et al., *Spectral-domain optical coherence tomography measures of outer segment layer progression in patients with X-linked retinitis pigmentosa.* JAMA Ophthalmol, 2013. **131**(9): p. 1143-50.
187. Tee, J.J.L., et al., *Quantitative Analysis of Retinal Structure Using Spectral-Domain Optical Coherence Tomography in RPGR-Associated Retinopathy.* Am J Ophthalmol, 2017. **178**: p. 18-26.
188. Sandberg, M.A., et al., *Disease course of patients with X-linked retinitis pigmentosa due to RPGR gene mutations.* Invest Ophthalmol Vis Sci, 2007. **48**(3): p. 1298-304.
189. Beltran, W.A., et al., *Successful arrest of photoreceptor and vision loss expands the therapeutic window of retinal gene therapy to later stages of disease.* Proc Natl Acad Sci U S A, 2015. **112**(43): p. E5844-53.

DECLARATION OF AUTHORSHIP

Except where otherwise indicated, this thesis is entirely my own work. This includes all lab work, data acquisition, statistical analysis and writing of the manuscript.

The following parts of the thesis involve work not undertaken by myself:
In Chapter 2, all murine retinal tissue was obtained from a preclinical trial run by Dominik Fischer (Nuffield Laboratory of Ophthalmology (NLO), University of Oxford, UK). The Rhesus macaques (*Macaca mullata*) retinal tissue was obtained from the Medical Research Council Centre for Macaques (Porton Down, UK) by Alun Barnard (NLO, University of Oxford, UK). The original plasmids containing codon optimized and wild type *RPGR* were designed by Dominik Fischer and synthesized by GenScript (Piscataway, USA).
In Chapter 3, Alex Ochakovski (University Eye Hospital Tübingen, Germany) undertook the generalized linear mixed model (GzLMM) analysis. Both Aline Naumann (Institute of Clinical Epidemiology and Applied Biometrics, University of Tübingen, Germany) and Philipp Berens (Neural Data Science for Vision Research Lab, University of Tübingen, Germany) kindly provided advice on the statistical analysis. Immanuel Seitz (University Eye Hospital Tübingen, Germany) performed the data acquisition of the patients from the University Eye Hospital, Tübingen, Germany.

Tübingen, 22.10. 2018

PUBLICATIONS

Fischer, M.D., et al., *Codon-Optimized RPGR Improves Stability and Efficacy of AAV8 Gene Therapy in Two Mouse Models of X-Linked Retinitis Pigmentosa.* Mol Ther, 2017. **25**(8): p. 1854-1865.

Bellingrath, J.S., et al., *High Symmetry of Visual Acuity and Visual Fields in RPGR-Linked Retinitis Pigmentosa.* Invest Ophthalmol Vis Sci, 2017. **58**(11): p. 4457-4466.

Bellingrath, J.S., et al*., Gene therapy as a treatment concept for inherited retinal diseases*. Ophthalmologe, 2015. **112**(9): p. 720-7.

ACKNOWLEDGEMENTS

First and foremost, I would like to express my immense gratitude to Dominik Fischer, for his guidance, support, patience and mentorship throughout every step of the way of this journey. I am so thankful for the opportunities he has opened up for me and the lessons learned along the way.

Robert MacLaren, who welcomed me into his lab and gave me the invaluable opportunity to spend ten months learning from him and his extraordinary team in the magical place that is Oxford University.

My colleagues and friends at the Nuffield Laboratory of Ophthalmology, who made coming into the lab every day a wonderful experience: Alun Barnard, Michelle McClements, Marco Bellino, Maria Patrício, Jasmin Balmer, Saun Wood, Daniyar Dauletbekov, Doron Hickey, Mark Hassall, Anna Paola Salvetti, Jasleen Jolly, Matthew Simunovic, Kanmin Xue and Thomas Edwards.

Michelle McClements for taking time every week for genetics tutorial and answering every question I had in the lab.

Maria Patrício, who gave me invaluable guidance and taught me many of the practicalities of lab work.

Jasleen Jolly, who was a huge help in deciphering handwriting and explaining patient charts at the Oxford Eye Clinic.

Mark Hassall for being a wonderful friend and bench partner during those months in Oxford.

My fantastic team of colleagues and friends at the Institute for Ophthalmic Research in Tübingen: Ahmad Zhour, Immanuel Seitz, Felix Reichl, Jonas Neubauer and Alex Ochakovski.

Immanuel Seitz and Alex Ochakovski for their wonderful work on the *RPGR*-XLRP patient data.

Philip, who is responsible for introducing me to Dominik Fischer in the first place.

Elisa, with whom I shared the parallel challenges and joys of doing experimental lab work and discovering a new country.

Nikhil, for his help, feedback and moral support with much of the *RPGR*-XLRP patient data.

My extraordinary group of childhood friends: Monika, Dorothea, Anna, Anna-Katharina and Lenny.

Rebecca and Kiri, my kindred spirits.

My wonderful friends Max and Johanna.

“Nanny” Joan - I cherish every moment we get to spend together.

My aunt Lexie, whose extraordinary spirit I am so grateful to have in my life.

Lastly, my thanks go to my parents, whose love and unwavering support are the bedrock of me being able to make my way in this world. You taught me the ability to get up after every fall and cherish the wonderful moments that life brings, however small or big they may be. I am proud to be your daughter.